# OPTIMIZATION OF ELECTRODE SYSTEM FOR ELECTROHYDRODYNAMIC (EHD) DRYER

**by**

**Ivanna Bashkir**

**Submitted in partial fulfilment of the requirements**

**for the degree of Master of Science**

**at**

**Dalhousie University**

**Halifax, Nova Scotia**

**March 2020**

## Table of Contents

## List of Tables

## List of Figures

## Abstract

Electrohydrodynamic (EHD) drying is a non-thermal dewatering technology, based on the phenomenon of high-voltage corona discharge in the gaseous medium. It is offering high product quality and less energy consumption compared to commonly used thermal drying. Since EHD drying was not commercialized yet, this research was focused on the optimization of discharge and collecting electrodes for industrial application of this drying technology. Three types of needles in discharge electrodes and mesh-type collecting electrodes with different open area, wire diameter, and grounded wires percentage have been studied. Discharge electrode fabricated with sharp pins or construction nails was found to be the most suitable to use in EHD dryers. Mesh collecting electrode significantly enhanced drying rate compared to a solid plate and it is recommended to use in the large scale EHD dryers. The results of this research are critical for further industrial upscaling of the EHD drying technology.

## List of Abbreviations Used

### Abbreviations:

| | |
|---|---|
| EHD | Electrohydrodynamic |
| AC | Alternating current |
| DC | Direct current |
| DR | Drying rate, g/h |
| OA | Open area, % |
| RH | Relative humidity, % |

### Nomenclature:

| | |
|---|---|
| A | area, $m^2$ |
| $b$ | ions mobility, $m^2/(V \cdot s)$ |
| $d$ | gap, cm |
| $E$ | electric field strength, kV/cm |
| $E_0$ | breakdown electric field strength, kV/cm |
| $\varepsilon_0$ | dielectric permittivity of vacuum, $8.86 \cdot 10^{-12}$ F/m |
| $I$ | current, A |
| $j$ | current density, $A/m^2$ |
| $L$ | spacing between needles/wires, cm |
| $l$ | sample thickness, mm |
| $P$ | pressure, kPa |
| $\rho$ | air density, $kg/m^3$ |
| $\rho_c$ | space charge, $C/m^3$ |
| $r$ | needle/wire body radius, mm |
| $r_{tip}$ | needle tip radius, mm |
| $T$ | absolute temperature, K |
| $V$ | applied voltage, kV |
| $v$ | kinematic viscosity of air, $m^2/s$ |

## Acknowledgements

Being at high school, I used to read books every evening and late night. One night after reading I realized how lucky we all are by having electricity at our homes. We could not overestimate the importance of the electricity, which is a part of our life and all industrial development. That's how I become passionate about my future career in power engineering and energy saving technologies. Since January 2018 when I started my Master study at Dalhousie University, it was exciting journey in the field of electrical and power engineering. I am very lucky to be a part of Dr. Alex Martynenko's Bioprocess Engineering research team.

I would like to express my special thanks to my supervisor Dr. Alex Martynenko for the opportunity to do this project as well as his guidance and support throughout my graduate years at Dalhousie University. I am thankful to Dr. Thijs Defraeye and Dr. Tadeusz Kudra for giving me the valuable advices in writing of scientific papers. In addition, I thank Dr. Peter Havard and Department of Engineering for providing all technical support for design of EHD experimental setups. I would also like to acknowledge Mr. Mark Mason (international student coordinator) for his thoughtful navigation through my MSc study, Dr. Daryl Hayes for improving my teaching skills, Ms. Mandi Wilson (administrative coordinator) for the continuous encouragement, and Mr. Chris Nelson (senior instructor) and Mr. Adam Wilson (technician) for their technical help. To my parents Mrs. Iryna Bashkir and Mr. Serhiy Bashkir, and all my relatives and friends, and others who shared their support, thank you. This work is dedicated to all of you.

# Chapter 1 Introduction

Drying is an important process of moisture removal from food and non-food materials. It is the most common method for food preservation by reducing water activity, used by small scale farmers and food processing industry. Dried foods have many benefits compared to raw products, including an extended shelf-life as well as reduced packaging, storage, handling and transportation costs. However, the process of drying is energy intensive, accounting for roughly 12-20% of energy consumed in the manufacturing industry (Moses et al., 2014).

Over 85% of industrial dryers are the convective types; however, convective drying requires a huge amount of energy. Despite its simplicity and low investment cost, this drying is time-consuming and generally requires elevated air temperatures, often resulting in microstructural damage and loss of nutritional value (Li et al., 2019). To increase the shelf stability of products and save their initial nutritional value, the industry and academics are looking for a new energy-saving drying technology. One of the potential candidates is electrohydrodynamic (EHD) drying, based on phenomenon of corona discharge in the gaseous medium, which enhances moisture removal from food sample placed between two electrodes. It performs effectively at room temperature (20°C). Once EHD commercial unit is developed, it has the potential to have several strong advantages.

Electrohydrodynamic drying is regarded as a non-thermal dewatering technology, suitable for drying heat-sensitive materials because it offers high product quality (Kudra and Martynenko, 2015). Compared to traditional convective drying at elevated temperatures, EHD drying is a non-thermal technology and has been reported to reduce drying time and increase drying rate (DR). A foremost benefit of EHD drying is its non-

thermal processing, resulting in superior quality of dried products, such as enhanced color (or at least similar to the fresh samples) (Bajgai and Hashinaga, 2001a, 2001b; Bai et al., 2008; Esehaghbeygi et al., 2014; Martynenko et al., 2019a), reduced shrinkage (Alemrajabi et al., 2012; Singh, 2014; Martynenko and Zheng, 2015), uniform texture (Singh, 2014; Martynenko and Kudra, 2016a), higher rehydration capacity (Yang and Ding, 2016), better retention of nutritional compounds (Tirawanichakul et al., 2009; Ding et al., 2015), and flavor (Martynenko and Kudra, 2016a).

Additionally, the EHD drying technique has many beneficial features such as simplicity (no moving parts involved) (Feng and Seyed-Yagoobi, 2004), lightweight construction, low acoustic noise (Tansakul and Lumyong, 2008), and rapid control of the drying process by varying of the applied voltage (Feng and Seyed-Yagoobi, 2004). The EHD drying does not require additional high-temperature airflow and operates effectively at room temperature (20°C) and low relative humidity (RH). Energy consumption used in EHD drying is reported to be much lower compared to traditional thermal drying (Singh, 2014; Dinani et al., 2014, Martynenko and Zhang, 2015; Martynenko at al., 2019).

Overall, compared to the traditional drying techniques, including high-end technologies such as freeze-drying, the hardware requirements and the operational costs of EHD drying are expected to be much lower (Kudra and Martynenko, 2015). Hence, it is an excellent alternative for drying of heat-sensitive agricultural biomaterials, which contain highly sensitive nutritional compounds (Giri et al., 2007).

Currently the actual mechanism of the mass transfer in EHD drying is still unclear. One of the reasons is that the couplings between electrostatic field, ion flow, resulting ionic wind, and heat and mass transfer in the product are not fully understood. There are

numerous factors, which affect EHD drying; however, since previously published results obtained at different conditions are barely comparable, better understanding of the combined effects on EHD drying is required.

Because most of previous research was conducted on small lab-scale EHD setups, this research was dedicated for further industrial up-scaling of the EHD drying technology based on optimization of discharge and collecting electrode configuration. Critical analysis of findings on the lab scale is essential for better understanding of EHD drying processes. To this end, the main goals of this research are:

- Analyzing and categorizing of key factors affecting the drying process in EHD technology (Chapter 2);
- Investigating of the effect of needle shape in a multiple needle discharge electrode on ionic wind, drying rate and energy consumption (Chapter 3);
- Studying the effect of metal mesh collecting electrode as compared to a solid metal plate on the drying rate and energy consumption (Chapter 4);
- Quantifying the effect of open area, wire diameter, and grounded wires percentage in mesh collecting electrode on drying rate and energy consumption (Chapter 4).

# Chapter 2 Literature Review

The EHD technology is relatively new and not yet explored extensively for drying; because of that, a profound and comprehensive understanding of EHD effects on drying rate is very important. To this end, critical analysis of findings on lab-scale is essential for upscaling and further commercializing of the EHD drying technology. Therefore, the purpose of this review is to analyze the effects of key factors and drying conditions on the drying rate of fruits, vegetables, and other plant-based materials. The EHD is a complex phenomenon, involving multiple factors, and the contribution of some factors to the moisture removal is still underexplored and will require thorough investigation.

## 2.1 Mechanism of EHD Drying

Electric wind, also known as ionic or corona wind, is considered to be the principal driving force in EHD drying (Ramachandran and Lai, 2010). The ionic wind results from a flow of ions from discharge electrode (such as a sharp pin/needle or thin wire) under high voltages. The air around discharge electrode is ionized with unipolar ions, which are moving towards the collecting (grounded) electrode at high ion velocity about 80 - 200 m/s (Drew and Pister, 2017; Monrolin et al., 2017). Along their path, these ions collide with neutral air molecules, transferring their momentum to the neutral air molecules and creating air flow with velocity in the range of 0.1-10 m/s (Defraeye and Martynenko, 2018). Figure 2.1 schematically portrays the EHD flow due to corona discharge from two-needle electrodes.

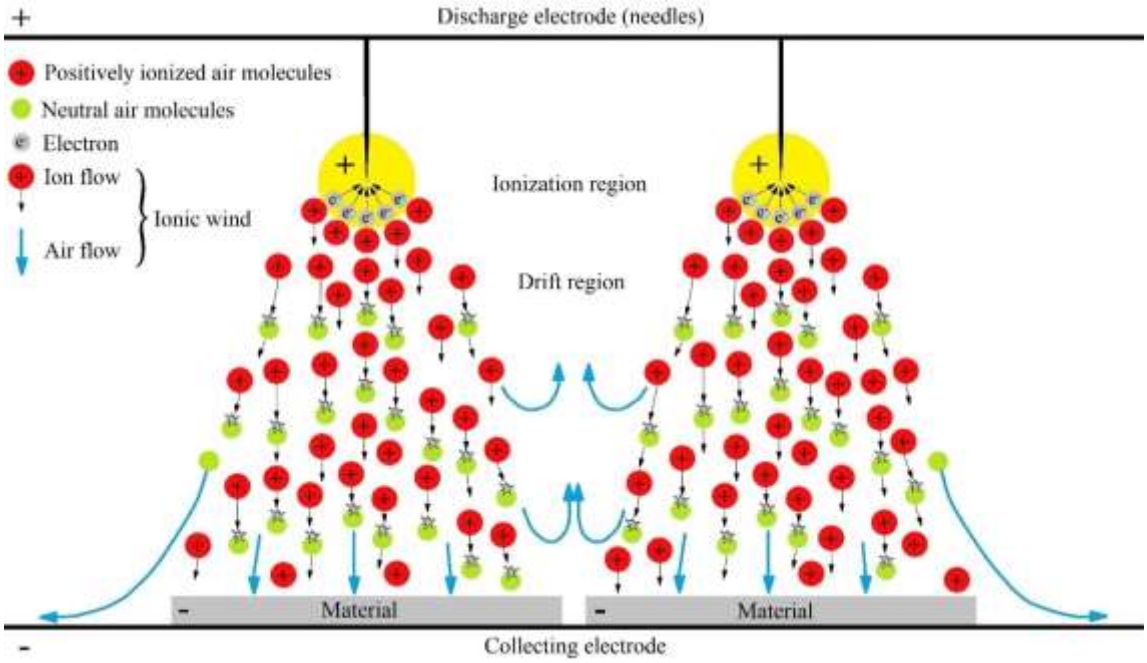


Figure 2.1 EHD-induced ionic wind from two-needle electrodes, showing ions flow as black arrows, and air flow as blue arrows (modified from Martynenko et al., 2019, with permission (Appendix B))

Most researchers consider that the main effect of ionic wind on the drying is the convective destabilization of a boundary layer at the gas-material interface (Moreau, 2007). This leads to a substantial enhancement of heat and mass transfer (Lai and Wong, 2003) and induces an increase of moisture removal from the surface of wet material (Ramachandran and Lai, 2010). However, the EHD is a complex phenomenon, involving multiple factors. The contribution of some factors to the moisture removal is already confirmed, whereas others are still underexplored and will require thorough investigation.

## 2.2 Key Factors in EHD Drying

An analysis of previously published works enabled to classify the key factors of EHD drying technology into the following four categories:

1. Electrical process parameters: voltage, electric field strength, current, polarity, type of current (direct or alternating).
2. Geometry and configuration of discharge needles/wires, spacing, gap, and collector (solid/mesh) electrodes.
3. Environmental parameters: air temperature, relative humidity (RH), pressure, as well as velocity and direction of additional external (fan-driven) air flow with respect to ionic wind.
4. Material characteristics: initial moisture content, porosity, tortuosity, capillarity, surface roughness, sorption isotherms, mechanical properties, equilibrium moisture content.

Electrical process parameters, configurations of electrodes, environmental conditions, and their effects on the drying of plant-based materials are summarized in Table A.1 (Appendix A). An optimal combination of these key factors can be sought for developing the most energy efficient drying technology, leading to the shortest drying process and the best product quality. This knowledge is also critical for industrial upscaling of EHD drying.

The effects of geometry factors on DR have been briefly discussed by Martynenko et al. (2017a). For multiple-needle discharge electrodes, an interaction between ionic jets depends on the space between the needles and affects charge and mass transfer (Martynenko et al., 2017a). Therefore, the electrode geometry and configuration are significant factors affecting EHD drying. Ideally, the jets of ionic wind should cover most of the wet material surface and do not interfere with others leaving the path for rebounding jets of ionic wind and loading of the recirculating air with evaporated moisture.

The information on the effects of environmental conditions and material properties on the DR of plant-based material is very scarce. Most of the review papers were focused on the description of EHD phenomenon and its application in industry, mainly for drying purposes (Bajgai et al., 2006; Singh et al., 2012; Filladitakis et al., 2014; Kudra and Martynenko, 2015; Martynenko and Kudra, 2016a; Zhang et al., 2017). Additionally, Singh et al. (2012) reviewed the EHD application for postharvest storage, and Fylladitakis et al. (2014) reviewed EHD application for thrusts and pumps.

The effects of material properties on EHD drying is the least explored topic. Chen and Barthakur (1994) reported that drying efficiency decreased with material thickness, whereas Martynenko et al. (2017b) found that drying rate depends on the material microstructure, in particular the material surface properties. The effects of density, porosity, tortuosity, capillarity, surface roughness, sorption properties require further research.

### *2.2.1 Effect of Electrical Parameters on EHD Drying*

Experimental research showed that there is no effect on the DR of the wet material when the discharge and collecting electrodes are flat and parallel (Sumorek and Pietrzyk, 2004; Atungulu et al., 2005). This configuration of electrodes provides a uniform electrostatic field, which prevents ionization and current flow and therefore it is not applicable for drying purpose. Only non-uniform electric fields, which originate from corona discharge and create ionic wind, could facilitate dehydration (Panchenko et al., 1980). The effect of non-uniform electric field on the enhancement of the DR could be explained by the fact that polar water molecules are driven from the region with lower

electric field to the higher one. This implies a movement of water from the inside of the product to the tip of the discharge electrode (Liang and Ding, 2006).

In EHD, a non-uniform electric field is created by the high voltage between an emitting electrode with very small radius thus large curvature (wire or needle), and a grounded collecting electrode, which is usually the flat plate/mesh or large-diameter cylinder (Figure 2.1). The overall electric field in EHD drying is characterized by the electric field strength $E$ (kV/cm), defined as the ratio of the applied voltage $V$ (kV) to the gap between the electrodes, $d$ (cm):

$$E = \frac{V}{d} \tag{2.1}$$

In EHD, ionic wind or charge flow appears after ionization of the air in the vicinity of the discharge electrode. This occurs if the electric field strength $E_0$ on the spherical needle tip is reaching a critical value determined by Peek' law (Peek, 1929):

$$E_0 = 3.1 \cdot 10^6 \left(1 + \frac{0.308}{\sqrt{0.5 \cdot r}}\right) \tag{2.2}$$

where $r$ is the radius of curvature of discharge electrode (cm).

This onset value $E_0$ is the condition to initiate corona discharge and ionic flow. Thereafter, the corona discharge current is determined by the electric field strength above the onset value. The equation for corona discharge current in the needle-plate geometry has been first proposed by Warburg in early 1899. According to Warburg law, the corona discharge from the needle or thin wire causes non-uniform distribution of electric current at the plane surface of collecting electrode (Equation 2.3):

$$j = j_0 cos^5\theta \tag{2.3}$$

where $j$ is the current density, $\mathrm{A/m^2}$; $j_0$ quantifies the maximum current density just underneath of a needle/wire, $\mathrm{A/m^2}$; and $\theta$ is the Warburg angle between perpendicular from discharge point to collecting electrode and the vector from discharge point to any point at the surface of the collecting electrode (usually this angle does not exceed 60°). The three-dimensional shape of Warburg distribution reproduced in MATLAB for a single-needle (Figure 2.2 a) and single-wire electrodes (Figure 2.2 b), and for two-needle (Figure 2.2 c) and two-wire electrodes (Figure 2.2 d) (Martynenko et al., 2017b), visualize the non-homogeneous distribution of current at the surface of the collecting plate electrode.

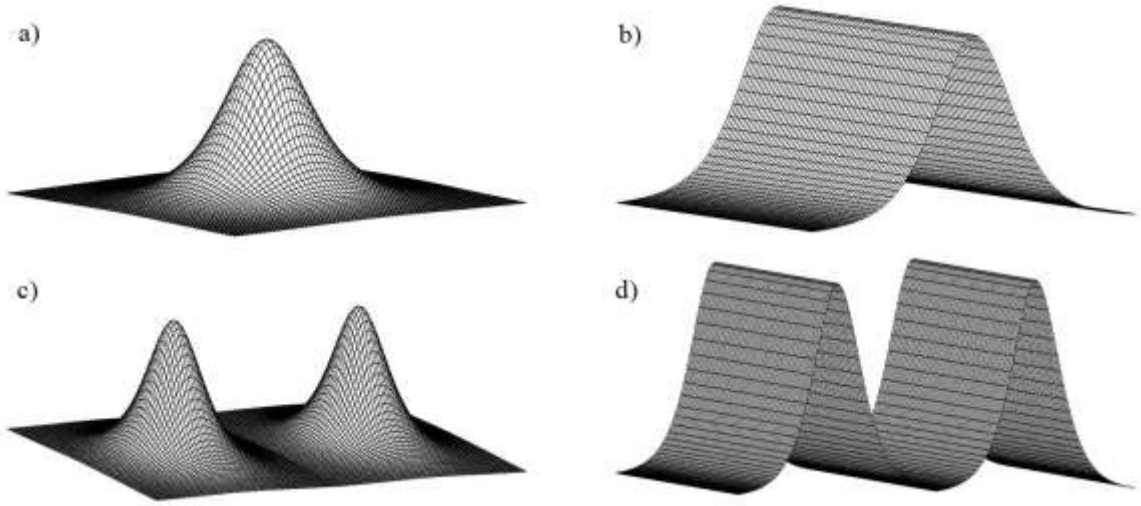


Figure 2.2 Current density distribution for single-needle (a), single-wire (b), two-needle (c), and two-wire (d) electrodes (Martynenko et al., 2017b, with permission (Appendix B))

Current density is determined by the space charge density, ions mobility and electric field strength (Stuetzer, 1959):

$$j = \rho_c b E \tag{2.4}$$

where $\rho_c$ is a space charge, $\mathrm{C/m^3}$.

Robinson (1961) derived the relationship between current density and ionic wind velocity at the surface of the collecting electrode:

$$u_e = \sqrt{\frac{jd}{\rho b}} \tag{2.5}$$

where $u_e$ is the ionic wind velocity, m/s; $\rho$ is the air density, $\mathrm{kg/m^3}$.

Equations (2.3-2.5) describe spatial distribution of electric current density and ionic wind velocity at any point of the collecting electrode (Figure 2.2). The total electric current over the entire area of collecting electrode could be approximated with equation, proposed by Warburg (1927):

$$I = cV(V - V_0) \tag{2.6}$$

where $V$ is the voltage applied to the electrodes; $V_0$ is the onset voltage, required to initiate the corona discharge; and $c$ is the dimensional constant depending on the inter-electrode distance, the needle electrode radius, the ion mobility in the drift region and other geometrical factors. It was found that this constant increases with the diameter of the discharge electrode and decreases with the needle-to-plate gap (Townsend, 1915).

In 1961, Robinson found that the constant $c$ is equal to $g\varepsilon_0 b$, so the Warburg relationship becomes:

$$I = g\varepsilon_0 b \cdot V(V - V_0) \tag{2.7}$$

where $\varepsilon_0$ represents dielectric permittivity of vacuum, $8.86 \cdot 10^{-12}\mathrm{F/m}$; $b$ stands for the ion mobility, $\mathrm{m^2/(V{\cdot}s)}$, being equal to $b^+ = 1.6 \cdot 10^{-4}\mathrm{m^2/(V{\cdot}s)}$ for positive ions and $b^- = 2.1 \cdot 10^{-4}\mathrm{m^2/(V{\cdot}s)}$ for negative ions; $g$ is a geometrical parameter, depending on electrode geometry and configuration (1/m).

This equation was found to be accurate for single needle/wire-to-plate geometry. Independently, Stuetzer (1959) proposed different formula for the current from needle/wire to the collecting electrode:

$$I = \frac{g_0 \varepsilon_0 b A}{d^3}(V - V_0)^2 \tag{2.8}$$

where $A$ is the area of the collecting electrode ($m^2$); $g_0$ is dimensionless geometry factor, independent of the gap between the electrodes, while in Equation 2.7 the parameter $g$ is dimensional.

In 1983, Henson analyzed theoretically both models and he proved that equation 2.6 holds only for currents below 100 μA, whereas Stuetzer's equation 2.8 is more universal and can be used for the currents higher than 100 μA. In 1987, McLean and Ansari proposed that model should not consider the physical gap between discharge and collecting electrodes, but rather the length of the drift zone. An increase of electric field strength would increase effective radius of the corona ionization region, thus reducing the length of the drift zone from $(d)$ to $(d - y)$:

$$I = \frac{g_0 \varepsilon_0 b A}{(d - y)^3}(V - V_0)^2 \tag{2.9}$$

where $y$ represents the effective radius of the corona ionization region, almost independent of the needle/wire diameter but increasing with the electric field strength (McLean and Ansari, 1987). Equation 2.9 could be also expressed through the average electric field strength (Equation 2.1):

$$I = \frac{g_0 \varepsilon_0 b A}{(d - y)}(E - E_0)^2 \tag{2.10}$$

which clearly reflects the relationship between corona discharge current and electric field strength above the onset value. It should be noted that gap between discharge and collecting electrodes depends also on the thickness and electrical conductivity of the drying material

as it alters the characteristics of the electric field. Material shrinkage and decrease of material conductivity make EHD drying as the non-stationary process.

The lack of a methodology for measurements and calculations of the electric field strength and current distribution in EHD drying makes it difficult to compare effects of electrical characteristics on the drying rate. Numerical Multiphysics simulations could shed light in this respect. With such simulations, information is available on the dependent variables (air velocity, voltage, space charge distribution) at each point in space and time (Martynenko et al., 2017b; Defraeye and Martynenko, 2018, 2019). Another problem is that often information on electrode geometry, material properties and experimental conditions is incomplete, which precludes correct interpretation and comparison with experimental results.

Experimental results published in topical literature clearly demonstrate that EHD-induced drying rate is controlled by voltage, current, electric field strength, or ionic wind intensity (Martynenko et al., 2017b). Due to interrelations between these factors, it is challenging to define the primary cause of EHD-induced moisture transfer.

*2.2.1.1 Effect of Voltage on Drying Rate*

It has been experimentally established that the DR of wet materials increases with applied voltage above the onset value. This finding holds for both direct current (DC) (Cao et al., 2004b; Bai et al., 2008, 2009, 2011; Basiry and Esehaghbeygi, 2010; Esehaghbeygi and Basiry, 2011; Dalvand et al., 2012b, 2013; Dinani et al., 2014; Elmizadeh et al., 2017) and alternating current (AC) (Xue et al., 1996; Ding et al., 2015; Yang and Ding, 2016). Overall, the range of applied voltages in experiments with EHD drying was from 4 kV to 30 kV for DC and from 4.3 kV to 32 kV for AC.

For most materials, the DR increased linearly with voltage (Cao et al., 2004b; Basiry and Esehaghbeygi, 2010; Esehaghbeygi and Basiry, 2011; Esehaghbeygi et al., 2014; Dinani et al., 2014; Dinani and Havet, 2015; Elmizadeh et al., 2017). Drying of materials with dielectric barrier discharge (DBD) showed the same effect of voltage on DR (Thirumdas et al., 2016; Misra, 2018). However, for some materials, such as kelp and kiwi fruits, it was reported that DR increased exponentially with voltage (Bai et al., 2008; Dalvand et al., 2013). This inconsistency could be related to material transport properties (see section 4.1.1) and the mode of drying (convection-limited vs. diffusion-limited), and its initial moisture content.

It was found that the effect of voltage on drying rate was significantly reduced for the combination of EHD with hot air drying (60°C) (Dinani et al., 2014) and completely disappeared with forced airflow at 2.2 m/s (Dinani and Havet, 2015). This implies significant effect of environmental conditions on EHD drying. Unfortunately, authors did not analyze separate effects of temperature or forced airflow on drying rate. The interactions between EHD and convective air cross-flow, and EHD and high temperature should be further investigated.

*2.2.1.2 Effect of Gap on Drying Rate*

The gap between discharge and collecting electrodes is one of the most important parameters in EHD drying. Usually, the gap between electrodes is determined by the applied voltage and breakdown properties of the gas, and varies in the range from 1 cm to 10 cm. This literature review showed significant differences in the ways how gap was assessed. Some researchers assume the gap as the distance between a needle/wire emitter to the surface of the collecting electrode (Dinani et al., 2014), whereas the others consider

the distance between a needle/wire emitter to the surface of the material, placed on the collecting electrode (Chen and Barthakur, 1994; Singh et al., 2012; Singh, 2014; Bardy et al., 2016). The first assumption could be valid only for a thin layer of the wet material (Martynenko et al., 2017a), while the second one should consider the changes of material conductivity and shrinkage.

In most cases, DR of plant-based materials decreased with an increase of electrode gap because of decrease of electric field strength. This decrease was highly nonlinear for mushrooms slices (Dinani et al., 2014), agar gel (Isobe et al., 1999), and rice (Cao et al., 2004b). In a multiple needle/wire configuration it was found that there is an optimal gap, which leads to a maximal DR (Bai et al., 2011). These researchers explained such maximum by optimal exposure of the material surface to ionic wind flow pattern. This optimal gap depended on the spacing between two neighboring needles or wires in discharge electrode. With the spacing between wires of 9 cm and the gap below 9 cm, the surface of the material was underexposed to ionic wind, whereas for a gap larger than 9 cm, the ionic wind from neighboring jets partially overlapped, thus reducing the total effect of EHD drying. The existence of optimal ratio between spacing and gap was theoretically justified by Kudra and Martynenko (2019) (Figure 2.3).

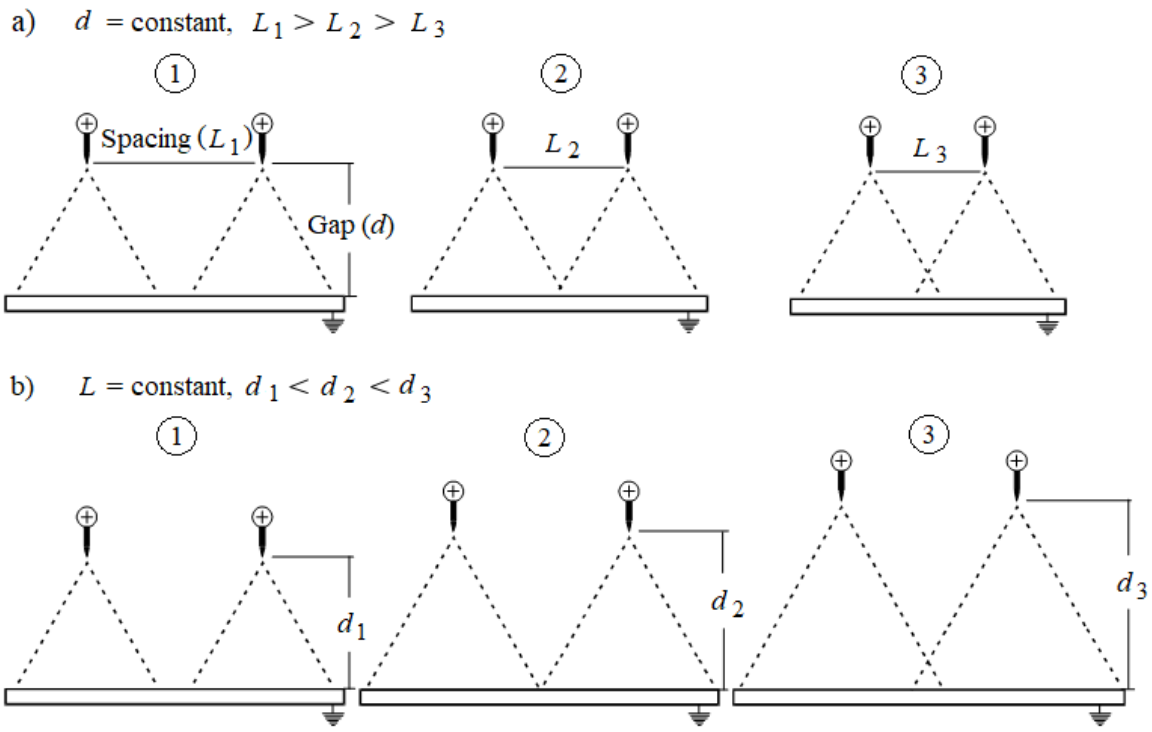


Figure 2.3 Sketch of ionic wind jets: (a) different spacing between emitters in discharge electrode; (b) different gaps between discharge and collecting electrodes (Kudra and Martynenko, 2019, with permission (Appendix B))

It follows that the gap is an important factor in the design of multiple needle/wire discharge electrodes and should be related to the spacing between emitters. Future research on EHD drying systems requires a unified approach to determine the optimum gap in EHD drying. For example, the gap between discharge and collecting electrodes would be determined by the material properties, which would provide a stable glow discharge even if the materials shrink during EHD drying. This gap will determine the optimal spacing between emitting needles/wires to maximize the total exposure of the wet material to ionic wind flow.

*2.2.1.3 Effect of Electric Field Strength on Drying Rate*

It is commonly accepted that electric field enhanced DR of biomaterials, such as agar gel, particulate solids (wheat grain) and sliced fruits (banana, apple) and vegetables (tomato) proportional to electric field strength (Isobe et al., 1999; Cao et al., 2004a; Sumorek and Pietrzyk, 2004; Martynenko and Zheng, 2015; Pirnazari et al., 2016). Either a decrease of the gap at constant voltage (Cao et al., 2004a), or an increase of voltage at the constant gap (Esehaghbeygi and Basiry, 2011; Martynenko and Zheng, 2015; Pirnazari et al., 2016), resulted in an increase of DR.

*2.2.1.4 Effect of Current on Drying Rate*

In some cases, the researchers reported that the DR was independent of the electric field strength, but dependent on the electric current (Sumorek and Pietrzyk, 2004; Martynenko et al., 2017a). This conclusion could be attributed to the strong correlation between intensity of ionic wind and charge transport (current). The current is the flow of electrically charged particles in the air, which are moving with ionic wind from the discharge electrode to the collecting electrode at EHD system. Depending on polarity of the DC, these particles can be positively or negatively charged.

Experiments carried out by Martynenko et al. (2017a) for different geometries of the multiple-needle electrodes showed a linear relationship between DR and square root of total current. It follows that for multiple-needle configuration the total current depends on the active area of discharge electrode, surface area of evaporation, spacing between emitters, electric field strength and the characteristics of the material under drying (Martynenko et al., 2017a). Corona current increased with an increase in electric field strength for both AC (Ding et al., 2015) and DC (Alemrajabi et al., 2012; Singh, 2014) due

to the more intense ionization. The effect of AC and DC current of different polarities on water evaporation is presented in Figure 2.4 (Zheng et al., 2011).

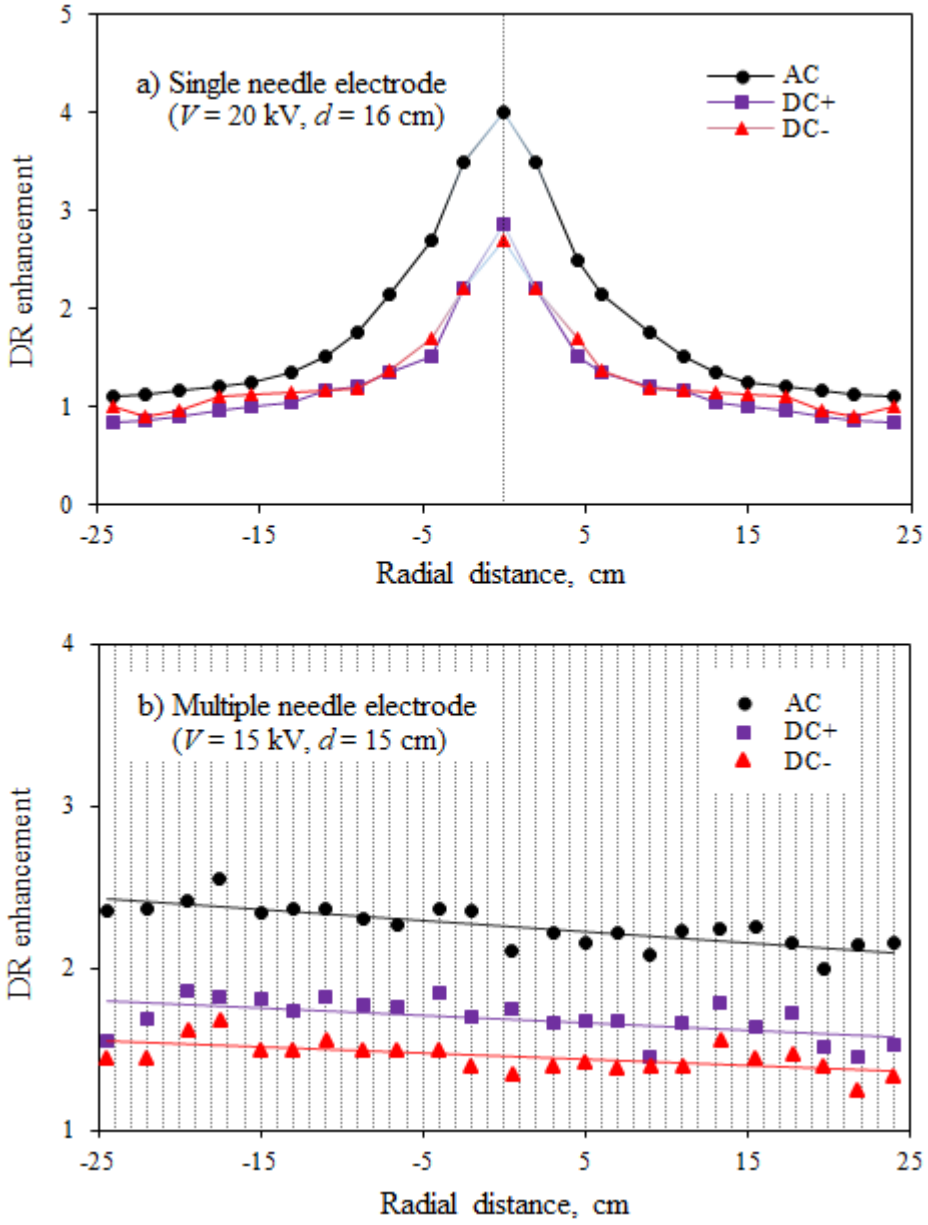


Figure 2.4 Effects of electric field polarity and electrode geometry on the drying rate enhancement for a single needle (a) and multiple needles array (b) with 1.0 cm spacing. Radial distance on the plane electrode is counted from the point just below emitter. Vertical dotted lines correspond to locations of discharge needles (modified from Zheng et al., 2011, with permission (Appendix C))

Increase of the total current with a decrease of the gap between discharge and collecting electrodes has been experimentally found in EHD drying of wet paper for electrode gaps in the range from 2 to 4 cm (Martynenko et al., 2017b). However, no significant effect of the gap from 1.5 to 2.5 cm on the current in EHD drying of wheat grain has been reported (Singh, 2014). Unfortunately, not all published papers report the values of total current, which makes it difficult to generalize relationship between charge and mass transfer for EHD drying.

*2.2.1.4.1 Effect of Current Polarity on Drying Rate*

Most of the time, researchers have been exploring positive DC (+) rather than negative DC (-) polarity for EHD drying. The EHD drying of sugar solutions, glycerin-water mixtures and agar gel (Al Bdour, 2000), Chinese wolfberries (Yang and Ding, 2016), and carrot slices (Alemrajabi et al., 2012) showed a non-significant effect of DC polarity on the DR, whereas the EHD evaporation of water (Hashinaga et al., 1995; Zheng et al., 2011), EHD drying of some fruits and vegetables (Pogorzelski et al., 2013) showed a significant effect of DC polarity. Interestingly, during EHD evaporation of water, the authors observed different results, where DC (+) provided higher enhancement of evaporation rate in experiments by Hashinaga et al. (1995), and lower evaporation rate in experiments by Zheng et al. (2011), compared to DC (-).

*2.2.1.4.2 Effect of Current Type on Drying Rate*

The difference between direct and alternating current is that DC creates flow in one direction, whereas commercial AC has a sinusoidal waveform, half the time in one direction and half the time in the other, changing its 120 times per second with 60-Hz and 100 times per second with 50-Hz frequency. Direct current was used in the majority of

EHD drying systems, while the effect of AC on DR was investigated only by a few researchers. There are only a few published papers (Hashinaga et al., 1995; Zheng et al., 2011; Yang and Ding, 2016), in which researchers compared DC with AC in EHD drying. All of them confirmed that the DR was significantly higher when using AC. This could be due a remarkable difference in currents at the same electric field strength. As an example, Yang and Ding (2016) reported 369 $\mu$A for AC as compared to 10 $\mu$A for DC at the same electric field strength 2.8 kV/cm. Based on this observation, it is important to have common basis for fair comparison of AC vs. DC current.

### *2.2.2 Effect of Electrode Geometry and Configuration on EHD drying*

#### *2.2.2.1 Effect of Discharge Electrode Geometry*

A larger curvature of needle electrode led to higher water evaporation rate, because the conical ends of needle was the most effective for water evaporation and the one with hemispherical top had the lowest drying rate (Zheng et al., 2011). The thin sharp sewing needle showed higher drying rate of apple slices than the thick cooper needle (Hashinaga et al., 1999). In the case of wire electrodes, the results of the research done by Kiousis et al. (2014) indicated that current, voltage, and electric field strength increased with decreasing of wire radius from 250 to 50 μm, which could lead to an increase in drying rate.

Also, a single-needle/wire discharge electrode has no potential for industrial application (Kudra and Martynenko, 2015). Upscaling of EHD dryer is possible only by using multiple needle/wire electrodes. During EHD drying of spinach leaves the authors found that the moisture removal increased with increasing of needles number up to seven but did not change with further increase of number to 11 (Bajgai and Hashinaga, 2001a),

which means there is an optimum in the number of needles and space between them (Martynenko et al., 2017a). It was also found that a needle electrode resulted in water evaporation, higher by almost two times, compared to the wire electrode (Zheng et al., 2011).

*2.2.2.2 Effect of Collecting Electrode Geometry (Solid/Mesh)*

Usually, the collecting electrode is located under the food sample, and it is made of a flat metal plate, while mesh collectors are used very rarely. Zheng et al. (2011) found that the drying rate with the plate collecting electrode and two mesh electrodes with different distance between wires (0.2 cm vs. 0.5 cm) was identical. However, the results of EHD drying of kiwi fruits indicated better efficiency of the mesh electrode compared to the flat plate electrode (Dalvand et al., 2012b). Moreover, this efficiency was increasing with an increase of electric field strength. The simulation of Defraeye and Martynenko (2019) confirmed that the mesh collector could be more effective compared to the flat plate one.

Kiousis et al. (2014) showed that the electric filed could be also dependent on the size of the collecting electrode. They found that the electric field strength increased with increasing in radius of the cylindrical collecting electrode in the range from 0.5 cm to 1.5 cm. It is important to note that the grid mesh placed in the gap between collecting and discharge electrodes allowed control of the corona current (Sumorek and Pietrzyk, 2004), which could be useful when designing a controllable EHD dryer.

*2.2.2.3 Effect of Electrode Material*

Different materials were used for discharge electrodes at EHD drying. Stainless steel needles were used in most of the experiments (Dalvand et al., 2012a, 2012b, 2013; Ding et al., 2015; Martynenko and Zheng, 2015; Martynenko and Kudra, 2016b). In the

case of a single needle, a copper needle electrode was used (Hashinaga et al., 1999) as well as stainless steel sewing needles (Chen and Barthakur, 1994); however, the effectiveness of these needles could not be compared because of the difference in methodology.

The collecting electrodes have been made from a variety of materials: aluminum (Singh, 2014; Dinani et al., 2014; Martynenko and Zhang, 2015; Martynenko and Kudra, 2016b), stainless steel (Xue et al., 1996; Bai et al., 2011; Alemrajabi et al., 2012; Ding et al., 2015; Yang and Ding, 2016), copper (Dalvand et al., 2012b, 2013), galvanized iron (Dalvand et al., 2012a), titanium (Isobe et al., 1999), and molybdenum (Panchenko et al., 1980). Of those materials, aluminum and stainless steel meshes/plates were used the most often for EHD drying of food materials. It was found that the aluminum plate collecting electrode was the most effective for drying, while copper electrode lead to lower drying rate of kiwi fruits, and galvanized iron plate resulted in the lowest drying rate of kiwi fruits (Dalvand et al., 2012b). Panchenko et al. (1980) indicated the effectiveness of molybdenum for EHD dryer electrodes as it possesses a low coefficient of thermal expansion and a high level of thermal conductivity. Titanium could be very effective for EHD dryer too, as it has high strength, stiffness, toughness, low density, and good corrosion resistance.

### *2.2.3 Effect of Environmental Parameters on EHD Drying*

#### *2.2.3.1 Effect of Air Temperature*

Most experiments using electrically-assisted drying usually demonstrated advantages of EHD drying at low-temperature drying, while high temperature significantly reduced positive effect of EHD on the drying process. In the range of ambient temperatures from 20 to 25°C, EHD enhanced drying rate from 2 to 6 times (Alemrajabi et al., 2012). EHD drying of radish (Bajgai and Hashinaga, 2001a), carrots (Alemrajabi et al., 2012),

mushrooms (Bashkir et al., 2018), and kiwi fruits (Dalvand et al., 2012a) at ambient temperatures was faster than thermal drying at 55-60°C. Dalvand et al. (2012a) found that the EHD drying rate of kiwi fruits increased with increasing of temperature from 15 °C to 29°C. However, with further increase of temperature, the positive EHD effect decreased. It was reported that the EHD enhancement effect on DR reduced from 1.9 to 1.6 and 1.5 for temperatures 20, 35, and 50ºC, respectively (Cao et al., 2004a).

*2.2.3.2 Effect of Relative Humidity (RH)*

Effect of relative humidity on DR could be related to the decrease of ion mobility in humid air (Zhang et al., 2017). Almost linear decrease of current with the increase of RH was reported by Maskell (1970) and Zhang et al. (2017). Gallo et al. (1969) explained that current decreased with increasing of RH due to the formation of ion hydrates $H^+(H_2O)_n$. The onset voltage also decreased at high RH. The experiments on EHD drying of white champignons (Martynenko et al., 2019) confirmed that the drying time increased with an increase of relative humidity. Moreover, equilibrium moisture content of mushroom slices increased with an increase of RH (Martynenko et al., 2019).

*2.2.3.3 Effect of Pressure*

Another factor which can affect the EHD drying process is air density (pressure) (Maskell, 1970; Grosu et al., 2014; Zhang et al., 2017). Maskell (1970) reported that the decrease of barometric pressure from 102.0 to 33 kPa accelerated charge transfer. Grosu et al. (2014) noted that the onset voltage increased with increasing of pressure. To describe dependence of ions mobility from humidity and pressure, authors applied the modified Langevin's model (Equation 2.11):

$$b = b_0 \cdot \frac{T}{273.15} \cdot \frac{101.325}{P} \tag{2.11}$$

where $b_0$ is the ion mobility ($m^2/(V \cdot s)$) at standard conditions (0 °C, 101.325 kPa atmospheric pressure); $T$ is the absolute temperature (K); $P$ stands for the pressure (kPa). This most widely used model also predicts that ion mobility should increase with the temperature.

*2.2.3.4 Effect of External Air Flow Velocity*

The effect of EHD drying compared to air flow in the range from 0 to 1.0 m/s was reported to be higher by 1.1-2.0 times (Sumorek and Pietrzyk, 2004). It is important to note that the effect of EHD on DR gradually decreased with an increasing of air cross-flow velocity from 1 to 5 m/s (Martynenko and Zheng, 2015). The EHD enhancement of DR at 6 kV/cm was 3.9 at 1.0 m/s, decreasing to 1.73 at 3.0 m/s and 1.46 at 5 m/s of air velocity (Martynenko and Zheng, 2015). The same relationship between EHD drying and forced convective drying was found at the temperature of 60°C (Dinani and Havet, 2015), where the effect of EHD drying combined with 0.4 m/s air flow was higher in 1.40 - 1.78 times as compared to sole 0.4 m/s air drying, while at 2.2 m/s there were no significant enhancement of EHD in combination with air flow observed compared to sole forced air drying at the same velocity.

### *2.2.4 Effect of Material Characteristics on EHD Drying*

The decrease of moisture content with time was found to be linear (Isobe, 1999; Al Bdour, 2000; Martynenko et al., 2017b) or exponential (Dinani and Havet, 2015; Bashkir et al., 2018). Such a difference could be explained by the mode of EHD drying, which depends on the material and drying period (Martynenko et al., 2017b). A linear kinetics

means that the moisture is readily available and drying process is limited by convection (constant drying rate period). The example could be a paper towel (Martynenko et al., 2017b), agar gel (Isobe et al., 1999), solutions of sugar, glycerin, and many other food powders with high amount of water (Al Bdour, 2000). The constant drying rate implies constant water content on the surface of the material with constant coefficient of convective mass transfer and negligible effect of diffusion. But when there is no more water on the surface, it is more difficult to transport water from the inside of the sample, and the drying process becomes diffusion-limited (Martynenko and Kudra, 2016b; Martynenko et al., 2019). This period of falling drying rate is governed by Fick's law and characterized by exponential kinetics of reducing the moisture content. This exponential drying behavior was reported for capillary-porous materials, such as mushrooms, bananas, and others (Dinani and Havet, 2015; Pirnazari et al., 2016; Martynenko et al., 2019).

### 2.3 Relevance for the Industry

The target of this research is to provide a way of optimization procedure for EHD dryer configuration for further commercialization of the drying technology, considering all possible factors which can affect the EHD drying process. Once the objectives of the proposed research have been achieved, a scalable EHD dryer can be adapted for the food industry, which will allow to dry heat-sensitive plant-based materials with desirable high quality, uniform texture, and rich nutritional content for different groups of consumers. Also, because of low energy consumption, the EHD drying technology can be affordable for small farms, communities and developing countries. Overall, it is predicted to be in a high demand on the market because of its simplicity, which would allow to design small-scale as well as large-scale industrial dryers.

# Chapter 3 Optimization of Discharge Electrode Configuration

## 3.1 Introduction

Most of previously published research was conducted on a lab scale, using a single needle/wire electrode. However, single needle/wire discharge electrode has no potential for industrial application (Kudra and Martynenko, 2015). Dalvand et al. (2013) and Pogorzelski et al. (2013) reported that the drying rate decreased with an increase of needle number in a discharge electrode, which indicated that there is possible interaction between ionic wind jets created by needles, which should be further investigated. The effect of a discharge electrode with multiple needles/wires on the drying rate is still underexplored, but essential for upscaling.

It was already found that there are a few most important geometrical characteristics of a discharge electrode, which affect the drying process in EHD technology, and they are curvature of the emitting needles (Zheng et al., 2011) and spacing between these emitters, where spacing should be optimized with a gap between discharge and collecting electrode (see Figure 2.3, Chapter 2) (Kudra and Martynenko, 2019). However, it is still unclear which geometry of needles would be better to use in a multiple-needle discharge electrode. Also, further upscaling to industrial prototypes should consider energy consumption and stability of EHD system. So, the *objectives* of this chapter are to find:

1) which shape of needles in the discharge electrode has minimum inception voltage and maximum discharge stability

2) is there any effect of needle shape on ionic wind flow

3) which shape of needles in multiple needle discharge electrode provides the highest drying rate and lowest energy consumption in EHD system

The initial *hypotheses* for the above objectives were:

1) Sharper needles are more suitable for EHD drying

2) Needle shape affects the ionic wind flow

3) Multiple needle electrode with sharp needles results in the highest drying rate.

## 3.2 Optimization of Needle Configuration

One of the most important geometrical characteristics of a discharge electrode is the curvature of the emitting needles. Hashinaga et al. (1999) and Zheng et al. (2011) found that the sharper needles were more effective compared to the thicker (blunt) ones. However, there were no explanation of why the sharper needles resulted in a significantly higher drying rate. Because of that, in this set of experiments, the goal was not only to compare the effect of differently shaped needles on the drying rate, but also to investigate deeper how the ionic wind, created by needles, is changing with needle shape.

It is already confirmed that ionic wind flow consists of two streams: unipolar ions flow and air flow (see Figure 2.1 in Chapter 2). While the charged ions move towards the collecting electrode, the air flow as a part of ionic wind flow, has a rotation trajectory when using both needle or wire discharge electrodes (Taylor, 1966; Yabe et al., 1977). To investigate the ionic wind flow depending on the needle shape, a special methodology of ionic wind visualization has been developed. Moreover, multiple needle discharge electrodes with different needle shapes were built and their effect on the drying rate and energy consumption was investigated.

### *3.2.1 Methodology*

In the first part of the research four types of emitters were examined: (#1) stainless steel nails with diameter $d_1 = 1.8$ mm and tip radii $r_{tip1} = 0.25$ mm, thick conical sewing

needles (#2) with $d_2 = 1.2$ mm and $r_{tip2} = 0.11$ mm, and thin pins (#3) with $d_3 = 0.7$ mm and $r_{tip3} = 0.09$ mm, and sharp machine sewing needles with ellipsoidal profile ($R_a = 0.44$ mm, $R_b = 0.32$ mm) and $r_{tip4} = 0.08$ mm (#4). Shapes of these needle electrodes are shown in Figure 3.1. The multiple needle electrodes were modeled with two needles of the same shape spaced by 3 cm.

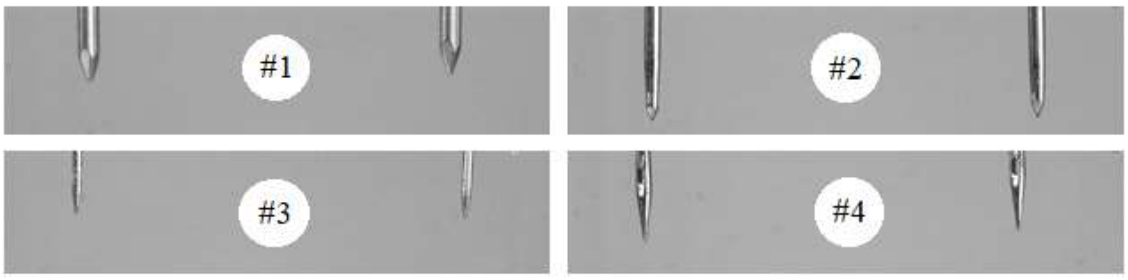


Figure 3.1 Shapes of needles: stainless steel nails (#1), thick conical sewing needles (#2), thin pins (#3), and sharp machine sewing needles (#4)

Discharge stability of different shape needles was determined by the magnitude of fluctuations of discharge current at constant voltage. To find configuration of discharge electrode with minimum inception voltage and maximum discharge stability, volt-ampere characteristics were recorded at relative humidity of 40% and temperature 20°C. The inception voltage was determined from volt-ampere characteristics, and the ionic wind jets have been visualized with a high resolution (1388×1038) digital camera in the dark.

The experiments were carried out using EHD setup shown in Figure 3.2. The needle discharge electrode (1) was connected to a positive pole, and the mesh collecting electrode (2) with open area of 55% and wire diameter of 0.1651 mm was connected to a negative pole of a direct current (DC) power supply (BAL-32-5, Voltronics, USA). The gap between two electrodes was kept constant at 3 cm. The camera (3) was connected to the computer and the images of ionic wind in the dark were recorded. Additionally, black-and-white

videos were recorded by increasing voltage from the inception to the breakdown (videos are available on request).

Computer software NI Vision Assistant 2018 (1999-2018 National Instruments, Version 2018 SP1 – (64-bit)) was used for taking images by monochromatic camera AVT Stingray F145B (ALLIED Vision Technologies, Canada) with a lens Fujinon HF50SA-1 (1:1.8/50 mm, Fujinon Corporation). The attributes used in the software were standard but gain and shutter were set at the maximum values of 680 and 4095, respectively.

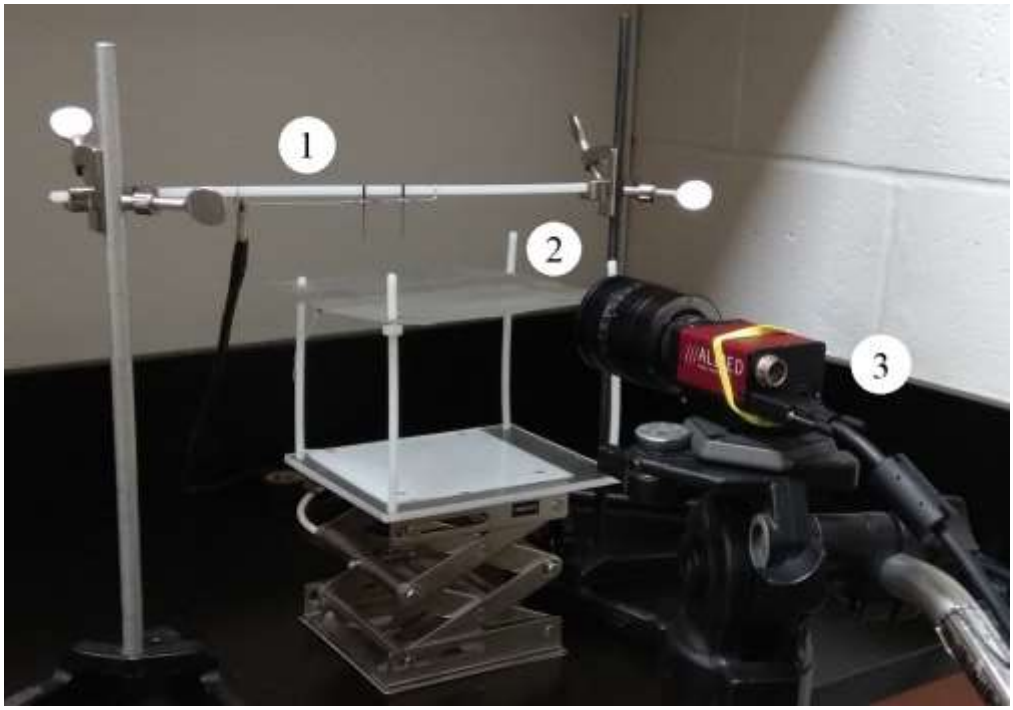


Figure 3.2 EHD setup for visualization of ionic wind: 1 – needle discharge electrode, 2 – mesh collecting electrode, 3 – camera

### *3.2.2 Results and Discussion*

#### *3.2.2.1 Volt-Ampere Characteristics*

Volt-ampere characteristics were measured with three replications. It could be seen in Figure 3.3 that the lowest current was observed when using thick construction nails (#1) and it was significantly lower compared to needles (#2-4). The current in the case of thick

sewing needles (#2) was not significantly different compared to thin pins (#3) and sharp machine sewing needles (#4) at voltages less than 21 kV (7 kV/cm). However, when voltage was over 21 kV, current of sewing needles (#2) and (#4) increased rapidly. This increase resulted in the random breakdowns, when current was extremely high creating lightening and the power supply was automatically disconnected.

Thick sewing needles (#2) had only a few breakdowns during experimental tests compared to sharp machine needles with continued breakdowns during tests. We concluded that construction nails (#1) and thin pins (#3) were the most suitable for using in EHD drying systems due to discharge stability. The inception and the breakdown voltages for all types of needles are presented in Table 3.1, where sharper needles (#2-4) lead to the lower inception and breakdown voltages compared to construction nails (#1). These results are in agreement with previously published by Precht (1883).

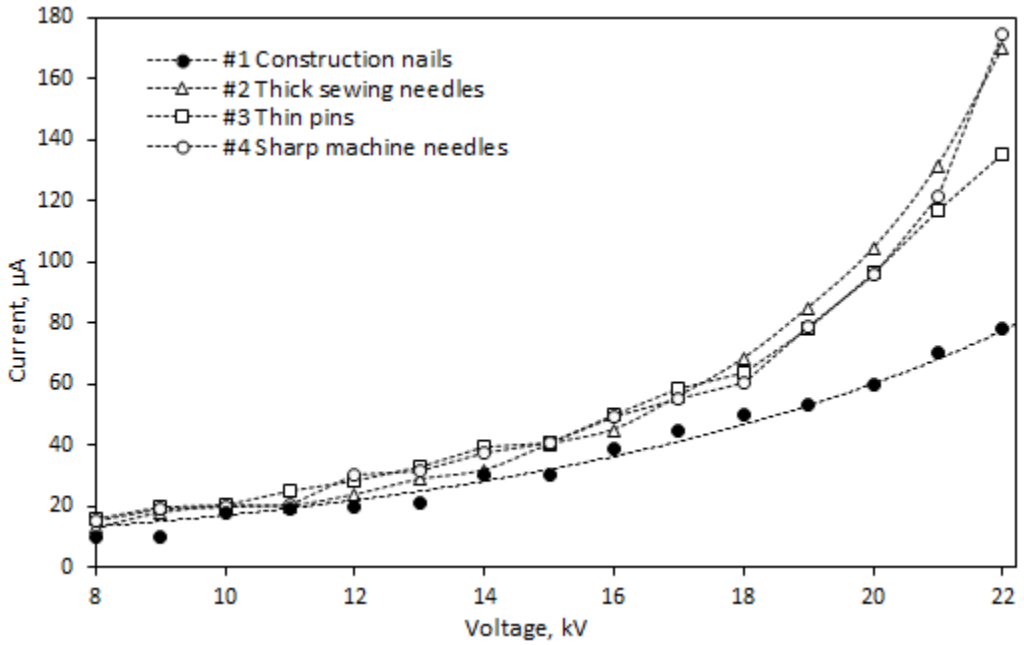


Figure 3.3 Volt-Ampere characteristics of different discharge needle shapes at 3 cm gap

Table 3.1 Inception and breakdown voltages for four needle shapes

| **Needle shape** | **Construction nails (#1) ($r_{tip1}$ = 0.25 mm)** | **Thick sewing needles (#2) ($r_{tip2}$ = 0.11 mm)** | **Thin pins (#3) ($r_{tip3}$ = 0.09 mm)** | **Machine needles (#4) ($R_a$ = 0.44 and $R_b$ = 0.32 mm)** |
|---|---|---|---|---|
| **Inception voltage, kV** | 10 | 8 | 7 | 8 |
| **Breakdown voltage, kV** | 25 | 23 | 22 | 22 |

*3.2.2.2 Ionic Wind Visualization*

From our experiments on EHD drying, we realized that ionic wind could be seen in the dark with human eye. The natural color of it is light purple blue. The camera settings let us to capture images of ionic wind in black-and-white. Practically, we cannot see the movement of air in the dark, so that we assume that the camera captured the traces of ions flow jets. The pictures of ionic jets in white are shown on the dark background in Figure 3.4 for all four needle shapes at 3 cm gap and 21 kV voltage (7 kV/cm electric field strength). Voltage of 21 kV at 3 cm gap was close to the breakdown voltage for needle types #2, 3, and 4, so that the ionic streamers were more intensive compared to needle type #1 (construction nails), where the breakdown voltage was over 25 kV at 3 cm gap. Real time imaging enabled to identify the coverage of material surface with ionic wind. The angle of ionic jets and diameter of the plum on the surface of the metal mesh have been measured from the images in Figure 3.4 and schematically presented in Figure 3.5.

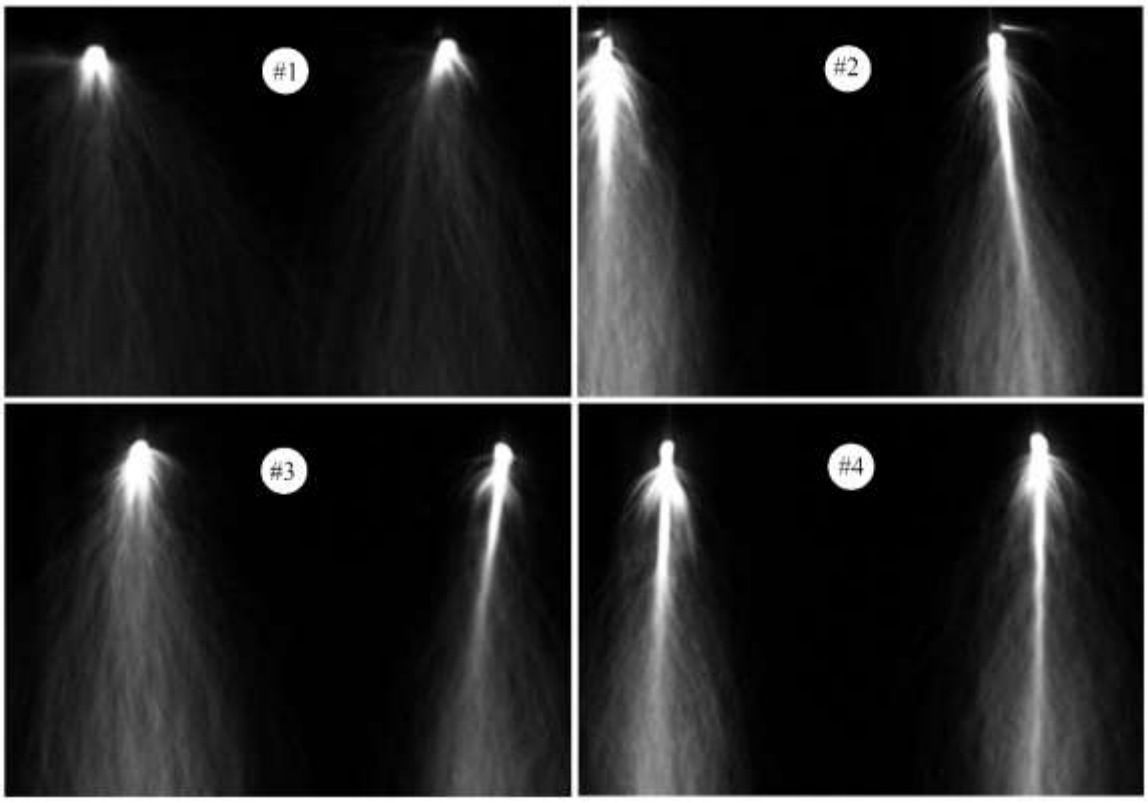


Figure 3.4 Visualized ionic jets for all four needle types at 3 cm gap and 21 kV: stainless steel nails (#1), thick conical sewing needles (#2), thin pins (#3), and sharp machine sewing needles (#4)

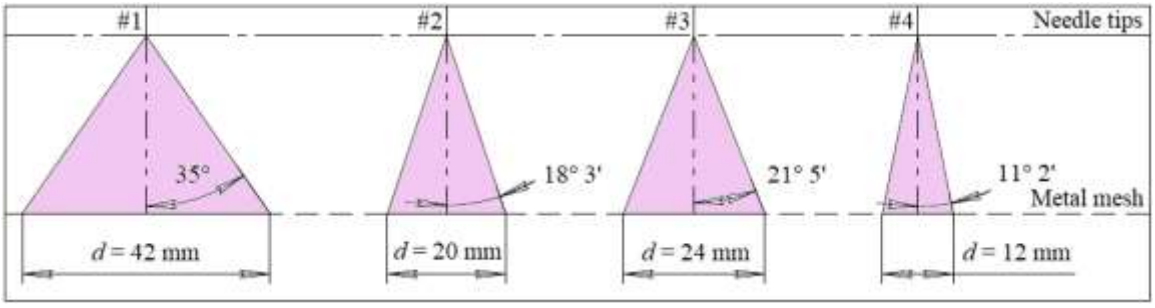


Figure 3.5 Diameter of ionic jets on the surface of the metal mesh collecting electrode at 3 cm gap and 21 kV: stainless steel nails (#1), thick conical sewing needles (#2), thin pins (#3), and sharp machine sewing needles (#4)

Figure 3.5 shows that the shape of ionic jets is getting smaller as the needle tip is getting thinner (sharper). The ionic jet shape is more stretched when using thick needle (construction nails, #1) and narrow when using sharp needle (sharp machine sewing

needles, #4). Measured angles of ionic jets spreading from the needle tip, and so the diameter of ionic plums on the surface of collecting electrode makes it possible to calculate the wet sample area exposed to the ionic wind jets during EHD drying with different needle shapes.

It is now found that the area of wet food sample covered by ionic jets is the biggest when using construction nails (#1, Figure 3.5) and it is significantly higher compared to area of the other three needle types: by 2.1 times compared to thick sewing needles (#2), 1.75 times compared to thin pins (#3), and 3.5 times compared to sharp machine sewing needles (#4). Sharp machine sewing needles (#4, Figure 3.5) resulted in the narrowest ionic jets and so the area of food sample, subjected to ionic flow. Thick sewing needles and thin pins (#2 and 3, Figure 3.5) resulted in almost the same angle of ionic flow spreading.

Another interesting finding was that the ionic flow jets are becoming more intensive with an increase of voltage at constant gap, as they are becoming brighter with higher density of ions (in white). As an example, the ionic streamers are shown for thick construction nails (#1) and thin pins (#3) at two voltages: close to the inception voltage and close to the breakdown voltage. When the voltage is 12 kV (Figure 3.6 a) or 9 kV (Figure 3.6 c) for thick construction nails (#1) and thin pins (#3), respectively, the ionic jets are darker and ions jets density is smaller compared to those at 24 (Figure 3.6 b) and 21 kV (Figure 3.6 d). The same situation was observed when using thick sewing needles (#2) and sharp machine sewing needles (#4).

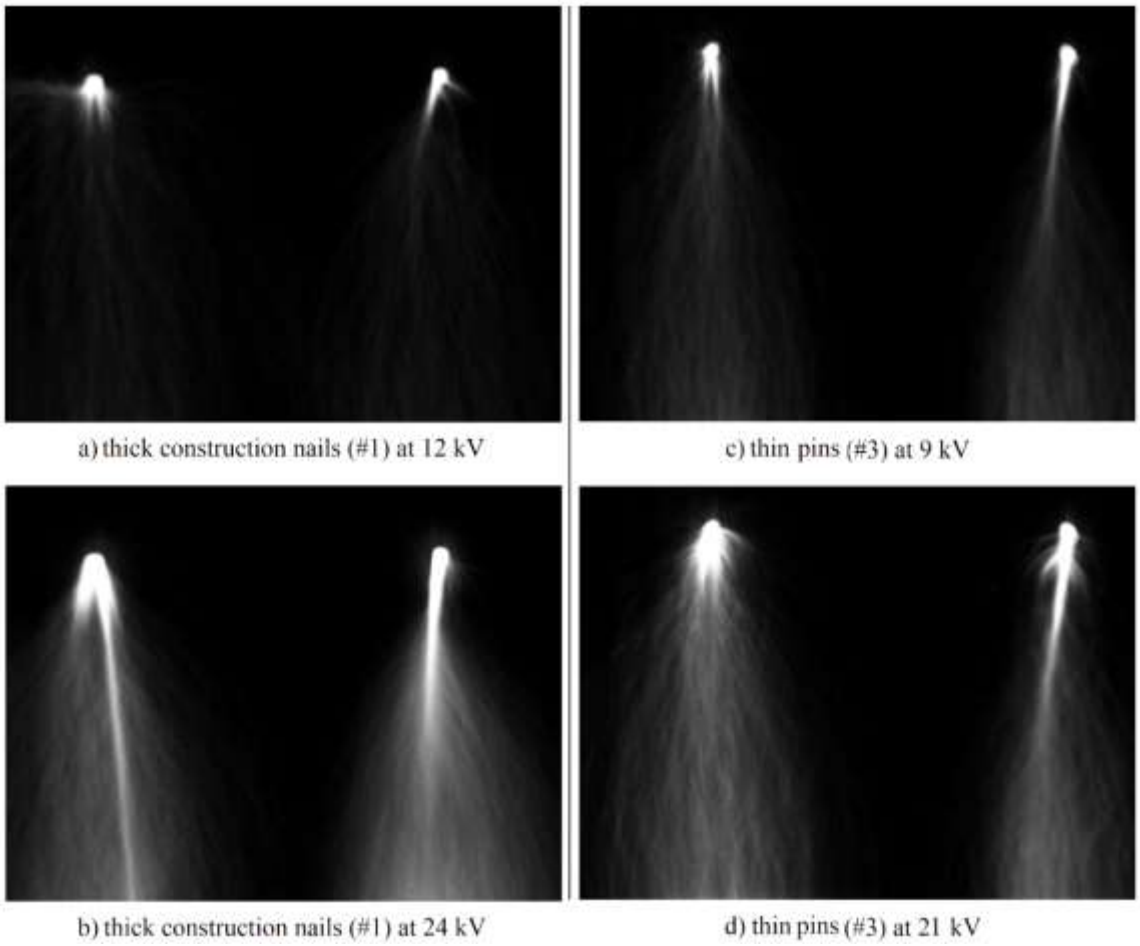


Figure 3.6 Intensity of ionic streamers at low and high voltages when using (#1) thick construction nails (a and b) and (#3) thin pins (c and d) at constant gap of 3 cm

It is important to note that while observing ionic jets in the dark, it seems that the ions jets themselves are moving on the circular direction, which reminds the ionic vortexes schematically illustrated by Yabe et al. (1977). It was already established that the trajectory of air flow as a part of ionic wind reminds small tornados vortexes (Taylor, 1966; Yabe et al., 1977), but it is commonly accepted that the ions in EHD systems are moving straight forward to collecting electrode from the discharge needles (Chen and Barthakur, 1991). However, these two statements are contradictory, as considering the following questions: how the charged ions, which collide with neutral air molecules, can create the air flow of

vortex trajectory, while the ions themselves are moving directly to the collecting electrode? Based on camera visualization, it seems that the ions jets are moving on vortex trajectory too, and this could be due to non-visible magnetic field directions. This question about movement of ions and ions jets, and overall, about ionic wind flow phenomena in EHD drying system, still require further investigation.

*3.2.2.3 Needles Arrangement in a Multiple Discharge Electrode*

It was already established that there is an optimum spacing-to-gap ratio in EHD drying (Martynenko et al., 2017a, Kudra and Martynenko, 2019). Figure 2.3 in Chapter 2 demonstrates this idea clearly. Martynenko et al. (2017a) found an optimum spacing-to gap ratio for construction nails based on the drying rate of wet paper towel. However, by knowing that different needle shapes result in a different angle of ionic wind jets spreading from the end of the needle (Figure 3.5), it is now possible to optimize spacing-to-gap ratio for multiple needles discharge electrodes using imaging of the angle of ionic wind jets. Overall, building of a multiple needle discharge electrode for the EHD drying technology is a task which should include multiple factors: spacing between emitters (needles), angle of ionic wind jets spreading, gap between the needle tip and collecting electrode, and the way of needle arrangement in the whole area of a discharge electrode.

Example. Let's consider optimization of a multiple needle discharge electrode using thin pins (#3) with $d_3 = 0.7$ mm and $r_{tip3} = 0.09$ mm. We already found that the angle of ionic wind jets spreading from the needle tip is $\alpha = 21° 5' \times 2 = 43°$ (Figure 3.5). Let's assume that we are going to use gap of 2 cm, and we have to find the optimum spacing between pins. Considering two factors such as angle (43°) and gap (2 cm), we can find optimum spacing between needles, which will be equal to the diameter of ionic wind jets

created by thin sewing needles (#3) at 2 cm gap. By geometrical representation of ionic wind jets spreading at 43° angle with 2 cm distance from the needle tip to collecting electrode (isosceles triangle with height of 2 cm) we can calculate that the diameter of ionic wind jets will be 16 mm (which is the base of a isosceles triangle) on the surface of collecting electrode (Figure 3.7). Then the optimum spacing between needles will be 16 mm too. Moreover, because we want to cover as much surface area of the material as possible by the ionic wind jets, we should arrange needles in a chess order rather than square arrays. Figure 3.8 represents the sketch of optimized multiple needle discharge electrode configuration with thin pins #3.

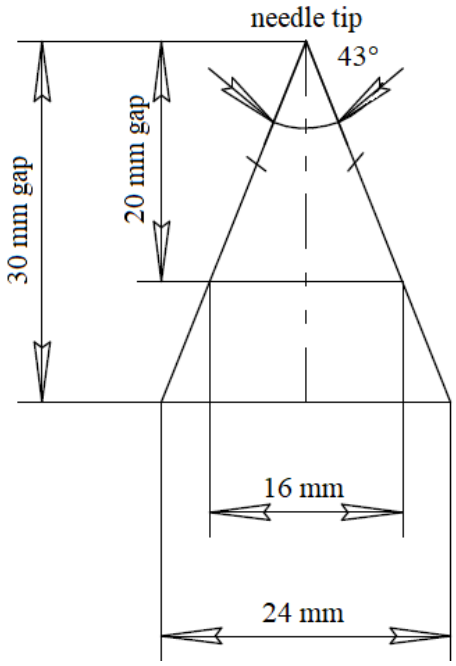


Figure 3.7 Geometrical interpretation of optimum spacing for thin pins (#3) with $r_{tip3} =$ 0.09 mm at 2 cm gap

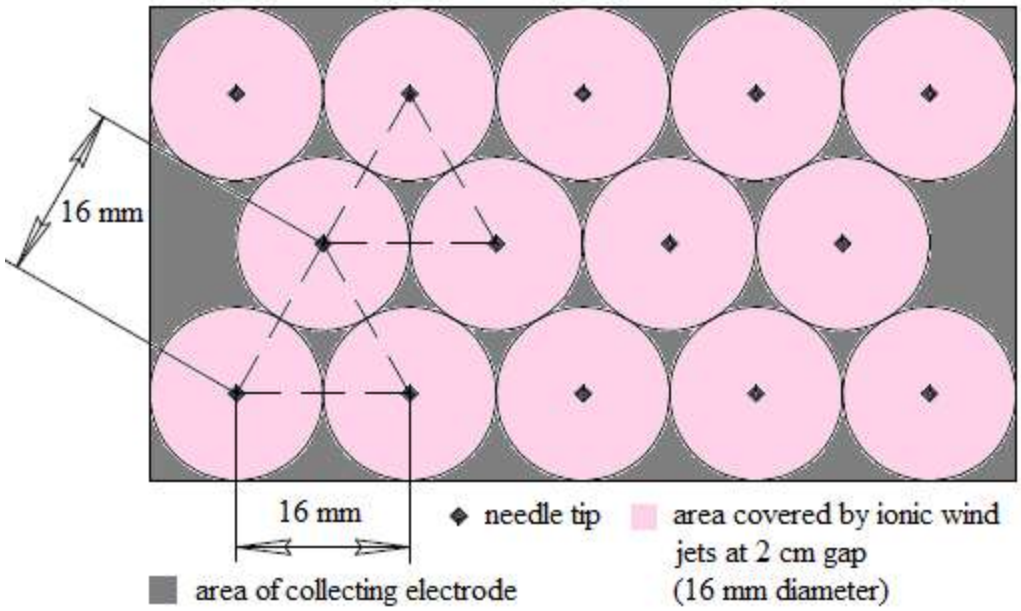


Figure 3.8 Optimized multiple discharge electrode configuration built with thin pins (#3) when gap between electrodes is 2 cm and optimum spacing between needles calculated to be 16 mm

### *3.2.3 Conclusions*

1) New approach to ionic wind visualization enabled to calculate the area of food material exposure to ionic wind created with different needle shapes. Sharper needles (#4) resulted in the narrower ionic flow jets, while thicker needles (#1-3) resulted in the wider spread of ionic wind jets. Because the drying rate is expected to be higher when the larger area of wet food sample is exposed to the ionic wind jets, the thicker needles are recommended for discharge electrodes in EHD drying technology.

2) Larger curvature of sharper needles (#2-4) results in the lower inception and lower breakdown voltages compared to small curvature of thicker needles (construction nails, #1).

3) Discharge stability was achieved when using thicker needles, while in sharp machine sewing needles (#4) discharge was unstable and resulted in random breakdowns

during experimental work. As a result, we concluded that sharp needles are not suitable for using them as the discharge emitters in the EHD drying technology.

4) Ionic wind jets brightness increases with an increase of electric filed strength; however, the angle of ionic jets spreading does not increase, it stays constant at all voltages. Brightness could be explained due higher intensity of ionization at the needle tip, so that there are more charged ions flowing from the discharge to collecting electrode per second (current), and the ionic wind jets looks more intensive and brighter.

5) When building of a multiple needle discharge electrode for the EHD drying technology the following factors should be considered: spacing between emitters (needles), angle of ionic wind jets spreading, gap between the needle tip and collecting electrode, and the way of needles arrangement (chess vs. square array) in the whole area of a discharge electrode.

## 3.3 Multiple Needle Discharge Electrode

This section has been designed to investigate which shape of needles, described in previous section 3.2, being arranged in a multiple needle discharge electrode, will provide the highest drying rate and lowest energy consumption in EHD system.

### *3.3.1 Methodology*

*Input*:

- Current type: DC+
- Discharge electrode (three configurations)
- Collecting electrodes (one configuration)
- Gap, cm (five levels)
- Voltage, kV (three levels for each gap)

- Electric field strength, kV/cm (three levels for each gap)
- Wet paper towel (50±1.0 g with constant initial moisture content of 72% wet basis)
- Relative humidity (35±5%)
- Temperature (~21°C)
- Pressure, kPa (100 kPa)

*Output*:

- Drying time, s
- Drying rate, g/h
- Current, μA
- Power, W ($P = V \cdot I$)
- Energy consumption, kJ/kg

Three multiple needle discharge electrodes were built for this set of experiments:

- (D1) construction stainless-steel nails (#1) with diameter 1.8 mm and $r_{tip1} = 0.25$ mm;
- (D2) thick sewing needles (#2) with diameter 1.2 mm and $r_{tip2} = 0.11$ mm;
- (D3) thin medium-steel pins (#3) with diameter 0.7 mm and $r_{tip3} = 0.09$ mm.

Each multiple discharge electrode was built with 32 needles of the same type with area of 10.3×15.8=162.74 $cm^2$ and space between needles 2×2 cm. Aluminum plate (3) with area of 12×16.4=196.8 $cm^2$ and thickness of 1.05 mm was used as a collecting electrode. Discharge electrode (2) was connected to the positive pole of a direct current (DC) high voltage power supply (5) model BAL-32-5 (Voltronics, USA) (Figure 3.9).

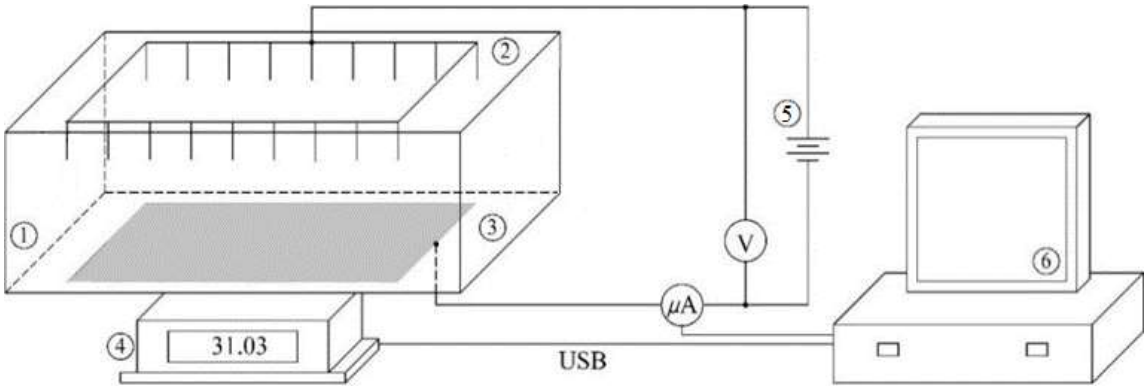


Figure 3.9 EHD lab setup for drying of wet paper towel using different discharge electrodes D1-D3: 1 – opened chamber, 2 – multiple needle discharge electrode, 3 – collecting plate electrode, 4 – digital scale, 5 – high voltage power supply, 6 – desktop computer

*3.3.1.1 Fabrication of Multiple Discharge Electrodes*

Plastic (ABS) holders for needles were modeled and printed for each type of needles with spacing of 2 cm between needles according to Martynenko et al. (2017a). 32 needles in each discharge electrode (D1-D3) were placed into the holes in the holder with the corresponding diameter (including printer error equal to nozzle diameter) and then soldered between each other with a stainless-steel wire of 0.5 mm in diameter. 2D Sketch and a 3D model of the holder for construction nails (D1) are shown in Figure 3.10. Models for D2 and D3 electrodes with thick sewing needles (#2) and thin pins (#3) were the same with the smaller diameter of the holes for the needles. Photos of completed three discharge electrodes are shown in Figure 3.11.

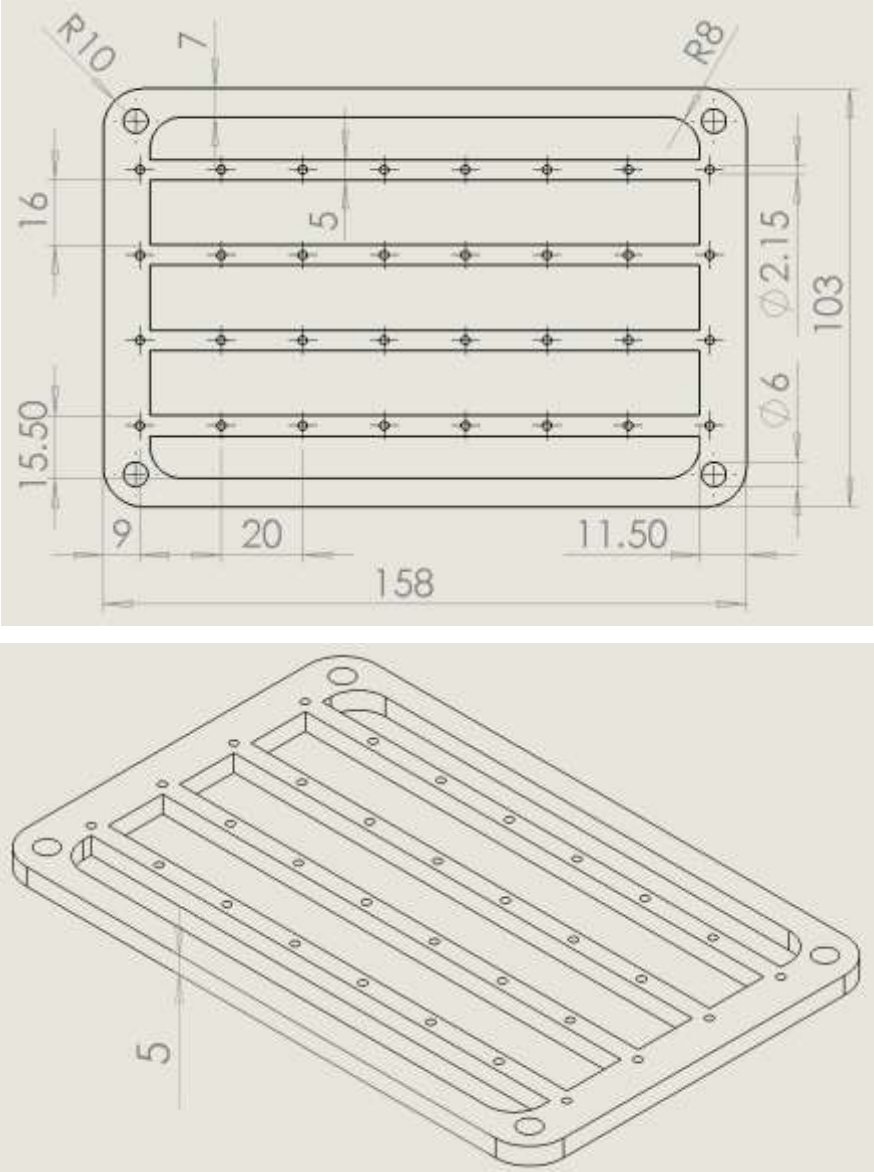


Figure 3.10 Holder for the discharge electrode with construction nails (2D and 3D views) (in mm)

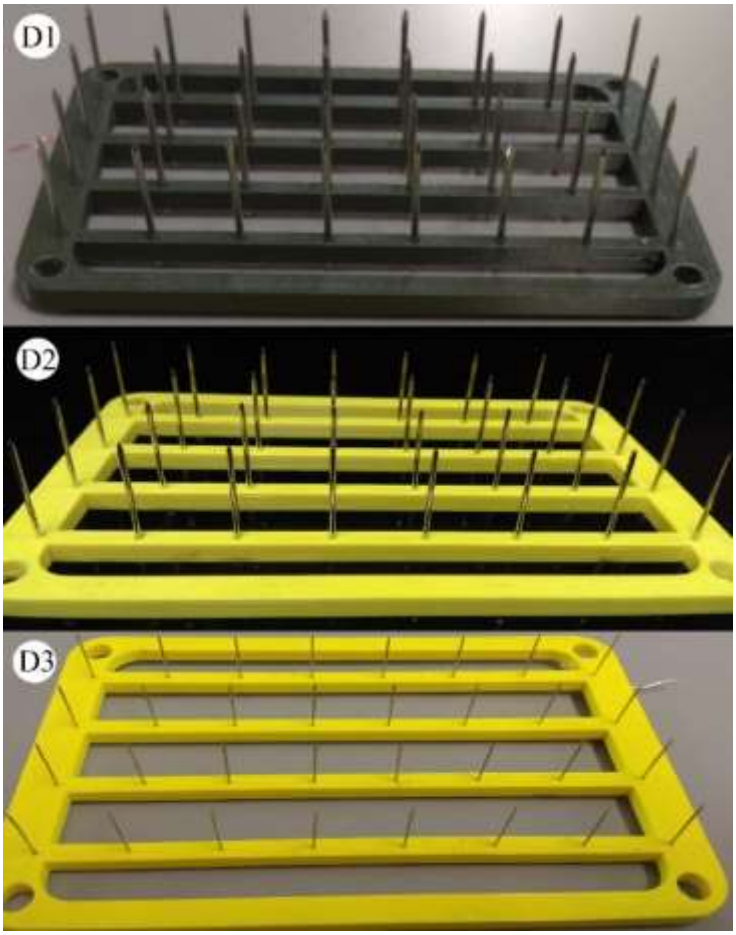


Figure 3.11 Photos of three multiple needle discharge electrodes: D1 with construction nails (#1), D2 with thick sewing needles (#2), and D3 with thin pins (#3)

SOLIDWORKS 2019 SP 5.0 Education Edition software (Javelin Technologies Inc., Canada) was used for 3D modeling of the plastic holders in order to print them on uPrint SE Plus™ 3D Printer. CatalystEX 4.5 software (Stratasys Inc., USA) was used to print 3D models on the 3D printer.

*3.3.1.2 Drying Experiments*

Wet paper towel was placed on the surface of collecting electrode (Figure 3.9) with the gap between needles tips and the surface of wet paper towel at 2, 2.5, 3, 3.5, and 4 cm. Drying rate in g/h was measured at each gap (5 levels) and each type of multiple discharge

electrode (3 levels) at three levels of voltages: close to the inception voltage (low), close to the breakdown voltage (high), and middle (middle) one between two mentioned voltages. So, the experimental design was three-factor factorial 5×3×3, where three replications were provided for each drying condition, and in total it required 135 experiments. Voltages were selected after measuring of volt-ampere characteristics for each multiple needle discharge electrode at each gap. This approach for drying of wet paper towel was chosen for each gap separately because of completely different voltage work ranges of the discharge electrodes. Moisture reduction (g) was measured with a digital scale (4) model HCB 1002 (Adam Equipment, Oxford, CT, USA) with 0.01 g resolution and recorded on the computer (6) every 30 seconds.

*3.3.1.3 Sample Preparation*

The 14 g sample pack of dry paper towels was wetted with tap water to 50.0±1.0 g and placed on the surface of the collecting electrode directly under the center of discharge electrode. The thickness of wet samples was 3±0.1 mm.

*3.3.1.4 Specific Energy Consumption*

For each experiment on drying of wet paper towel, level of current (μA) at a certain combination of gap (cm) and voltage (kV), which determined electric field strength (kV/cm), was recorded from the indicators on the high voltage power transformer. Power (mW) used in EHD lab setup was calculated by multiplying of voltage and current:

$$P = V \cdot I \tag{3.1}$$

Specific energy consumption (kJ/kg) was calculated by dividing of power (W) by drying rate $DR$ (g/h) measured at the first hour of drying, where specific energy means energy used directly for the drying in EHD system:

$$E = \frac{3600 \cdot V \cdot I}{DR} \tag{3.2}$$

*3.3.1.5 Statistical Analysis*

Changes in drying rate and energy consumption were analyze using ANOVA for two-factor factorial design, where the two factors were: gap between electrodes (2, 2.5, 3, 3.5, and 4 cm) and type of a discharge electrode (D1, D2, and D3). Model assumptions, such as normal distribution and constant variance were verified by examining the residuals (Montgomery, 2017). Independence of the error terms was verified through randomization. The analysis was completed using Minitab software (Minitab 18, Minitab Inc., State College, PA, USA). Statistical difference was determined using least significant difference (LSD) comparison test (*t*-test) and accepted at $p$-value $< 0.05$.

### *3.3.2 Results and Discussion*

*3.3.2.1 Volt-Ampere Characteristics*

Volt-ampere characteristics for three different discharge electrodes (D1-D3) were recorded using indicators of a high voltage power supply. There were no wet samples used in this set of experiments. An inception and breakdown voltages are shown in Table 3.2 for all electrodes and gaps. The inception voltage was usually lower at D3 electrode with thin pins and higher at construction nails (D1) and thick sewing needles (D2). The breakdown voltage was the highest at D3 electrode made of thin pins compared to construction nails (D1) and thick sewing needles (D2). While the inception voltage was the same at all gaps for both D1 and D2 electrodes, D1 made of construction nails resulted in the highest breakdown voltage compared to D2 made of thick sewing needles. Obviously, multiple needle discharge electrode D3 made of thin pins had the largest work range and

the best discharge stability, which is very important for EHD drying system. Thick sewing needles (D2) showed the smallest work range and discharge stability, which put this needle shape unsuitable for EHD drying technology.

Table 3.2 Inception and breakdown voltages (kV) for D1 (construction nails), D2 (thick sewing needles), and D3 (thin pins) discharge electrodes at 2, 2.5, 3, 3.5, and 4 cm gap

| **Gap,** | **D1 (construction nails)** | | **D2 (thick sewing needles)** | | **D3 (thin pins)** | |
|---|---|---|---|---|---|---|
| **cm** | **Inception** | **Breakdown** | **Inception** | **Breakdown** | **Inception** | **Breakdown** |
| **2** | 8 | 16 | 8 | 14 | 5 | 17 |
| **2.5** | 9 | 19 | 9 | 16 | 6 | 20 |
| **3** | 10 | 22 | 10 | 19 | 7 | 25 |
| **3.5** | 11 | 26 | 11 | 22 | 8 | 29 |
| **4** | 12 | 28 | 12 | 28 | 8 | 29 |

Volt-ampere characteristics of multiple discharge electrodes made of construction nails (D1), thick sewing needles (D2), and thin pins (D3) are presented in the Figures 3.12, 3.13, and 3.14, respectively. It follows that the current for all discharge electrodes increased with the voltage at all gaps, and this increase is slower when the gap between electrodes is bigger, and faster when the gap between electrodes is smaller.

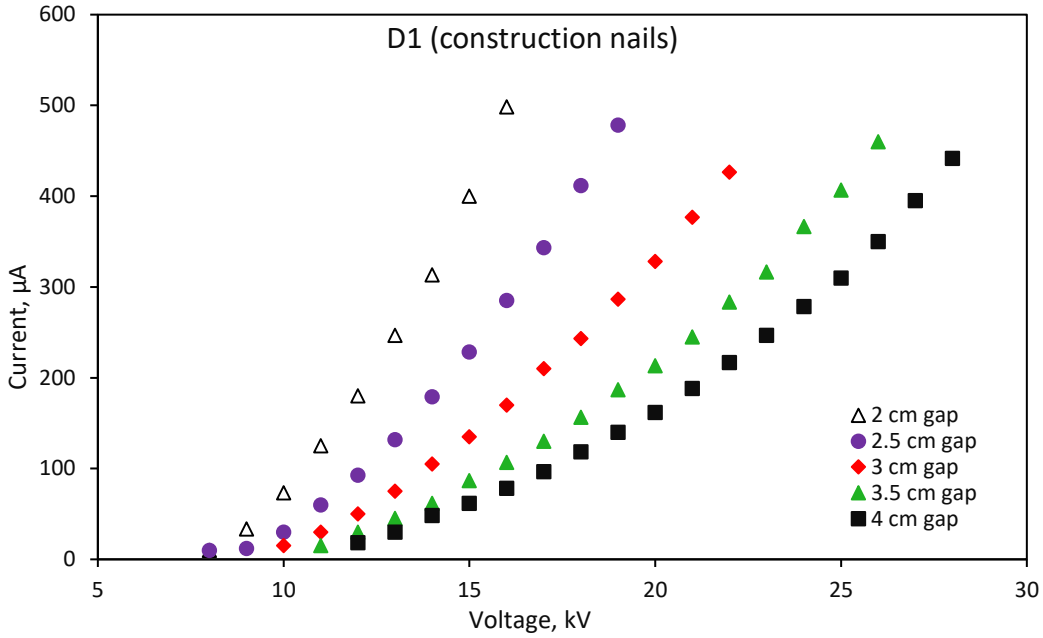


Figure 3.12 Volt-ampere characteristics at different gaps for multiple needle discharge electrode (D1) made of construction nails

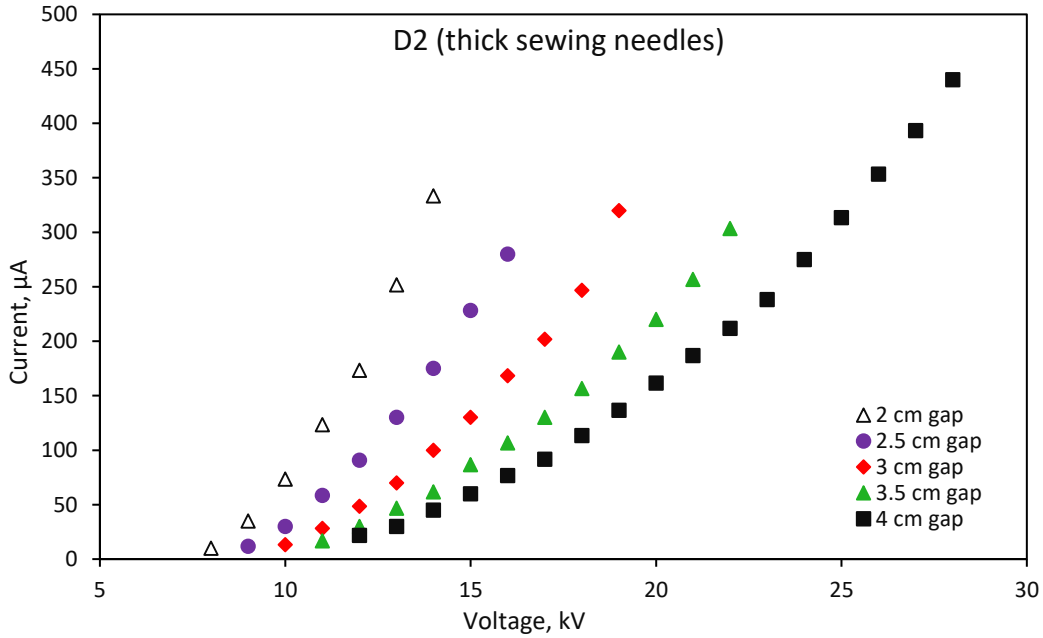


Figure 3.13 Volt-ampere characteristics at different gaps for multiple needle discharge electrode (D2) made of thick sewing needles

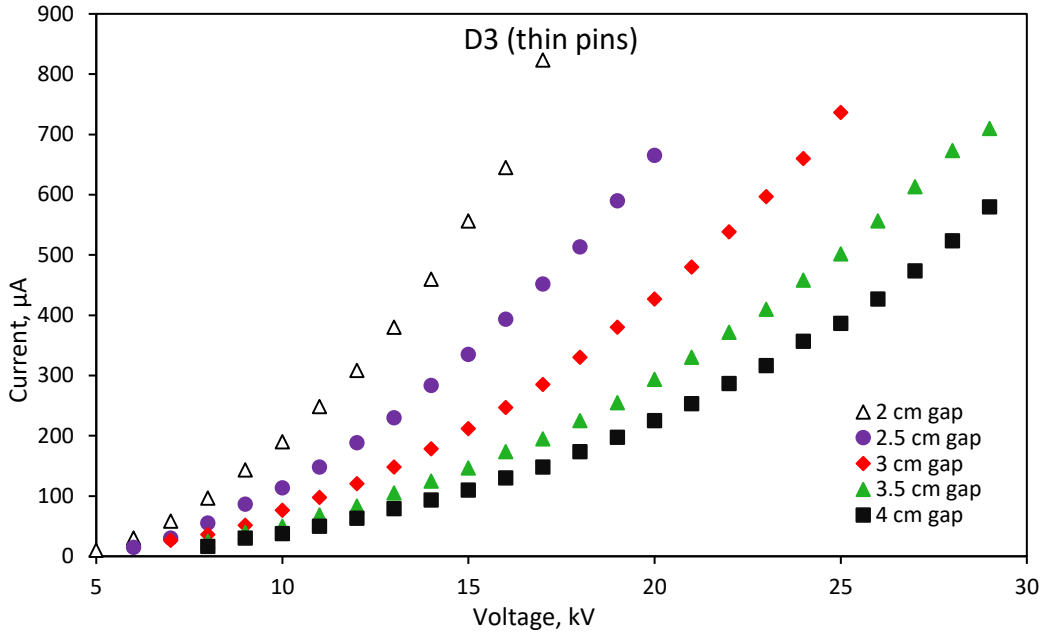


Figure 3.14 Volt-ampere characteristics at different gaps for multiple needle discharge electrode (D3) made of thin pins

The difference in volt-ampere characteristics between all three electrodes is shown in Figures 3.15, which represents volt-ampere characteristics of three electrodes at 2, 3, and 4 cm gap. Statistical analysis showed that current was significantly higher at D3 discharge electrode made with thin pins (#3) compared to electrode D1 (construction nails) and D2 (thick sewing needles) at all voltages and gaps. The current of D1 and D2 electrodes was not significantly different. Based on these results we expected that the drying rate of wet paper towel at the same voltage would be higher when using discharge electrode with thin pins (D3) and lower when using construction nails (D1) and thick sewing needles (D2) electrodes.

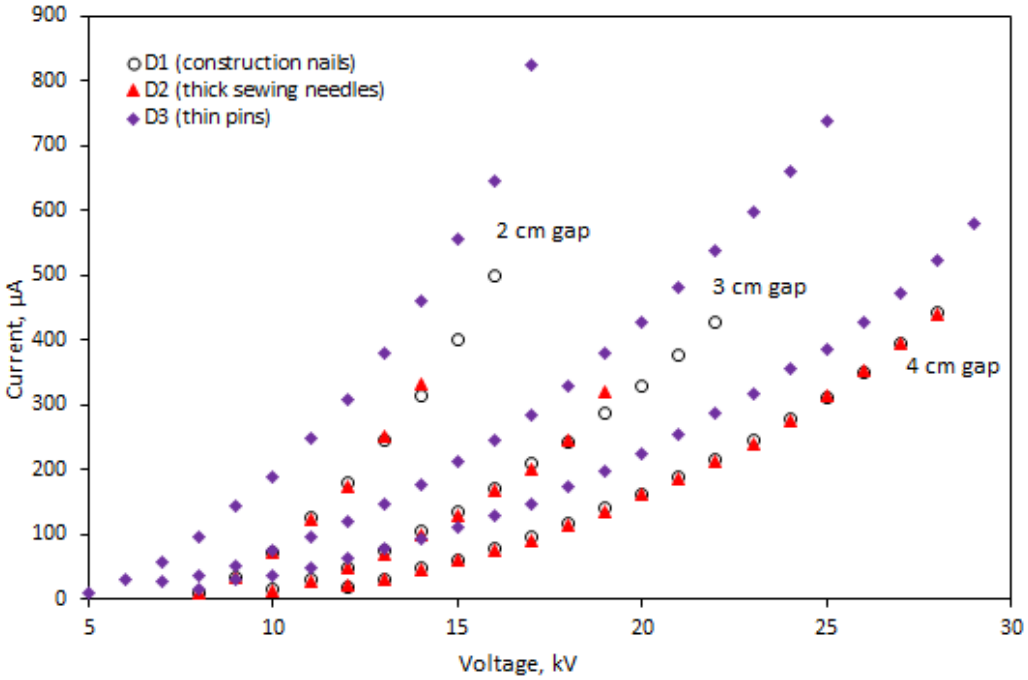


Figure 3.15 Volt-ampere characteristics of construction nails (D1), thick sewing needles (D2), and thin pins (D3) discharge electrodes at 2, 3, and 4 cm gap

Based on volt-ampere characteristics, certain voltages at certain gap of 2, 2.5, 3, 3.5, and 4 cm were selected for each of three discharge electrodes D1, D2, and D3 (Table 3.3).

Table 3.3 Selected voltages for drying of wet paper towel at certain gaps and multiple discharge electrodes

| Gap, cm | D1 (construction nails) Voltage, kV/Current, µA | | | D2 (thick sewing needles) Voltage, kV/Current, µA | | | D3 (thin pins) Voltage, kV/Current, µA | | |
|---|---|---|---|---|---|---|---|---|---|
| | Low | Middle | High | Low | Middle | High | Low | Middle | High |
| **2** | 9 kV<br>33 µA | 12 kV<br>180µA | 15 kV<br>400µA | 9 kV<br>35 µA | 11 kV<br>123µA | 13 kV<br>252µA | 7 kV<br>58 µA | 11 kV<br>248µA | 15 kV<br>557µA |
| **2.5** | 11 kV<br>60 µA | 15 kV<br>228µA | 18 kV<br>412µA | 11 kV<br>58 µA | 14 kV<br>175µA | 16 kV<br>280µA | 8 kV<br>55 µA | 14 kV<br>283µA | 19 kV<br>590µA |
| **3** | 12 kV<br>50 µA | 16 kV<br>170µA | 19 kV<br>287µA | 12 kV<br>48 µA | 15 kV<br>130µA | 18 kV<br>247µA | 9 kV<br>52 µA | 16 kV<br>247µA | 23 kV<br>597µA |
| **3.5** | 13 kV<br>45 µA | 19 kV<br>187µA | 24 kV<br>367µA | 13 kV<br>47 µA | 17 kV<br>130µA | 21 kV<br>257µA | 10 kV<br>50 µA | 19 kV<br>255µA | 27 kV<br>613µA |
| **4** | 14 kV<br>48 µA | 20 kV<br>162µA | 26 kV<br>350µA | 14 kV<br>45 µA | 21 kV<br>187µA | 27 kV<br>393µA | 11 kV<br>50 µA | 20 kV<br>225µA | 28 kV<br>523µA |

*3.3.2.2 Drying Rate*

Drying rate in g/h was measured for selected levels of voltage at all gaps (2, 2.5, 3, 3.5, and 4 cm). Results are shown in Figures 3.16, 3.17, and 3.18, for D1 (construction nails), D2 (thick sewing needles), and D3 (thin pins) multiple needle discharge electrodes, respectively. Drying rate did not exceed 22 g/h for all electrodes. It is important to note that the drying rate was more sensitive to the increase of voltage with the smaller gap between discharge electrode and the sample. This could be seen from the slopes of the drying rates at the certain gaps in Figures 3.16-3.18.

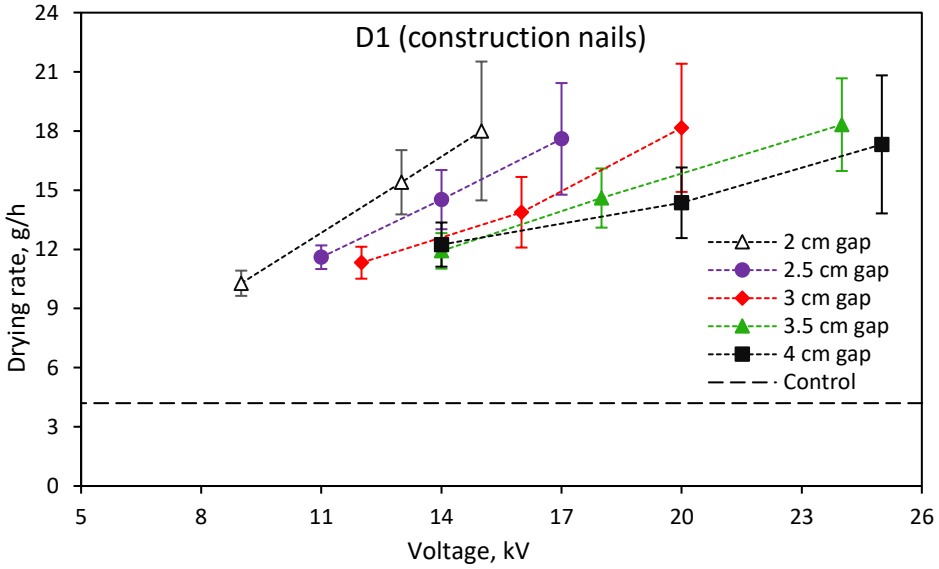


Figure 3.16 Drying rate depending on voltage at five gaps for D1 (construction nails) multiple needle discharge electrode

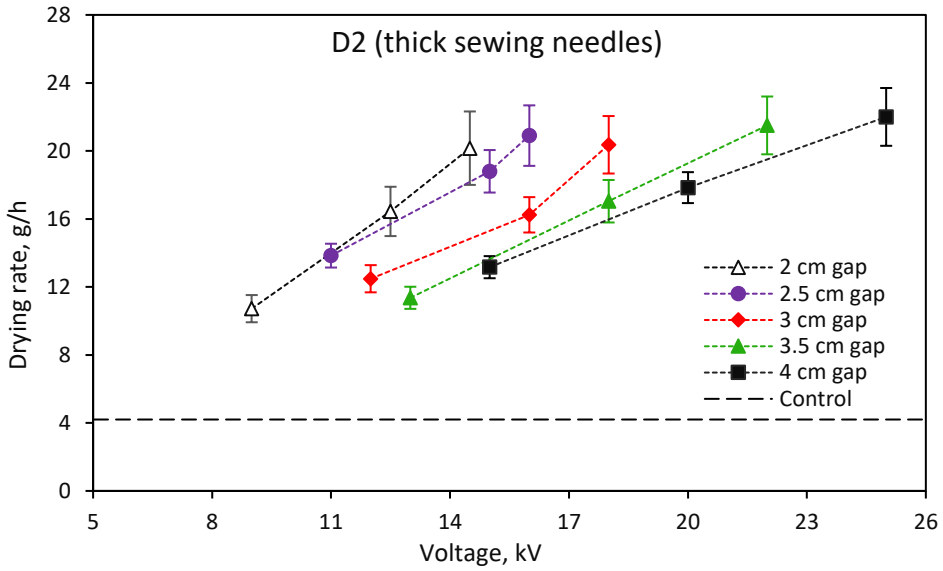


Figure 3.17 Drying rate depending on voltage at five gaps for D2 (thick sewing needles) multiple needle discharge electrode

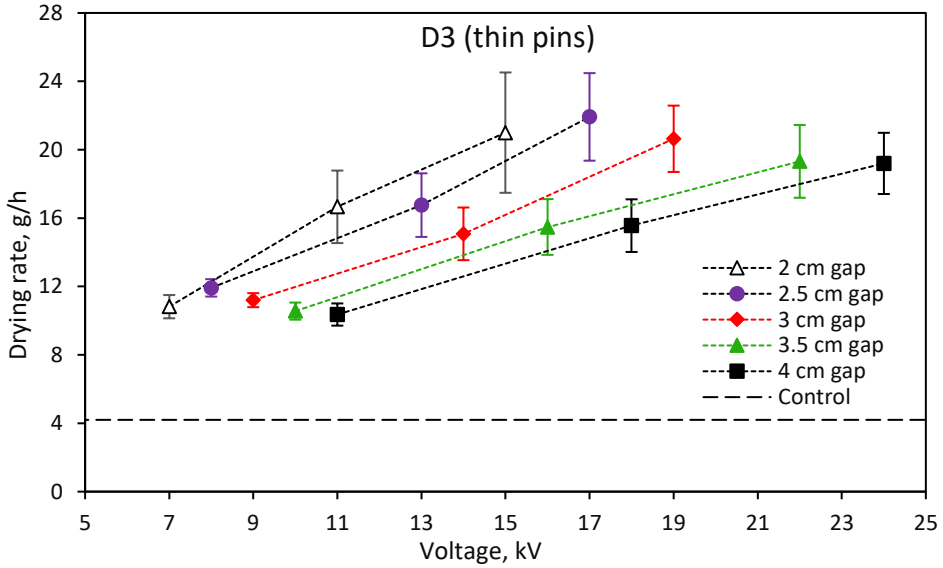


Figure 3.18 Drying rate depending on voltage at five gaps for D3 (thin pins) multiple needle discharge electrode

*3.3.2.3 Specific Energy Consumption*

Energy consumption for all three types of multiple needle discharge electrodes D1-D3 for each voltage (close to inception (low), close to breakdown (high), and the middle one between high and low (middle)) at each certain gap are shown on the bar chart (Figure

3.19). Multiple needle discharge electrode, made of thick sewing needles (D2), demonstrated the highest energy consumption compared to electrodes made of construction nails (D1) and thin pins (D3) at all gaps and voltage levels. For example, at high voltage (H), energy consumption when using D2 electrode made of thick sewing needles were 1.66 and 1.57 times higher compared to D1 and D3 electrodes at 2 cm gap, 1.64 and 1.59 times higher at 3 cm gap, and 2.84 and 2.46 times at 4 cm gap. Energy consumption were not significantly different between electrode with construction nails (D1) and electrode with thin pins (D3), which makes these shapes of needles the most suitable for EHD drying technology.

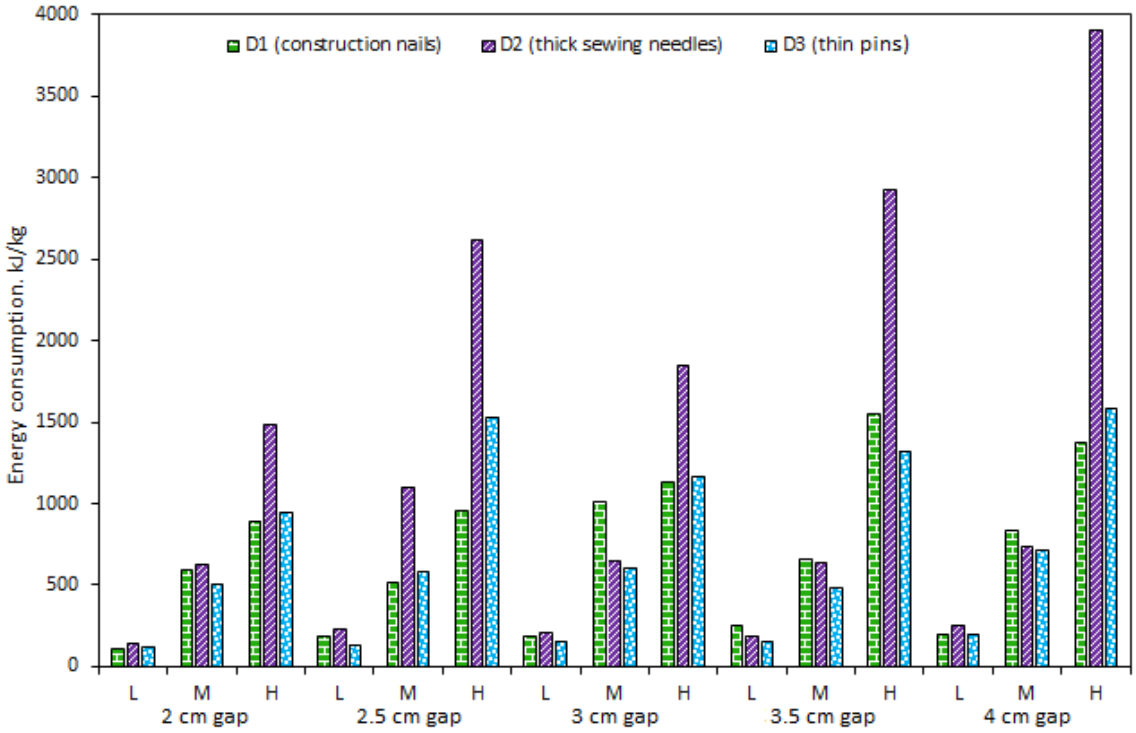


Figure 3.19 Specific energy consumption for construction nails (D1), sewing needles (D2), and pins (D3) discharge electrodes: L – low voltage, M – middle voltage, H – high voltage

### *3.3.3 Conclusions*

1) Multiple needle discharge electrode D3 made with thin pins had the largest work range, which is very important for EHD drying technology. Thin pins (D3) and construction nails (D1) had the best discharge stability.

2) Thick sewing needles (D2) showed the worst discharge stability, which put this needle shape unsuitable for EHD drying technology.

3) Energy consumption in kJ per kg were the highest for multiple discharge electrode (D2) made of thick sewing needles with $d_2 = 1.2$ mm and $r_{tip2} = 0.11$ mm. Discharge electrodes made of construction nails (D1) with the biggest needle diameter $d_1 = 1.8$ mm and tip radii $r_{tip1} = 0.25$ mm and electrode made of thin pins (D3) with the smallest needle diameter resulted in the lowest energy consumption. Overall, construction nails ($d_1 = 1.8$ mm, $r_{tip1} = 0.25$ mm) and thin pins ($d_3 = 0.7$ mm, $r_{tip3} = 0.09$ mm) are the most suitable to use in EHD drying technology. An optimization of spacing to gap ratio based on ionic wind jets visualization and a needle arrangement (chess vs. square array) should be considered when building multiple needle discharge electrode.

## Connecting statement

It was possible to measure the area covered by ionic wind jets on the surface of collecting electrode, created by different needle shapes. The most suitable and effective needle shapes were selected and recommended for upscaling EHD drying technology. The possible way of optimization of needles arrangement in the discharge electrode has been proposed. Since EHD system include both discharge and collecting electrodes, the next objective was optimization of collecting electrode for large-scale dryers. Next in Chapter 4, the effect of different collecting electrodes on drying rate and energy efficiency has been studied.

# Chapter 4 Optimization of Collecting Electrode Configuration

## 4.1 Introduction

The solid metal plate was commonly used as a collecting electrode in EHD lab setups (see Table A.1). However, this type of the electrode restricts drying of wet material, which is in contact with non-permeable metal plate. Numerical analysis showed that openings in the collecting electrode can significantly improve heat and mass transfer and, at the same time, provide more uniform drying of the product (Defraeye and Martynenko, 2019). Therefore, mesh-type collecting electrode was proposed as a better alternative to the solid plate electrode.

There were only a few attempts to compare experimentally the drying of wet materials when using solid metal plate and plate with openings. While Zheng et al. (2011) found that the drying rate between solid metal plate and two mesh electrodes with different opening size resulted in an identical drying rate, the results of Dalvand et al. (2012b) were contradictory to those received by Zheng et al. (2011), saying that the drying rate was higher when using mesh collecting electrode compared to solid plate. This could be due to the fact, that Zheng et al. (2011) evaporated water, which, we assume, was hold in a dish, whereas Dalvand et al. (2012b) dried kiwi slices directly placed on the surface of the collecting electrode. Additionally, the research of Dalvand et al. (2012b) showed that this positive effect of mesh collector increased with the increase of applied voltage.

Based on these published findings, this research was initialized to compare the effect of solid plate collecting electrode and different mesh collecting electrodes. In this case, the main mesh characteristics, such as wire diameter, opening size, and open area, is very important, as all these factors can possibly affect the drying rate.

Experiments have been conducted to answer three *research questions*:

1) What is the effect of open area on the drying rate and energy consumption at the same wire diameter? Do the openings in collecting electrode enhance the drying rate compared to solid plate?

2) What is the effect of wire diameter on the drying rate and energy consumption at the same open area?

3) What is the impact of percentage of grounded wires in mesh collecting electrode on the drying rate and energy consumption at different voltages and gaps?

The *hypotheses* are:

1) Openings in collecting electrodes significantly increase the drying rate compared to solid metal plate collecting electrode. Open area of mesh collecting electrodes has a significant effect on the drying rate and energy consumption.

2) Wire diameter has a significant effect on the drying rate and energy consumption.

3) Percentage of grounded wires in the collecting electrode can significantly affect both the drying rate and energy consumption.

## 4.2 Methodology

*Input*:

- Current type: DC+
- Discharge electrode (one configuration)
- Collecting electrodes (eight configurations)
- Gap, cm (three levels)
- Voltage, kV (three levels for each gap)
- Electric field strength, kV/cm (3, 4.5, and 6.5 kV/cm)

- Wet paper towel (50±1.0 g with constant initial moisture content of 72% wet basis)
- Relative humidity (35±5%)
- Temperature (~21°C)
- Pressure, kPa (100 kPa)

*Output*:

- Drying time, s
- Drying rate, g/h
- Current, μA
- Power, W ($P = V \cdot I$)
- Energy consumption, kJ/kg

In this research the drying rate of wet paper towel placed on the different collecting electrodes was measured. The collecting electrode configurations were as follows: solid aluminum plate (C1), three stainless steel meshes (C2, C3, and C4) with different open area but the same wire diameter ($d_w$ =0.254 mm), three stainless steel meshes (C5, C6, and C7) with different wire diameter but the same open area (46%), and nylon plastic mesh collecting electrode (C8), where each fourth nylon thread in width was replaced with a stainless steel wire of the same diameter, creating 12.5% of metal material and 87.5% of plastic material in the mesh (Figure 4.1). Full description of these electrodes is presented in Table 4.1 and some of them are shown in Figure 4.2. All collecting electrodes had the same area of 0.03712 $m^2$. The opening size ($l_{os}$) and wire diameter ($2r$) of mesh collecting electrode is shown in Figure 4.3. Term "open area" ($OA$) describes the percentage part of all apertures across the entire surface area of the mesh electrode (Figure 4.3):

$$OA = \left(\frac{l_{os}}{l_{os} + 2r}\right)^2 \cdot 100\% \quad (4.1)$$

Figure 4.1 Nylon plastic mesh collecting electrode (C8) with 12.5% of stainless steel wires

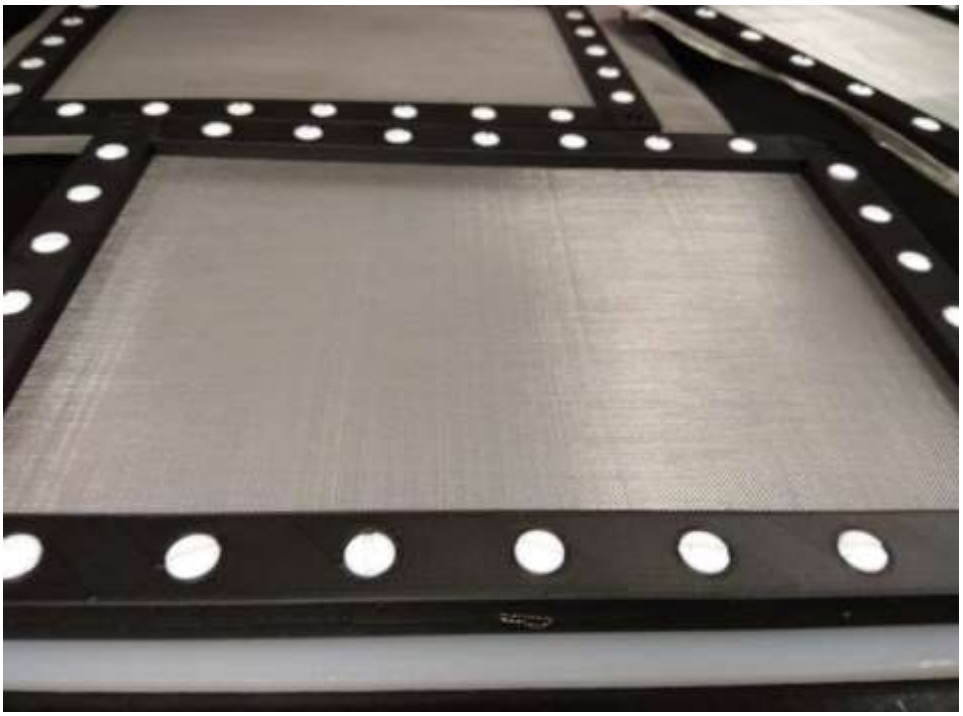

Figure 4.2 Overall view of stainless steel mesh collecting electrodes

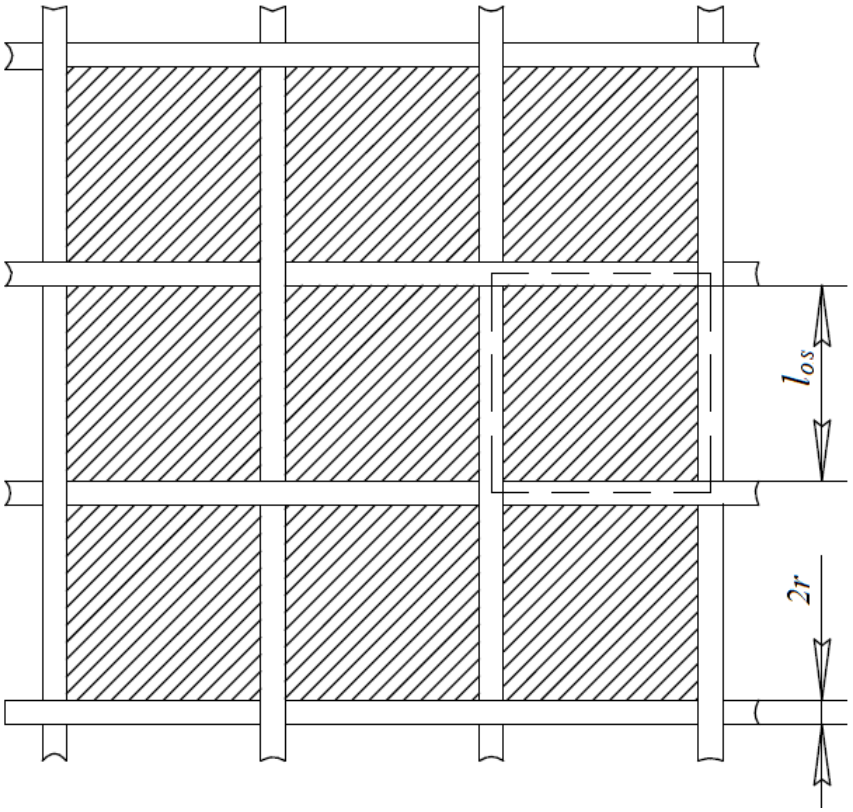


Figure 4.3 Meaning of opening size ($l_{os}$) and wire diameter ($2r$) in woven mesh collecting electrode

Table 4.1 Characteristics of metal plate and woven mesh collecting electrodes

| | **C1** | **C2*** | **C3*** | **C4*** | **C5**** | **C6**'** | **C7**** | **C8'** |
|---|---|---|---|---|---|---|---|---|
| **Market name** | - | 40×40 | 28×28 | 15×15 | 200×200 | 20×20 | 10×10 | 20×20 |
| **Construction** | Plate 0.03712 $m^2$ | Woven mesh | Woven mesh | Woven mesh | Woven mesh | Woven mesh | Woven mesh | Woven mesh |
| **Material** | Aluminum | 304 SS | 304 SS | 304 SS | 304 SS | 304 SS | 304 SS | 304 SS 25% Nylon 175% |
| **Wire diameter ($2r$)** | Thickness 1.05 mm | 0.01" 0.254 mm | 0.01" 0.254 mm | 0.01" 0.254 mm | 0.0016" 0.0406 mm | 0.016" 0.406 mm | 0.032" 0.813 mm | 0.0159" 0.404 mm |
| **Opening size ($l_{os}$)** | 0 | 0.015" 0.381 mm | 0.026" 0.6604 mm | 0.057" 1.45 mm | 0.0034" 0.0864 mm | 0.034" 0.864 mm | 0.068" 1.73 mm | 0.0334" 0.848 mm |
| **Open area ($OA$)** | 0 | 36% | 52% | 73% | 46% | 46% | 46% | 46% |

58 *Note*. C* used to compare the effect of mesh open area (constant wire diameter); C** used to compare the effect of wire diameter of mesh collecting electrode (constant open area); C' used to quantify the impact of percentage of grounded wires of the mesh collecting electrode.

### *4.2.1 Fabrication of Collecting Electrodes*

3D frames for all collecting electrodes (Table 4.1) were modeled and printed using Markforged 3D printer (Mark Two) with two components of the material, plastic (Onyx, which is 40% stiffer than ABS) and carbon fiber. The length and the width of the frame were modeled separately as the board of the printer was smaller than the frame for the electrode. Sketches and 3D models of these two parts are shown in Figure 4.4 and 4.5. Epoxy glue was used to connect two width and two length together. The mesh was put between two frames and connected with polyethylene plastic press-fit binding barrels and screws, shown in Figure 4.6.

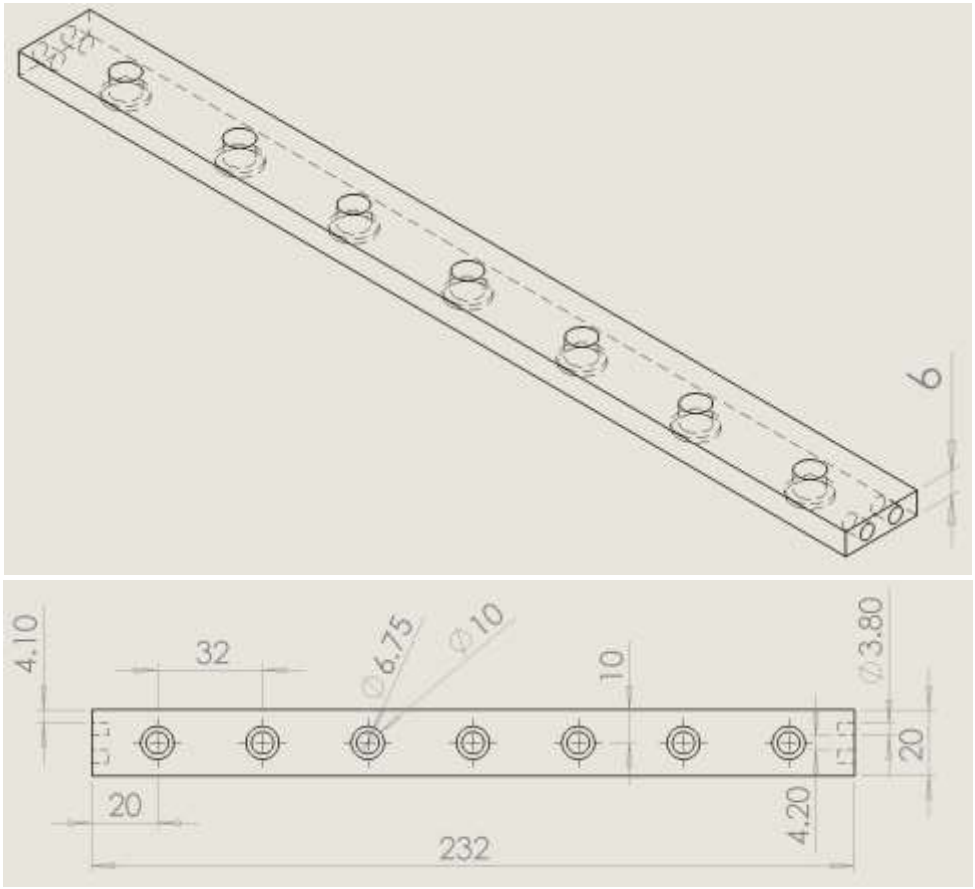


Figure 4.4 Length of the frame for mesh collecting electrode (in mm)

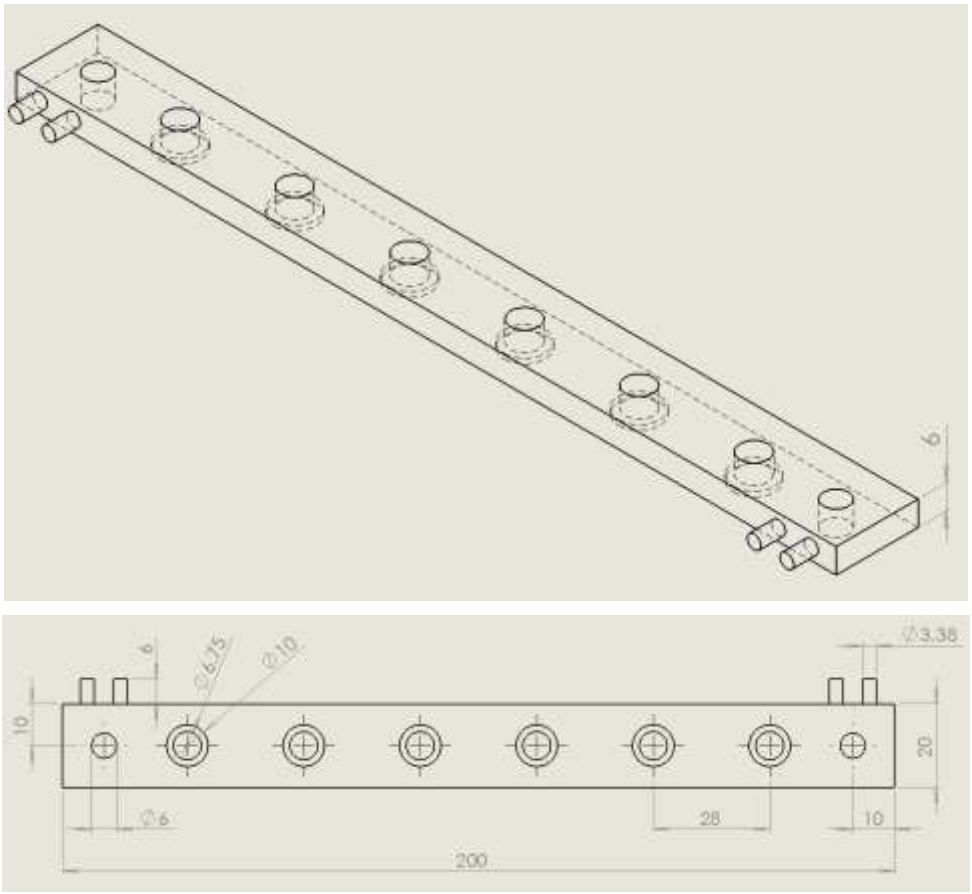


Figure 4.5 Width of the frame for mesh collecting electrode (in mm)

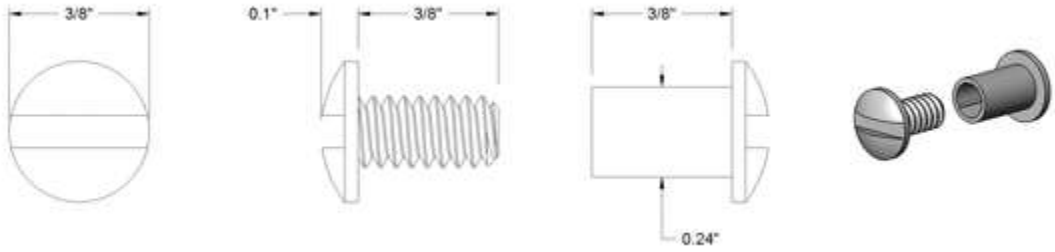


Figure 4.6 Plastic press-fit binding barrels and screws (retrieved from https://www.mcmaster.com/90249a620)

SOLIDWORKS 2019 SP5.0 Education Edition software (Javelin Technologies Inc., Canada) was used for 3D modeling of the parts for 3D printing. Markforged Eiger 3D printing software (Markforged Inc., USA) for Mark Two Markforged 3D Printer was used for 3D printing of the collecting electrode frames.

### *4.2.2 Sample Preparation*

The 14 g sample pack of dry paper towels was wetted with tap water to 50.0±1.0 g before each experiment. The thickness of wet samples was 3±0.1 mm and the surface area was 0.01955 $m^2$.

### *4.2.3 Drying Experiments*

Wet paper towel (1) was placed on the surface of collecting electrode (2) (Figure 4.7) with the gap between needles ends of the discharge electrode (3) and the surface of wet paper towel at 2, 3, and 4 cm. Drying rate (DR in g/h) was measured at different gaps, but the same electric field strength of 3, 4.5, and 6.5 kV/cm. So that the voltage level for each gap was: 6, 9, and 13 kV for 2 cm gap; 9, 13.5, and 19.5 kV for 3 cm gap; and 12, 18, and 26 kV for 4 cm gap. These voltages, and as a result electric field strength, were selected based on volt-ampere characteristics, starting from the *inception* voltage and ending with *breakdown* voltage. For example, at 2 cm gap the inception voltage was 5 kV and breakdown voltage was 15 kV, so that the levels of voltages were selected as one the closest to the inception voltage, second one as the closest to the breakdown voltage, and the third one was selected between these two voltages. In order to make the results comparable between all different collecting electrodes, we decided to keep the same levels of electric field for drying of wet paper towel when using different collecting electrodes.

Discharge electrode with the surface area of 0.016274 $m^2$ was made with 32 thin conical sewing needles with $d_3 = 0.7$ mm and $r_{tip3} = 0.09$ mm and spacing between them was set at 2 cm (see Figures 3.9 and 3.10 in section 3.2, Chapter 3). Discharge electrode was connected to the positive pole of a direct current (DC) high voltage power supply model BAL-32-5 (Voltronics, USA). Moisture reduction (g) was measured with a digital

scale model HCB 1002 (Adam Equipment, Oxford, CT, USA) with 0.01 g resolution and recorded on the computer every 30 seconds.

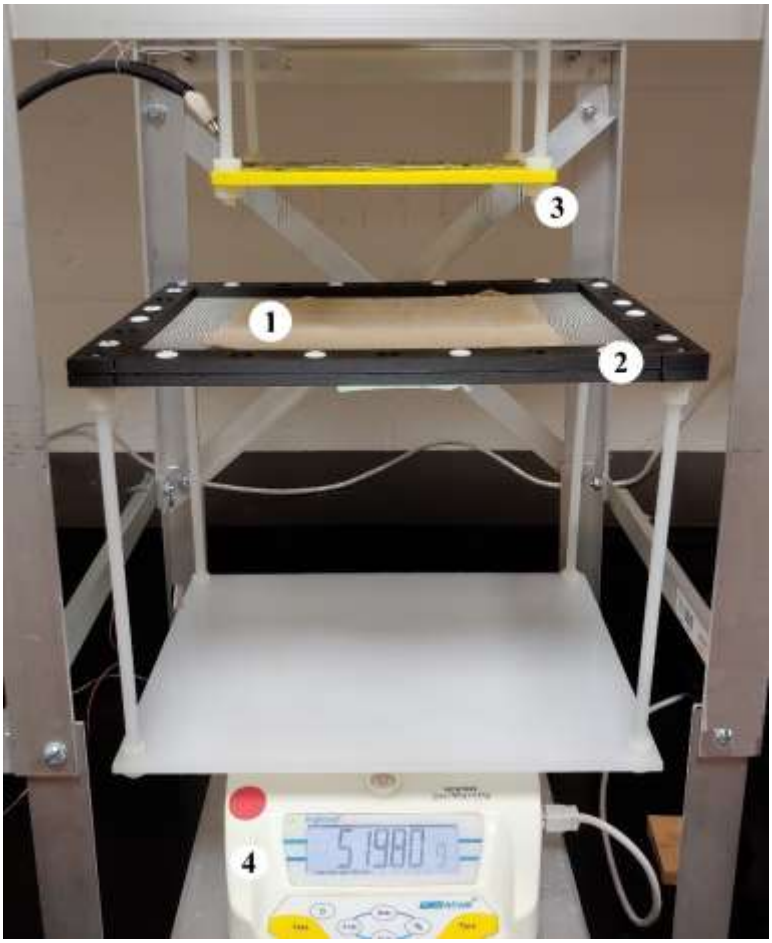


Figure 4.7 EHD lab setup for drying of wet paper towel at different collecting electrodes: wet paper towel (1), mesh collecting electrode (2), needle discharge electrode (3)

### *4.2.4 Specific Energy Consumption*

For each experiment on drying of wet paper towel, level of current (μA) at a certain gap and voltage (kV) was recorded from the indicators on the high voltage power transformer. Power (mW) used in EHD lab setup was calculated by multiplying of voltage and current:

$$P = V \cdot I \tag{4.2}$$

Specific energy consumption (kJ/kg) was calculated by dividing of power (W) by drying rate (g/h) measured at the first hour of drying, where specific energy means energy used directly for the drying in EHD system:

$$E = \frac{3600 \cdot V \cdot I}{DR} \tag{4.3}$$

### *4.2.5 Statistical Analysis*

Changes in drying rate and energy consumption were analyzed using ANOVA for three-factor factorial design, where the factors were: gap between electrodes (three levels), electric field strength (three levels), and type of collecting electrode. Model assumptions, such as normal distribution and constant variance were verified by examining the residuals (Montgomery, 2017). Independence of the error terms was verified through randomization. The analysis was completed using Minitab software (Minitab 18, Minitab Inc., State College, PA, USA). Statistical difference was determined using least significant difference (LSD) comparison test (*t*-test) and accepted at $p$-value $< 0.05$.

## 4.3 Results and Discussion

### *4.3.1 Effect of Open Area of Collecting Electrode*

This section represents experimental study, designed to answer following research questions:

*What is the effect of open area (C2 vs. C3 vs. C4) on the drying rate and energy consumption at the same wire diameter ($2r = 0.254$ mm)? Do the openings in collecting electrode enhance the drying rate compare to solid plate (C1)?*

#### *4.3.1.1 Volt-Ampere Characteristics*

Figures 4.8-4.10 show volt-ampere characteristics of mesh collecting electrodes with the same wire diameter but different open area (C2 vs. C3 vs. C4). Each Figure represents volt-ampere characteristics at a certain gap. There was no effect of the open area on the current and so, current was not significantly different between solid plate (0% open area) and all mesh collecting electrodes with different open areas at 3 and 4 cm gap. The same was observed at 2 cm gap in the range of voltages below 12 kV. However, above 12 kV or 6 kV/cm, current was 1.1-1.13 times higher for mesh collecting electrodes compared to a solid plate with 0% open area, respectively.

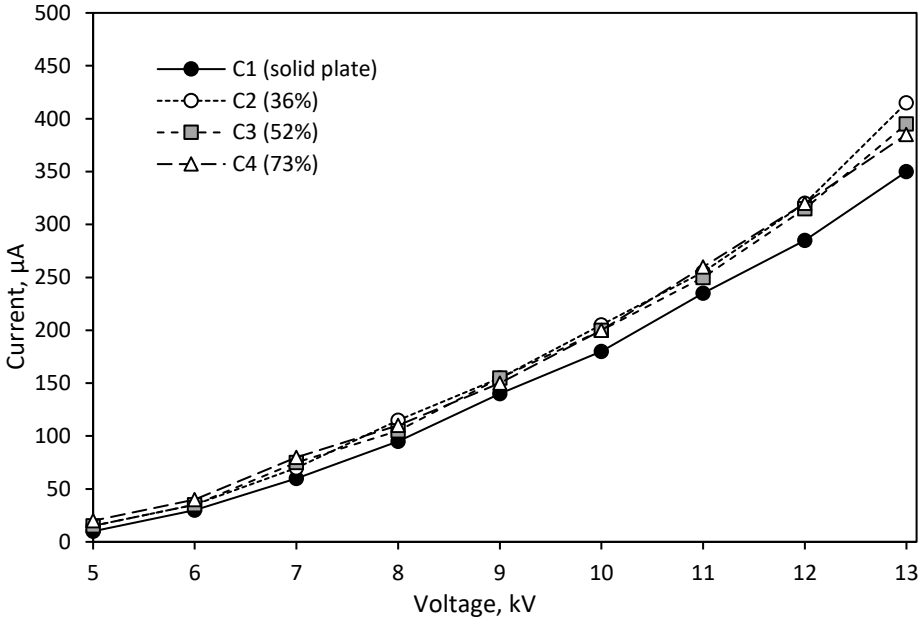


Figure 4.8 Current at 2 cm gap and all voltages for C1, C2, C3 and C4 mesh collecting electrodes

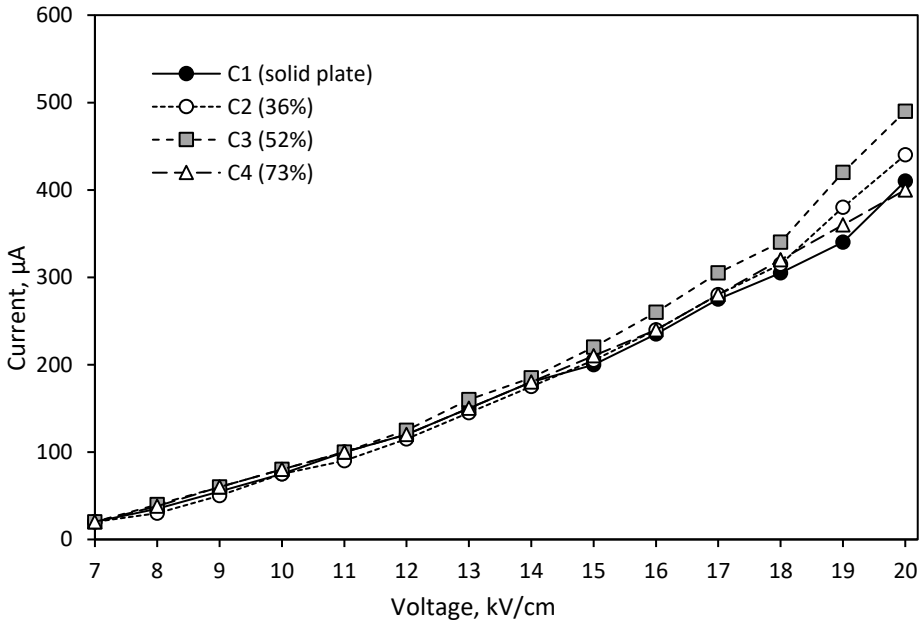


Figure 4.9 Current at 3 cm gap and all voltages for C1, C2, C3 and C4 mesh collecting electrodes

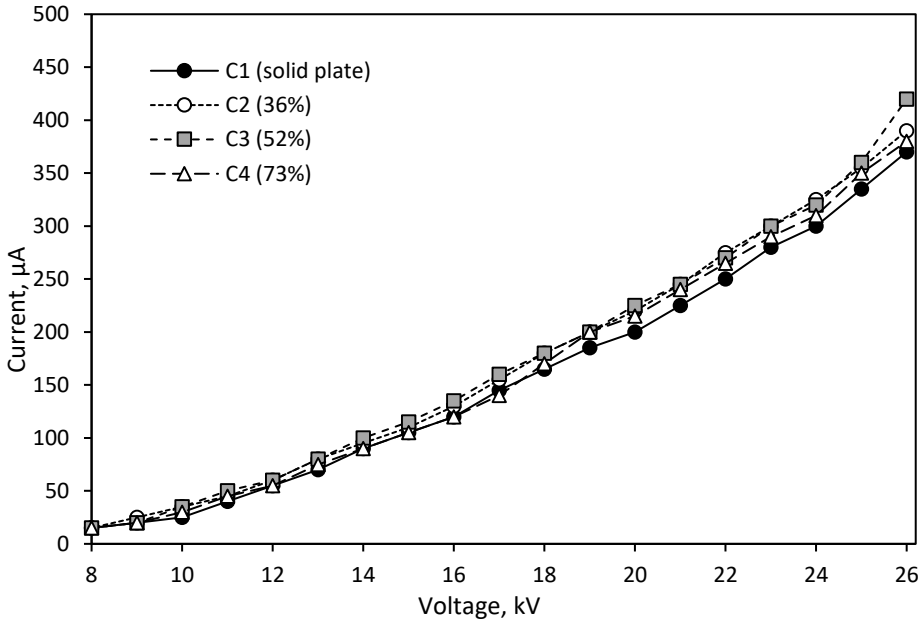


Figure 4.10 Current at 4 cm gap and all voltages for C1, C2, C3 and C4 mesh collecting electrodes

*4.3.1.2 Drying Rate*

Following Figures 4.11-4.13 (a) represent drying rate of wet paper towel depending on open area when using solid metal plate with 0% open area (C1) and three mesh collecting electrodes (C2 vs. C3 vs. C4) with the same wire diameter but different open area. There was no linear relationship observed between open area and drying rate. Statistical analysis showed that using of both C2 (36%) and C4 (73%) electrodes resulted in the highest drying rate, which was significantly higher compared to C1 (0%) and C3 (52%) electrodes. For example, at 2 cm gap and 3 kV/cm electric field, the drying rate was 1.3 and 1.4 times higher when using 36% and 73% collecting electrode, respectively, compared to a solid plate (0%). This difference decreased with an increase of electric field strength: at 4.5 kV/cm the drying rate was 1.3 and 1.22 times higher, and at 6.5 kV/cm it was only 1.16 and 1.14 times higher, compared to the solid metal plate.

At 3 cm gap, collecting electrodes with open area of 36% (C2) and 73% (C4) resulted in the highest drying rate, but the drying rate at 3 and 6.5 kV/cm and open area of 36% (C2) was not significantly different compared to a solid plate. At 4 cm gap the same 36% (C2) and 73% (C4) collecting electrodes showed the highest drying rate, but it was not significantly different compared to a solid plate (C1) at the smallest electric field strength of 3 kV/cm. The same situation was observed at 4 cm gap, but there was no significant difference observed at 3 and 6.5 kV/cm electric field strength. At 4 cm gap, solid plate (C1) and mesh plate with 52% open area (C3) resulted in the smallest drying rate. Mesh collecting electrode with open area of 52% (C3) led to the same drying rate as the solid metal plate (C1) at all gaps and electric field strength. Overall, collecting electrode with openings can significantly increase drying rate compared to a solid metal plate. Therefore, mesh collecting electrodes with 36 and 73% open area are recommended to use in EHD technology for its further upscaling.

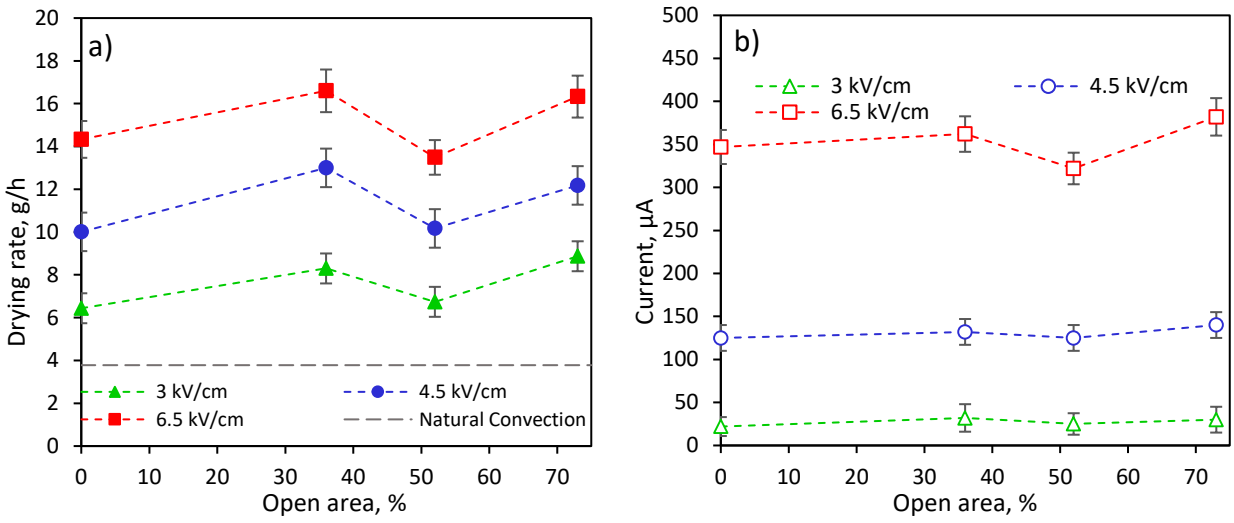


Figure 4.11 Drying rate (a) and current (b) at different open area of mesh collecting electrodes at 2 cm gap

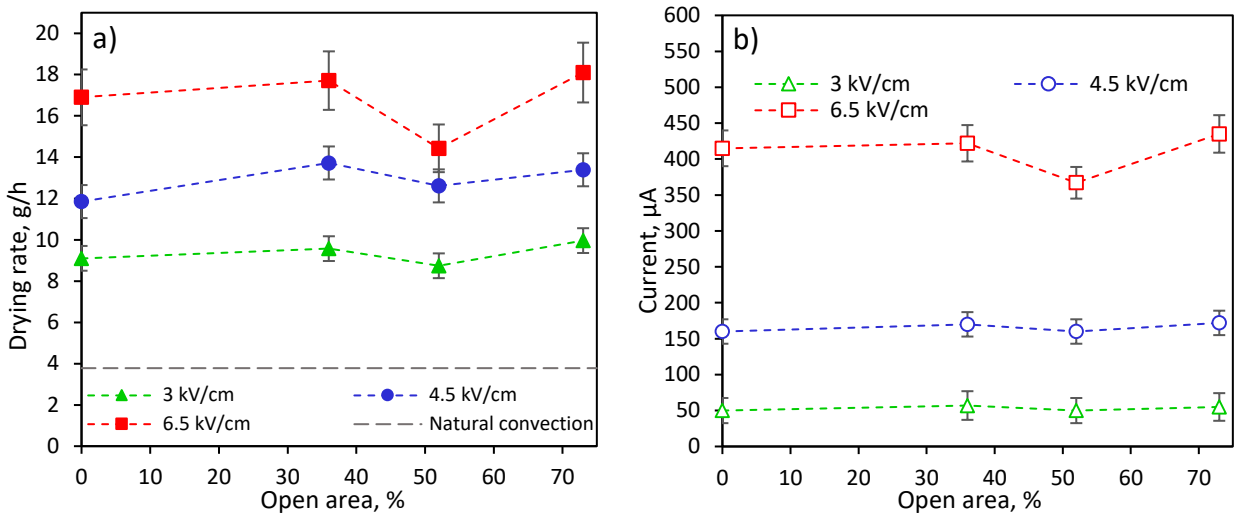


Figure 4.12 Drying rate (a) and current (b) at different open area of mesh collecting electrodes at 3 cm gap

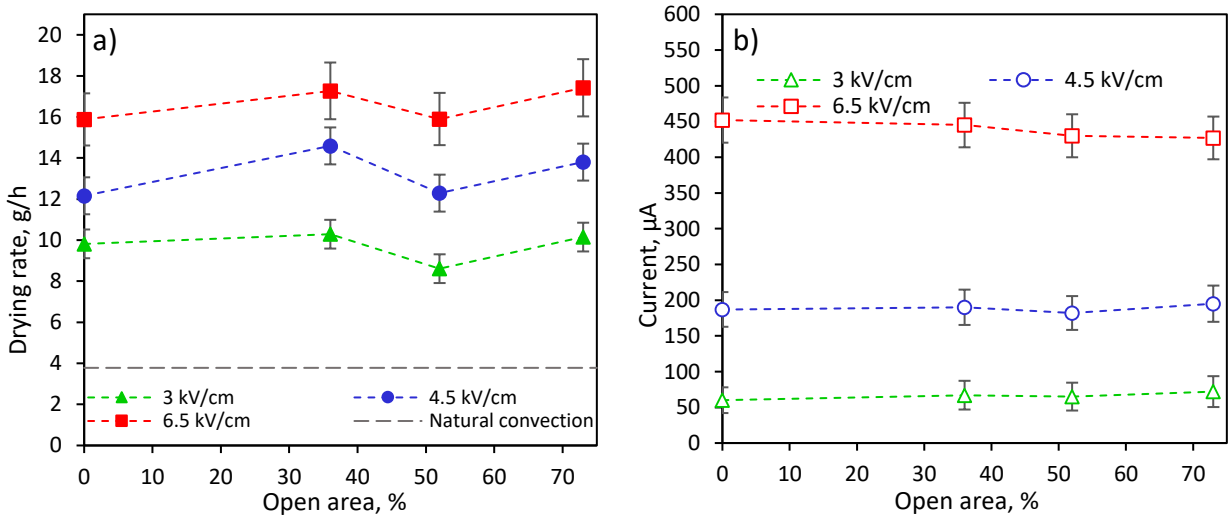


Figure 4.13 Drying rate (a) and current (b) at different open area of mesh collecting electrodes at 4 cm gap

*4.3.1.3 Specific Energy Consumption*

The level of current, measured during drying of wet paper towel as a function of the open area of collecting electrode is presented in Figures 4.11 (b), 4.12 (b), and 4.13 (b) for the gaps 2, 3, and 4 cm, respectively. Overall, there were no significant difference in the level of current between all four collecting electrodes, but, there was one exception: at

6.5 kV/cm and gap of 2 and 3 cm, mesh collecting electrode with open area of 52% resulted in a significantly lower current compared to all other three collecting electrodes with open area of 0 (C1), 36 (C2) and 73% (C4). This observation corresponds to consistently smaller drying rate; however, the reason for this anomaly behavior should be further investigated.

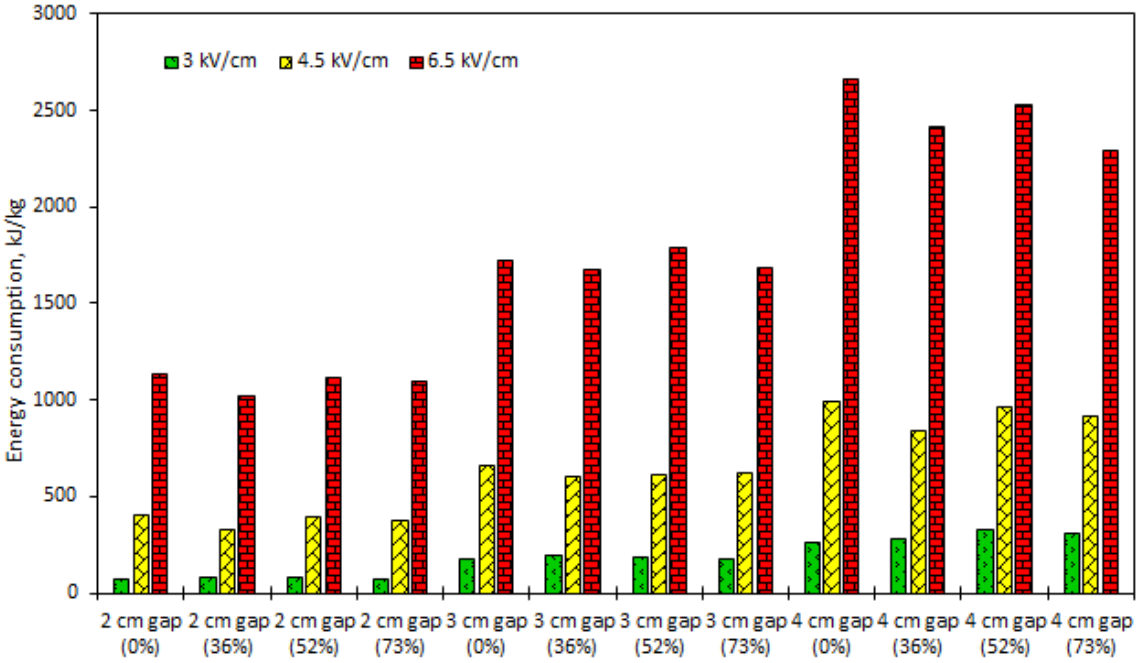


Figure 4.14 Specific energy consumption for 0% (C1), 36% (C2), 52% (C3) and 73% (C4) open area of mesh collecting electrodes at 2, 3, and 4 cm gap and 3, 4.5, and 6.5 kV/cm electric field strength

Specific energy consumption in kJ/kg are presented in Figure 4.14 and the data is shown in Table 4.2. Statistical analysis showed that the effect of open area on energy consumption was negligible, so that energy consumption was not significantly different between all collecting electrodes C1 vs. C2 vs. C3 vs. C4.

Table 4.2 Specific energy consumption in kJ/kg according to Figure 4.14

| E, kV/cm | 2 cm gap (0%) | 2 cm gap (36%) | 2 cm gap (52%) | 2 cm gap (73%) | 3 cm gap (0%) | 3 cm gap (36%) | 3 cm gap (52%) | 3 cm gap (73%) | 4 cm gap (0%) | 4 cm gap (36%) | 4 cm gap (52%) | 4 cm gap (73%) |
|---|---|---|---|---|---|---|---|---|---|---|---|---|
| **3** | 73.79c | 83.28c | 80.12c | 73.06c | 178.02b | 192.98b | 185.35b | 178.92b | 263.95a | 281.28a | 326.13a | 306.44a |
| **4.5** | 404.6c | 328.98c | 398.23c | 372.41c | 656.2b | 602.19b | 616.65b | 624.29b | 996.51a | 843.87a | 959.61a | 915.65a |
| **6.5** | 1133.26c | 1020.58c | 1117.09c | 1094.77c | 1723.85b | 1672.75b | 1785.41b | 1687.13b | 2664.18a | 2411.81a | 2531.32a | 2294.33a |

*Note*. Means sharing the same letter in the row are not significantly different.

*4.3.1.4 Conclusions*

1. There was no linear relationship between the drying rate and an increase of open area, but electrode with open area of 52% resulted in the smallest drying rate. The highest drying rate at 36% open area could be explained by the highest number of holes (openings) as they were the smallest (see opening size in Table 4.1) which possibly can affect the distribution of electrostatic field. The highest drying rate at 73% open area could be due convection of wet material on the bottom of the material because of the large open area and so, bigger area of an interaction of wet material with environmental air. Overall, mesh collecting electrodes are preferable to use in EHD drying compared to solid plates without openings.

2. Effect of open area on energy consumption was negligible.

### *4.3.2 Effect of Wire Diameter of Collecting Electrode*

These experiments have been designed to answer the following research question:

*What is the effect of wire diameter on the drying rate and energy consumption at the same open area of collecting electrode (46%)?*

*4.3.2.1 Volt-Ampere Characteristics*

Volt-Ampere characteristics for collecting electrodes with the same open area (46%) but different wire diameter (C5 (0.0406 mm) vs. C6 (0.406 mm) vs. C7 (0.813 mm)) are shown in Figures 4.15, 4.16, and 4.17 for gap between electrodes of 2, 3, and 4 cm, respectively.

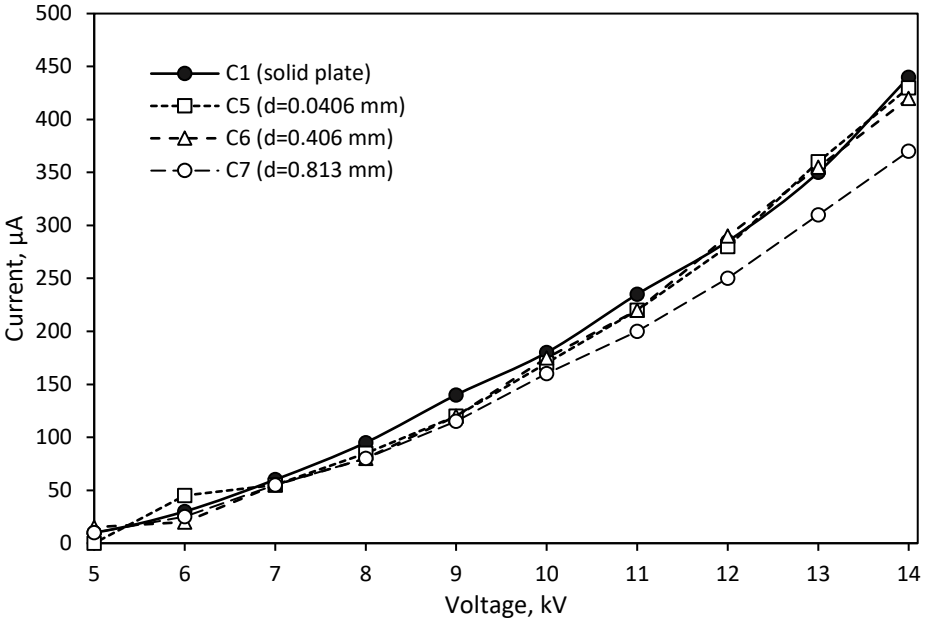


Figure 4.15 Current at 2 cm gap and all voltages for C1, C5, C6 and C7 mesh collecting electrodes

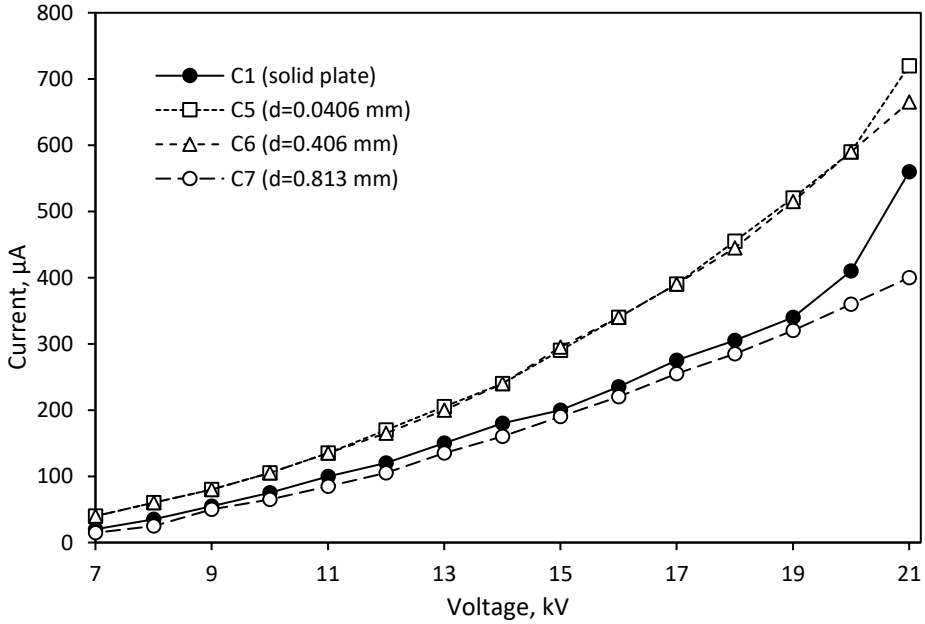


Figure 4.16 Current at 3 cm gap and all voltages for C1, C5, C6 and C7 mesh collecting electrodes

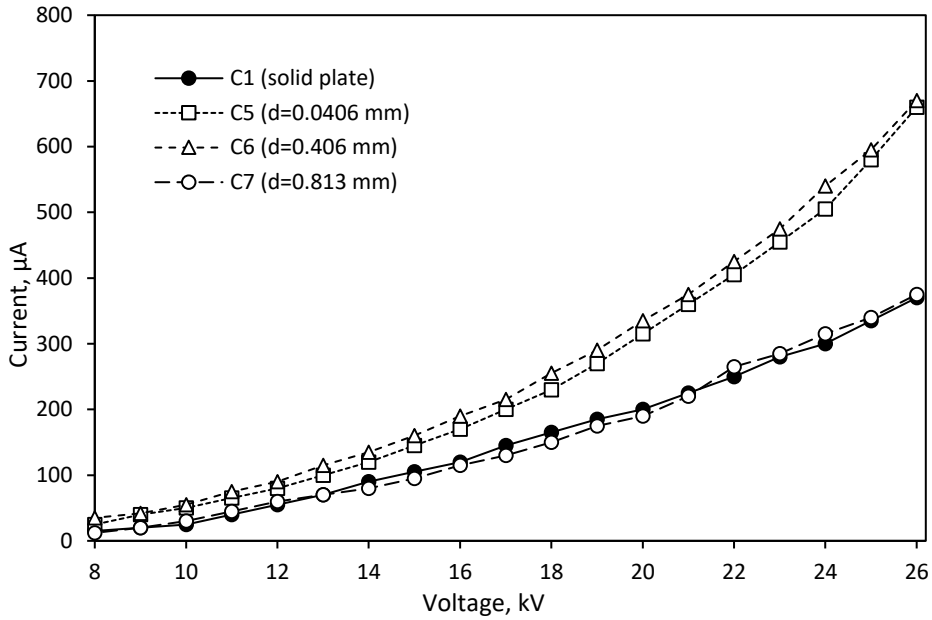


Figure 4.17 Current at 4 cm gap and all voltages for C1, C5, C6 and C7 mesh collecting electrodes

It could be seen that the current was the same between all electrodes (C1 vs. C5 vs. C6 vs. C7) at 2 cm gap, but above 11 kV the current was slightly lower when using mesh electrode with the biggest wire diameter of 0.813 mm. This result was confirmed by measurements at 3 and 4 cm gap, which proved the finding that current decreases with increase of wire diameter (0.813 mm) (C7) and solid plate (C1). The highest current was observed when using electrodes with smaller wire diameter such as 0.406 mm (C6) and 0.0406 (C5) mm. These results show that wire diameter can potentially affect energy consumption.

*4.3.2.2 Drying Rate*

This set of experiments was carried out to investigate the effect of wire diameter on drying rate. Relationship between drying rate and wire diameter are presented in the Figures 4.18 (a), 4.19 (a), and 4.20 (a). Statistical analysis showed that there was no

significant difference in drying rate between three electrodes at 2, 3, and 4 cm gaps. The wires diameter in the mesh collecting electrode did not affect the drying rate.

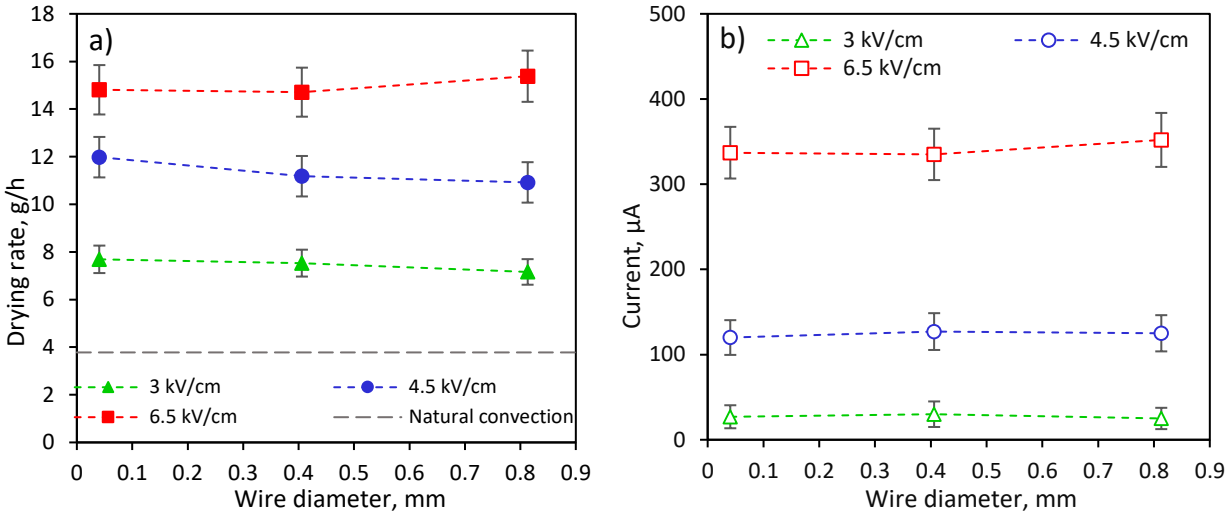


Figure 4.18 Drying rate (a) and current (b) at different wire diameter of mesh collecting electrodes at 2 cm gap

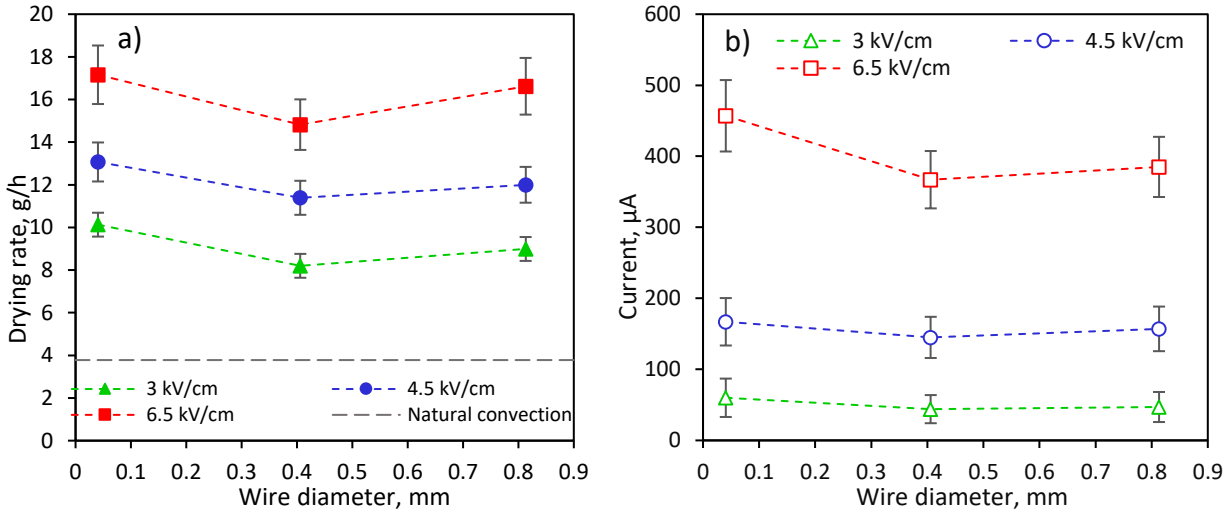


Figure 4.19 Drying rate (a) and current (b) at different wire diameter of mesh collecting electrodes at 3 cm gap

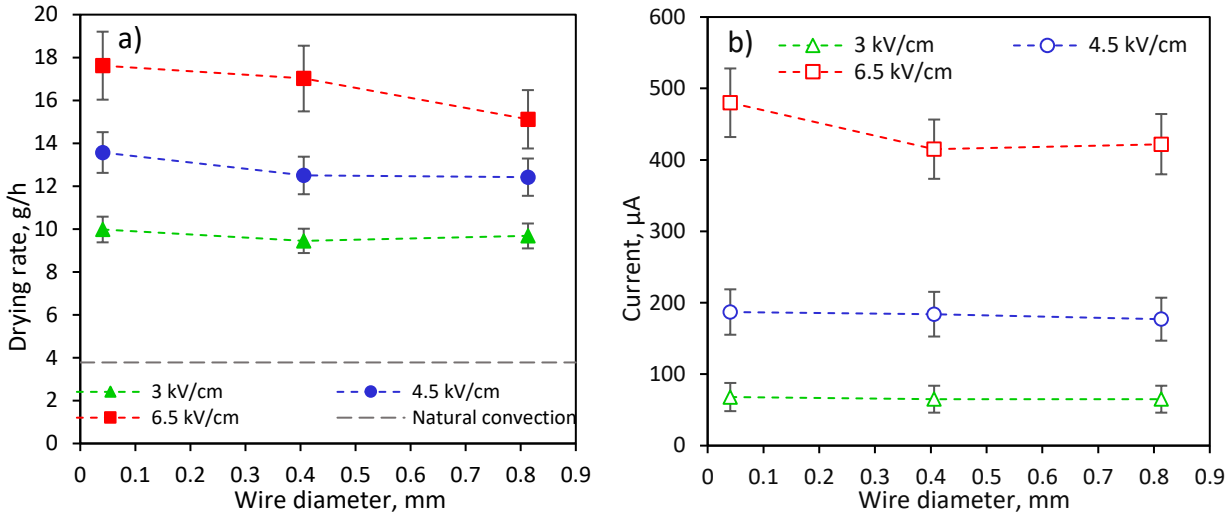


Figure 4.20 Drying rate (a) and current (b) at different wire diameter of mesh collecting electrodes at 4 cm gap

*4.3.2.3 Specific Energy Consumption*

The level of current, measured during drying of wet paper towel, depending on wire diameter is presented in Figures 4.18 (b), 4.19 (b), and 4.20 (b) for a certain gap of 2, 3, and 4 cm, respectively. There was no significant difference in the level of current at a certain electric field strength and gap between all wire diameters.

Specific energy consumption in kJ/kg are presented in Figure 4.21 and the data is shown in Table 4.3. Statistical analysis confirmed that energy consumption was not significantly different between three electrodes.

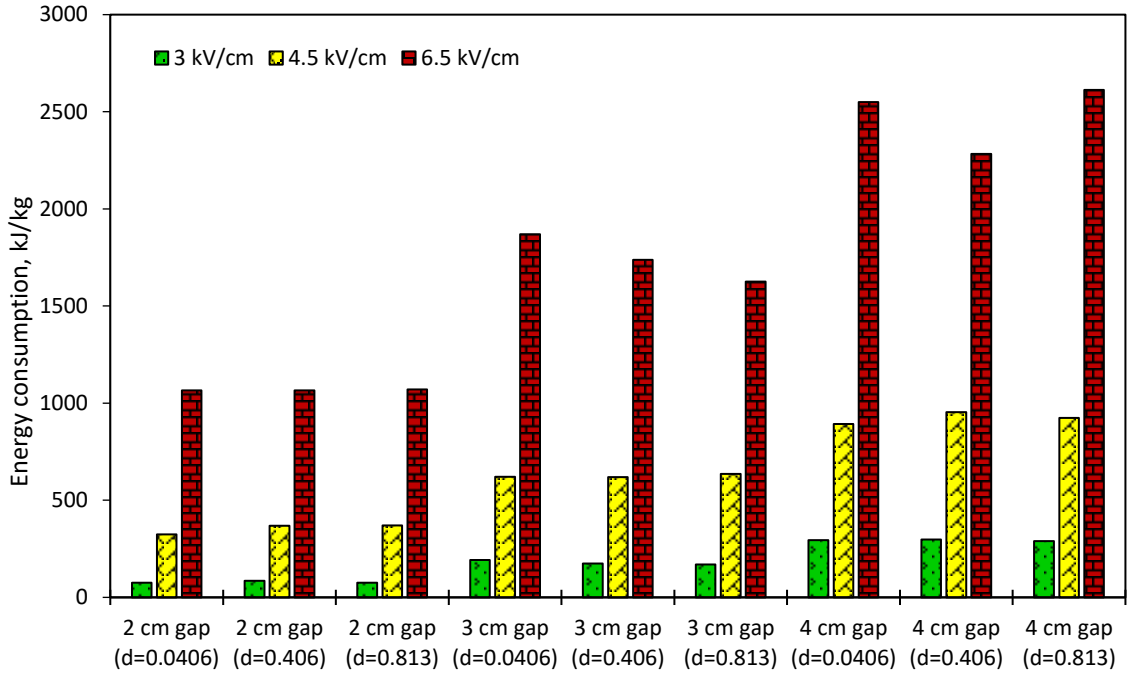


Figure 4.21 Specific energy consumption for 0.0406 mm (C5), 0.406 mm (C6), and 0.813 mm (C7) wire diameters of mesh collecting electrodes at 2, 3, and 4 cm gap and 3, 4.5, and 6.5 kV/cm electric field strength

Table 4.3 Specific energy consumption in kJ/kg according to Figure 4.21

| E, kV/cm | 2 cm gap d=0.0406 | 2 cm gap d=0.406 | 2 cm gap d=0.813 | 3 cm gap d=0.0406 | 3 cm gap d=0.406 | 3 cm gap d=0.813 | 4 cm gap d=0.0406 | 4 cm gap d=0.406 | 4 cm gap d=0.813 |
|---|---|---|---|---|---|---|---|---|---|
| **3** | 75.84 c | 86.06 c | 75.42 c | 191.91 b | 173.85 b | 169.39 b | 294.35 a | 297.14 a | 290.08 a |
| **4.5** | 324.54 c | 368.05 c | 370.88 c | 620.98 b | 618.7 b | 635.85 b | 892.97 a | 953.86 a | 923.48 a |
| **6.5** | 1064.93 c | 1065.81 c | 1071.11 c | 1869.55 b | 1738.42 b | 1626.17 b | 2549.83 a | 2282.26 a | 2612.38 a |

*Note*. Means sharing the same letter in the row are not significantly different.

*4.3.2.4 Conclusions*

1. Effect of wire diameter in mesh collecting electrode on the drying rate was not significant.

2. Effect of wire diameter in the mesh collecting electrode on energy consumption was negligible.

### *4.3.3 Effect of Percentage of Grounded Wires in Collecting Electrode*

The experiments, presented in this section, have been designed to answer the following research question:

*What is the impact of percentage of grounded (metal) wires in collecting electrode (C6 vs. C8) on the drying rate and energy consumption?*

#### *4.3.3.1 Drying Rate*

Drying rate (g/h) of wet paper towel at different electric field strength but the same gap between discharge and collecting electrodes for both C6 with 100% metal wires and C8 with 12.5% of metal wires is shown in Figures 4.22 (a), 4.23 (a), and 4.24 (a) for 2, 3, and 4 cm gap, respectively. Open area (46%) and wire diameter (0.848 - 0.864 mm) were the same for both C6 and C8 collecting electrodes.

In most cases, the drying rate was significantly higher when using mesh collecting electrode with 12.5% metal wires (C8) compared to fully metal electrode (C6). At constant gap of 2 cm, the drying rate when using nylon-metal mesh (C8) was 1.05, 1.19, and 1.2 times higher compared to mesh with 100% metal wires (C6) at 3, 4.5, and 6.5 kV/cm, respectively; however, at 3 kV/cm the difference was not significant in drying rate between both electrodes. At 3 cm gap, the drying rate when using C8 mesh electrode was 1.51, 1.21, and 1.2 times higher compared to C6 electrode with all metal wires at 3, 4.5, and 6.5 kV/cm, respectively. At 4 cm gap, the drying rate for C8 electrode was 1.21, 1.18, and 1.06 times higher compared to C6 at 3, 4.5, and 6.5 kV/cm, respectively; however, it was not significantly different at 6.5 kV/cm. Overall, it was found that electrode with less percentage (12.5%) of metal wires results in a higher drying rate compared to fully metal

electrode, and these experimental results are in agreement with numerical simulation of Defraeye and Martynenko (2019).

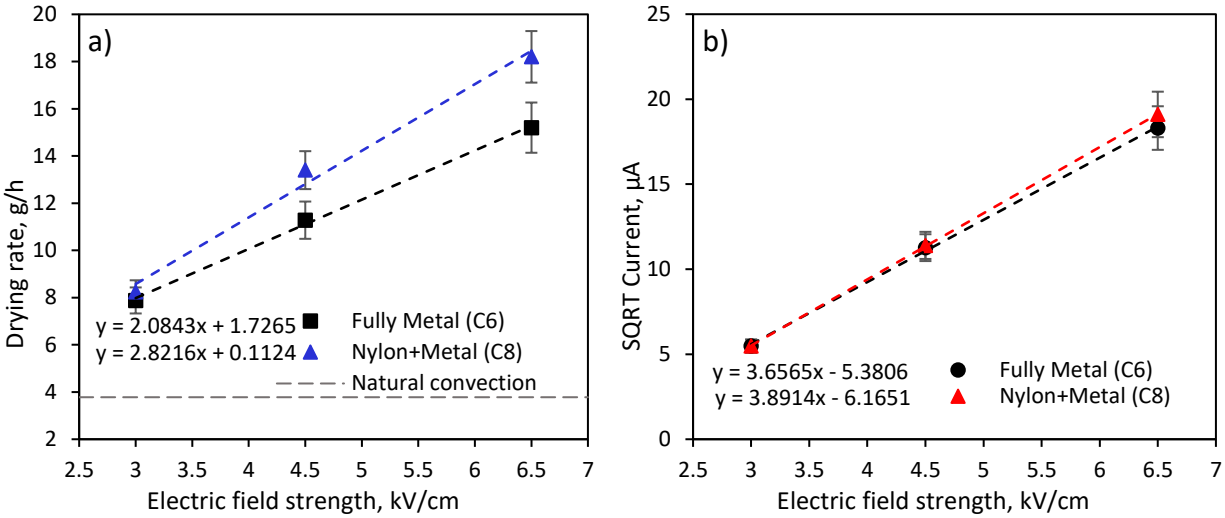


Figure 4.22 Drying rate (a) and square root of current (b) at 2 cm gap and different electric field strength for fully metal (C6) and nylon-metal mesh collecting electrode (C8)

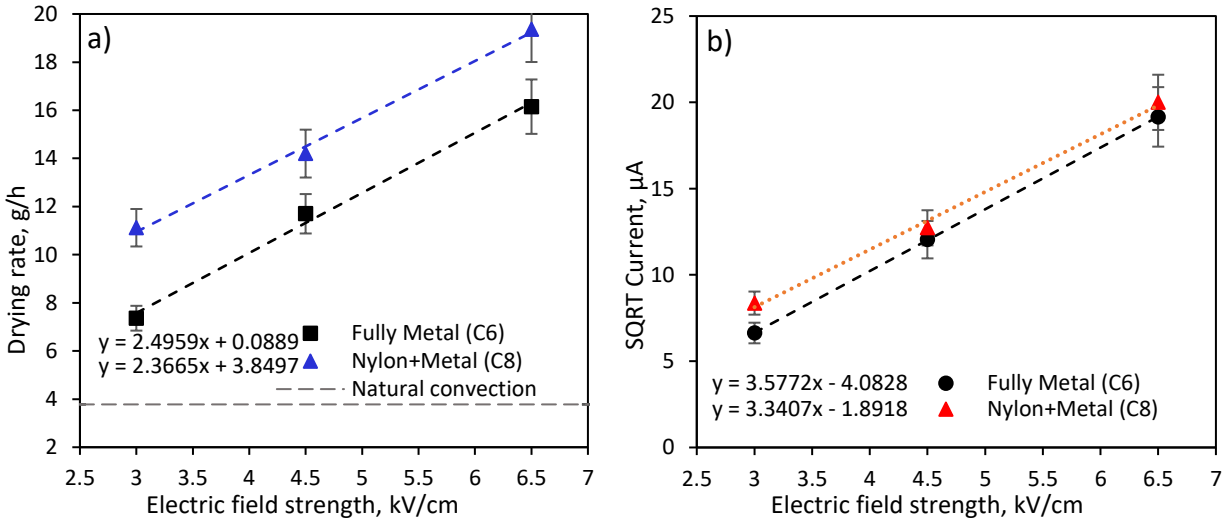


Figure 4.23 Drying rate (a) and square root of current (b) at 3 cm gap and different electric field strength for fully metal (C6) and nylon-metal mesh collecting electrode (C8)

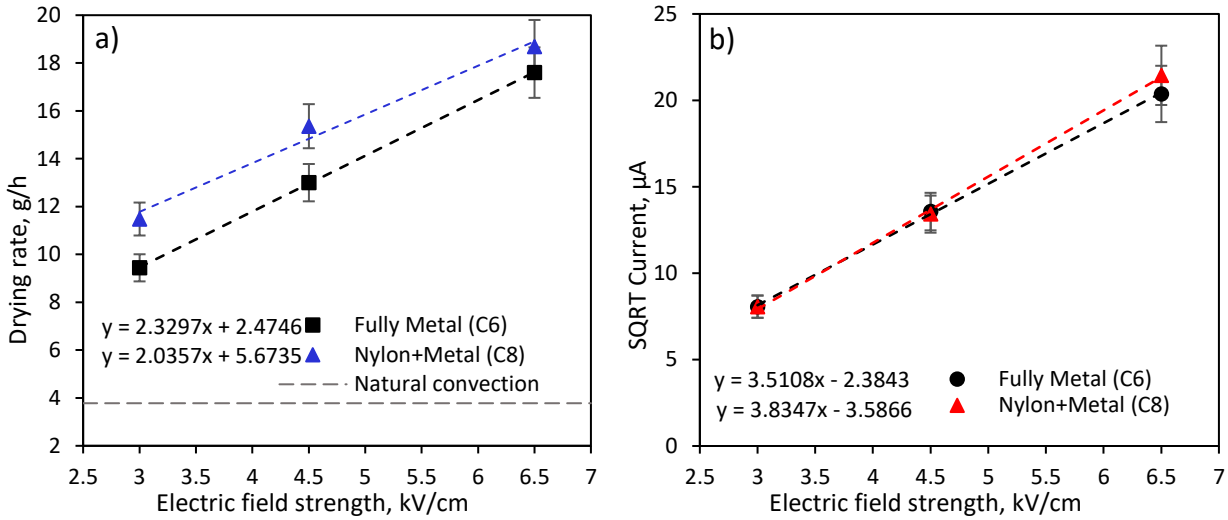


Figure 4.24 Drying rate (a) and square root of current (b) at 4 cm gap and different electric field strength for fully metal (C6) and nylon-metal mesh collecting electrode (C8)

*4.3.3.2 Specific Energy Consumption*

Square root of current for both C6 and C8 electrodes at 3, 4.5, and 6.5 kV/cm electric field strength is shown in Figures 4.22 (b), 4.23 (b), and 4.24 (b) at 2, 3, 4 cm gap, respectively. Current was the same for both electrodes at all conditions except 3 kV/cm at 3 cm gap, where current was significantly higher when using 12.5% metal mesh (C8) compared to 100% metal mesh (C6). Power used by each electrode in every second is shown in Figure 4.25. At 3 and 4.5 kV/cm, the power used by both electrodes was the same; however, at 6.5 kV/cm, the power used by C8 collecting electrode with 12.5% of metal wires was 1.09-1.11 times higher at all gaps compared to C6 100% metal electrode.

The bar chart in Figure 4.26 represents specific energy consumption calculated per first hour of drying. ANOVA analysis (Table 4.4) showed that there was no significant difference in energy consumption between C6 and C8 collecting electrodes at 3 kV/cm. Energy consumption in most cases were not significantly different at 4.5 and 6.5 kV/cm electric field strength, but at 4.5 kV/cm and 4 cm gap, energy consumption were

significantly higher when using fully metal mesh C6, while at 6.5 kV/cm and 4 cm gap the higher energy consumption were observed when using C8 electrode with 12.5% of metal wires.

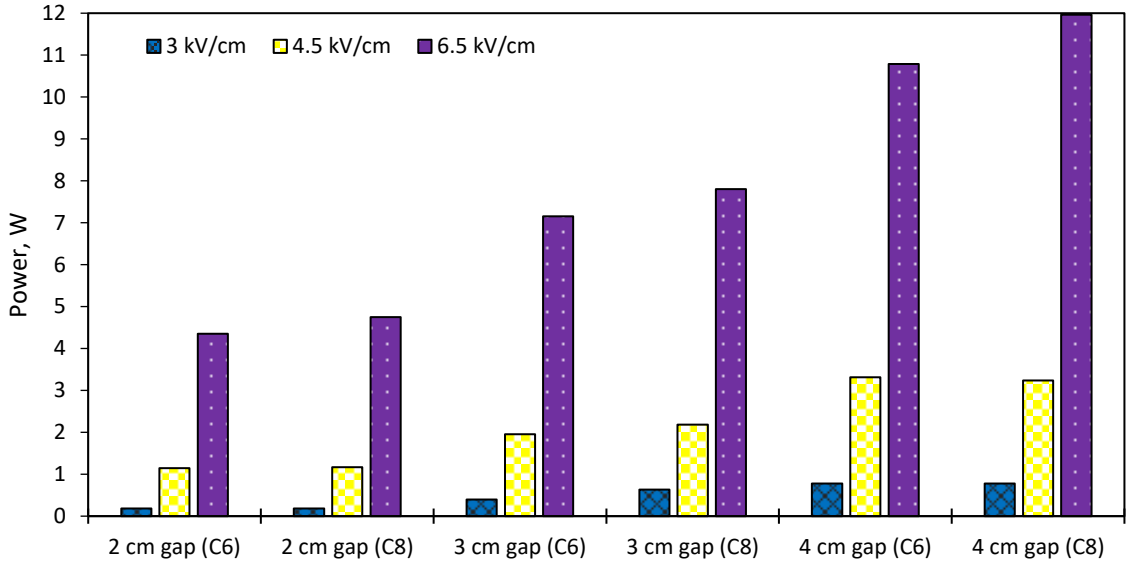


Figure 4.25 The values of power for C6 (100% of metal grounded wires) vs. C8 (12.5% of metal grounded wires) collecting electrodes at 2, 3, and 4 cm gap and 3, 4.5, and 6.5 kV/cm electric filed strength

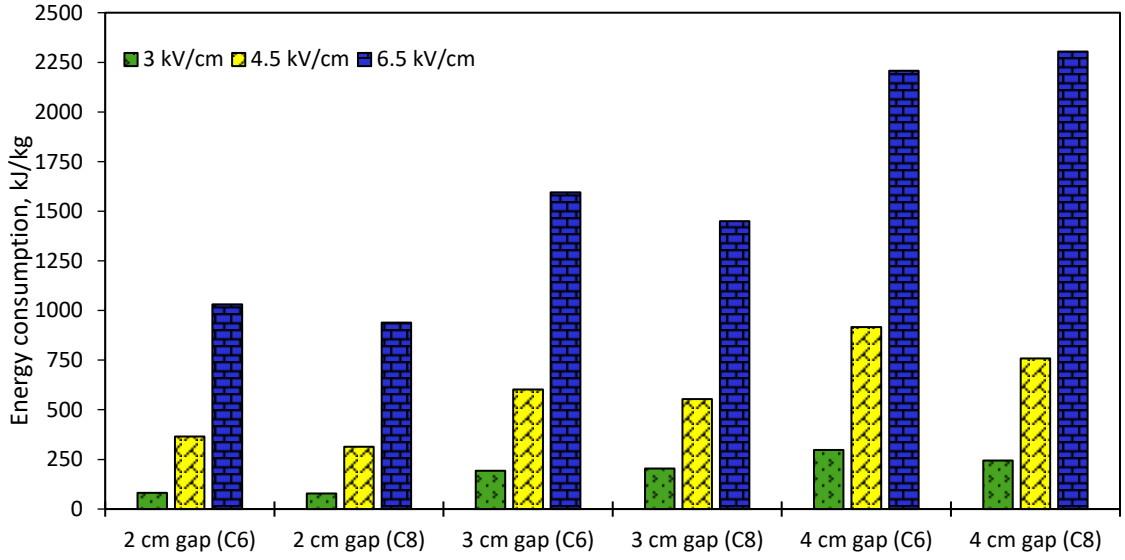


Figure 4.26 Specific energy consumption for C6 (100% of metal grounded wires) vs. C8 (12.5% of metal grounded wires) collecting electrodes at 2, 3, and 4 cm gap and 3, 4.5, and 6.5 kV/cm electric field strength

Table 4.4 Specific energy consumption in kJ/kg according to Figure 4.26

| E, kV/cm | 2 cm gap (C6) | 2 cm gap (C8) | 3 cm gap (C6) | 3 cm gap (C8) | 4 cm gap (C6) | 4 cm gap (C8) |
|---|---|---|---|---|---|---|
| **3** | 82.23 b | 78.64 b | 193.70 a | 203.96 a | 297.46 a | 244.60 a |
| **4.5** | 364.79 d | 314.33 d | 602.31 c | 554.45 c | 917.17 a | 759.375 b |
| **6.5** | 1031.45 e | 938.57 e | 1595.26 c | 1450.41 d | 2207.05 b | 2304.93 a |

*Note*. Means sharing the same letter in the row are not significantly different.

*4.3.3.3 Volt-Ampere Characteristics*

Volt-ampere characteristics were measured for both C6 vs. C8 electrodes at 2, 3, and 4 cm gap from the inception to the breakdown voltage with increment of one kV. These measurements were provided for both electrodes with or without wet paper towel on the surface. Volt-ampere characteristics are shown in Figures 4.27, 4.28, and 4.29 for the gap of 2, 3, and 4 cm gap, respectively. It follows that there were no significant different in volt-ampere characteristics for fully metal collecting electrode C6 with and without wet paper towel on the surface, while for nylon-metal collecting electrode C8 there was a significant difference observed in current. Current was significantly lower when C8 collecting electrode was used without wet paper towel on the surface. It is important to note that when using the wet paper towel, the values of current at certain voltages were not significantly different between both fully metal (C6) and 12.5% metal (C8) collecting electrodes, but when using these electrodes without wet paper towel, current was significantly lower at 12.5% metal (C8) collecting electrode. This could be due high moisture in the air between electrodes when using wet paper towel.

Another factor leading to these results could be the non-transparent nature of material placed on the surface of collecting electrode. Wet paper towel covered 52% of the collecting electrode area, shielding the convective effect of different meshes on the drying rate. It can be concluded that sample size and aerodynamic properties play significant role

in EHD drying. Possibly, mesh can enhance the drying rate of smaller samples of wet material compared to larger ones due to the better convective conditions.

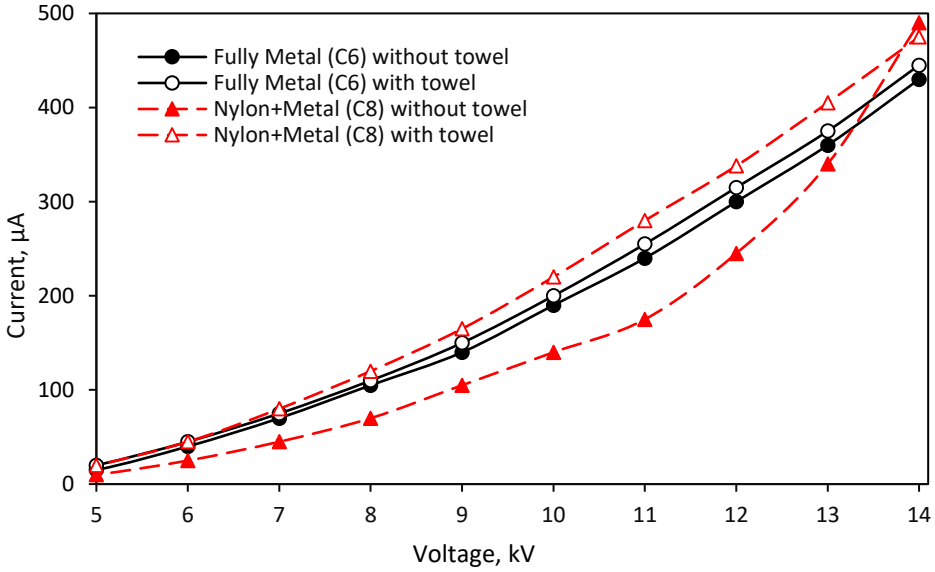


Figure 4.27 Current at 2 cm gap and all voltages for C6 (100% metal) and C8 (12.5% metal) mesh collecting electrodes with and without wet paper towel on the surface

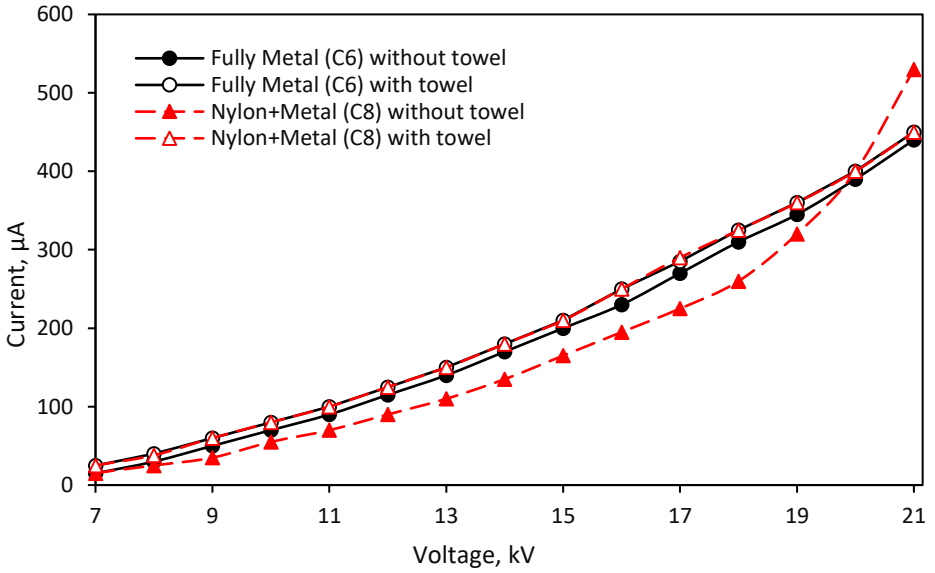


Figure 4.28 Current at 3 cm gap and all voltages for C6 (100% metal) and C8 (12.5% metal) mesh collecting electrodes with and without wet paper towel on the surface

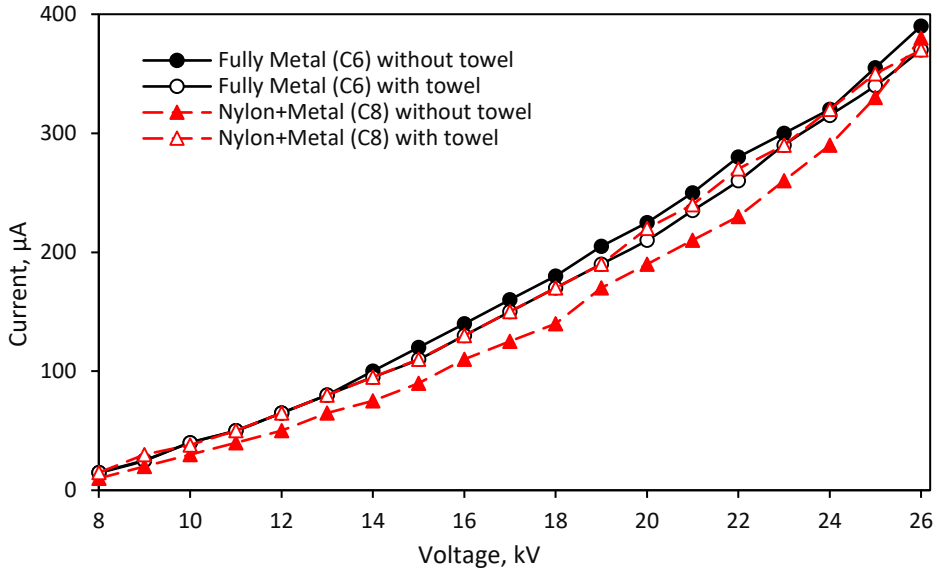


Figure 4.29 Current at 4 cm gap and all voltages for C6 (100% metal) and C8 (12.5% metal) mesh collecting electrodes with and without wet paper towel on the surface

*4.3.3.4 Conclusions*

1. Less percentage (12.5%) of grounded (metal) wires significantly improved drying rate of wet paper towel compared to 100% metal electrode.

2. Smaller percentage of grounded (metal) wires in mesh collecting electrode (C8) showed lower current when no wet paper towel was placed on the collecting electrode. However, the percentage of grounded wires did not affect current when collecting electrode was completely covered with the sheet of wet paper towel, which indicates that electrostatic field at collecting electrode is mostly determined by material properties.

3. Effect of percentage of grounded (metal) wires on energy consumption was significant for the EHD system without wet material on the surface of the collecting electrode, but was negligible for the drying of large area wet paper towel, possibly because of shielding effect of electrically conductive wet paper towel. The effect of material on the drying and volt-ampere characteristics should be further investigated.

# Chapter 5 General Conclusions and Recommendations

## 5.1 Achievements and General Discussion of the Results

To date, most researchers conducted their experiments on small lab setups with single wire or needle discharge electrodes in order to learn if EHD technology would enhance mass transfer. Although the researchers used different methodologies, they all confirmed that Electrohydrodynamic drying can be an excellent alternative to the currently existing drying technologies because of its low-cost, energy-efficiency, simplicity, and high quality of the dried product.

There was not enough information about all conditions the experiments were carried out at. In this thesis, previous research was analyzed and the key factors affecting EHD drying process were found and categorized (Chapter 2, Section 2.2). All these factors should be always considered for the further investigation of EHD drying processes. From this end, the thesis was focused on optimization of EHD electrodes configuration for further upscaling of the technology towards industrial prototype.

Ionic wind visualization described in Chapter 3 (Section 3.2) enabled to calculate the exposed area of food material to the ionic wind. Using this method, the angle of ionic wind spreading from the needle tip can be measured. It was found that sharper needles result in the narrower ionic wind cone, whereas thicker needles lead to the wider spreading of ionic wind jets. From this confirmation, thicker conical needles such as construction nails ($d_1 = 1.8$ mm, $r_{tip1} = 0.25$ mm) and pins ($d_3 = 0.7$ mm, $r_{tip3} = 0.09$ mm) are recommended to be used as emitters in the multiple discharge electrodes. Sharp needles are not recommended to use because of their discharge instability, low work range, and inefficiency compared to the thicker ones.

In upscaling of multiple needle discharge electrodes for EHD dryer, the following factors should be considered: needle shape and so angle of ionic wind jets spreading, optimum spacing between needles and gap between needles tips and collecting electrode, and needle arrangement (chess vs. square array). It is very important to mention one of the most important achievements of this work, which is a new methodology for engineering of a multiple needle/wire discharge electrode (Chapter 3, Section 3.3). Using 3D modeling and 3D printing, the highly precise dimensions were achieved in the discharge electrode configuration, which is one of the most critical conditions for uniform corona discharge. This methodology is one of the most convenient ways for upscaling of EHD drying electrodes from small scale to large industrial types.

Mesh collecting electrode was proposed as an alternative to a solid collecting plate in EHD dryer. The experimental results confirmed initial findings from numerical simulation, that metal mesh collecting electrodes can significantly increase drying rate while consuming the same amount of energy as compared to solid metal plates. Significant effect of open area on the drying rate was observed for mesh collecting electrode configuration. Electrode with the smallest open area of 36% (C2) and electrode with the largest open area of 73% (C4) were found to be the most effective in removing moisture. The effect of wire diameter in the collecting electrode on the drying rate and energy consumption was found to be negligible. Smaller number of grounded (metal) wires in a mesh collecting electrode was found to be more effective compared to fully metal mesh collecting electrode. Overall, mesh collecting electrodes are recommended to use in large scale EHD dryers due to a better convection regime.

## 5.2 Recommendations for Future Research

Based on the analysis in Chapter 2, the following gaps in EHD drying processes should be investigated:

- effect of electrodes material;
- effect of current type (AC vs. DC) and current polarity (DC+ vs. DC-) on drying rate and energy consumption;
- effect of polarization of water molecules and their movement in EHD system;
- the most efficient and effective way of EHD combination with air flow in order to move out of the EHD chamber the removed moisture from the sample; the most effective blower location for air movement through the EHD system should be found;
- effect of food material on the drying process.

The effect of electrodes material on the ionic wind and drying rate has been rarely investigated. Moreover, the material of electrodes should be chosen based on the engineering perspectives, such as long-term usage, corrosion resistance, material cost and others.

Even though Zheng et al. (2011) reported higher drying rate when using AC, it is important to note, that as a basis for the comparison, they used the same electric field strength (1.0-1.25 kV/cm) but did not provide comparison of the electric current. In contrast, Yang and Ding (2016) reported that AC current is much higher compare to DC at the same electric field strength (Yang and Ding, 2016), so that a fair comparison of AC vs. DC is required based on the drying rate and energy consumption.

Effect of moisture removal and water polarization in EHD system is still unclear as a trajectory of polarized water molecules is still unexplored yet. Visualization of ionic wind

with imaging gave us an idea about trajectory of charged particles, but trajectories of water molecules should be further investigated and confirmed experimentally. Once this research would be done, one would be able to design EHD apparatus with the optimal aerodynamic flow field, allowing to effectively remove water from the drying space.

Different material properties can affect the drying process in EHD system (section 2.2, Chapter 2). Further operation of EHD system should consider a transition from constant to falling drying rate period, when a diffusion-limited processes in the wet samples occur. Density, porosity, capillarity, diffusivity, texture and even surface properties such as surface roughness of wet material (Martynenko et al., 2017b) affect the drying process in EHD system. Because of that a method for food sample preparation before EHD drying should be developed by considering the most effective size, shape, thickness, and initial moisture content of food samples to be set before EHD drying. It is also important to note that the material shrinkage can affect the drying process. Hence, this factor should be monitored during drying in order to keep certain EHD drying conditions. This real-time monitoring can be done using computer vision proposed by Wang (2016).

Another interesting fact should be considered such as electrostatic attraction of dry samples towards discharge electrode. For example, during EHD drying of mushroom slices (Martynenko et al., 2019), the movement of a few samples towards discharge electrode created breakdown of EHD system. Because of that, an additional measure to prevent moving of food samples from the surface of collecting electrode is required.

Chapter 3 was focused on optimization of a multiple needle discharge electrode; the chess arrangement of needles should be considered as an alternative to the square array arrangement. It is worthwhile to investigate an additional rotation effect of created with needles ionic wind on the drying rate, confirmed by our ionic wind visualization. Also, it

is highly recommended to investigate the drying rate and energy consumption using multiple wire discharge electrode because of easier engineering. It would be also interesting to use our ionic wind visualization approach to see the ions movement in EHD system when using wires instead of sharp needles.

One of the key questions in EHD drying technology is to find an efficient high-voltage power transformer to use. Most of the previously published research did not distinguish between total power vs. discharge power (specific energy consumption). Specific energy consumption used by EHD drying was found to be extremely low compared to the total energy used by power equipment. In order to build the most efficient EHD dryer, energy losses in power transformer should be minimized.

Overall, the findings obtained in this research significantly contribute to the further upscaling of EHD drying technology towards industrial prototypes. Building EHD systems is a significant step for further commercialization of this technology, which can significanty decrease energy consumption in agricultural and food sector. EHD drying has a great potential for small- and medium-size farmers due to energy saving and low cost compared to other drying techniques. It is environmentally friendly and a great way to dehydrate heat-sensitive food materials with rich nutritional content. Because of its low cost and energy consumption, EHD technology can be in a high demand in the whole world, including developing countries, which are in a need of proper long storage of harvested crops.

## References


Al Bdour, K., 2000. Electrohydrodynamic drying of viscous materials and agar gel. MSc Thesis McGill University.

Alemrajabi, A., Rezaee, F., Mirhosseini, M., Esehaghbeygi, A., 2012. Comparative evaluation of the effects of electrohydrodynamic, oven, and ambient air on carrot cylindrical slices during drying process. Drying Technology 30: 88–96.

Atungulu, G., Atungulu, E., Okada, R., Nishiyama, Y., 2005. Efficacy of high voltage treatment on tomato storage. Journal of Food Technology 3 (2): 209–2015.

Bai, Y., Hu, Y., Li, X., 2011. Influence of operating parameters on energy consumption of electrohydrodynamic drying. International Journal of Applied Electromagnetics and Mechanics 35: 57–65.

Bai, Y., Hu, Y., Li, X., 2010. The Tofu's characteristics of electrohydrodynamic drying with wire electrode. Presented at 2010 Asia-Pacific Power and Energy Engineering Conference (APPEEC), IEEE: 1–4.

Bai, Y., Li, J., Mei, Y., Kang, D.M., 2008. Experiment of drying kelp with high voltage electric field. In: International Conference on High Voltage Engineering and Application, Chongqing, China. pp. 732–734.

Bajgai, T.R., Hashinaga, F., 2001a. High electric field drying of Japanese radish. Drying Technology 19 (9): 2291–2302.

Bajgai, T.R., Hashinaga, F., 2001b. Drying of spinach with a high electric field. Drying Technology 19 (9): 2331–2341.

Bajgai, T.R., Raghavan, G.S.V., Hashinaga, F., Ngadi, M.O., 2006. Electrohydrodynamic drying – a concise overview. Drying Technology 24: 905–910.

Bardy, E., Manai, S., Havet, M., Rouaud, O., 2016. Drying kinetics comparison of methylcellulose gel vs. mango fruit in forced convective drying with and without electrohydrodynamic enhancement. ASME Journal of Heat Transfer 138: 1–5.

Barthakur, N.N., Arnold, N.P., 1995. Evaporation rate enhancement of water with air ions from a corona discharge. International Journal of Biometeorology 39: 29–33.

Basiry, M., Esehaghbeygi, A., 2010. Electrohydrodynamic (EHD) drying of rapeseed (*Brassica napus* L.). Journal of Electrostatics 68: 360–363.

Bashkir, I., Kudra, T., Martynenko, A., 2018. Electrically enhanced drying of white champignons. In: IDS'2018 - 21st International Drying Symposium, Valencia, Spain. pp. 571–578.

Cao, W., Nishiyama, Y., Koide, S., 2004a. Electrohydrodynamic drying characteristics of wheat using high voltage electrostatic field. Journal of Food Engineering 62: 209–213.

Cao, W., Nishiyama, Y., Koide, S., Lu, Z.H., 2004b. Drying enhancement of rough rice by an electric field. Biosystems Engineering 87 (4): 445–451.

Carlon, H.R., Latham, J., 1992. Enhanced drying rates of wetted materials in electric fields. Journal of Atmospheric and Terrestrial Physics 54 (2): 117–118.

Chen, Y.H., Barthakur, N.N., 1991. Potato slab dehydration by air ions from corona discharge. International Journal of Biometeorology 35: 67–70.

Chen, Y.H., Barthakur, N.N., 1994. Electrohydrodynamic (EHD) drying of potato slabs. Journal of Food Engineering 23: 107–119.

Dalvand, M.J., Mohtasebi, S.S., Rafiee, S., 2012a. Determining the influence of drying conditions on EHD drying process. ARPN Journal of Agricultural and Biological Science 7 (6): 396–401.

Dalvand, M.J., Mohtasebi, S.S., Rafiee, S., 2012b. Study of effective structural parameter on drying rate of kiwi fruits in a solar EHD dryer. International Journal of Multidisciplinary Sciences and Engineering 3 (5), 66–70.

Dalvand, M.J., Mohtasebi, S.S., Rafiee, S., 2013. Effect of needle number on drying rate of kiwi fruit in EHD drying process. Agricultural Sciences 4 (1): 1–5.

Defraeye, T., Martynenko, A., 2018. Future perspectives for electrohydrodynamic drying of biomaterials. Drying Technology 36: 1–10.

Defraeye, T., Martynenko, A., 2019. Electrohydrodynamic drying of multiple food products: evaluating the potential of emitter-collector electrode configurations for upscaling. Journal of Food Engineering 240: 38–42.

Dinani, S.T., Havet, M., 2015. The influ1ence of voltage and air flow velocity of combined convective-electrohydrodynamic drying system on the kinetics and energy consumption of mushroom slices. Journal of Cleaner Production 95: 203–211.

Dinani, S.T., Havet, M., Hamdami, N., Shahedi, M., 2014. Drying of mushroom slices using hot air combined with an electrohydrodynamic (EHD) drying system. Drying Technology 32 (5): 597–605.

Ding, C., Lu, J., Song, Z., 2015. Electrohydrodynamic drying of carrot slices. PloS ONE 10 (4): e0124077. DOI: 10.1371/journal.pone.0124077.

Drew, D.S., Pister, K.S.J., 2017. Geometric optimization of microfabricated silicon electrodes for corona discharge-based electrohydrodynamic thrusters. Micromachines 8 (5): 1–13.

Elmizadeh, A., Shahedi, M., Hamdami, N., 2017. Comparison of electrohydrodynamic and hot-air drying of the quince slices. Innovative Food Science and Emerging Technologies 43: 130–135.

Esehaghbeygi, A., 2012. Effect of electrohydrodynamic and batch drying on rice fissuring. Drying Technology 30 (14): 1644–1648.

Esehaghbeygi, A., Basiry, M., 2011. Electrohydrodynamic (EHD) drying of tomato slices (*Lycopersicon esculentum*). Journal of Food Engineering 104: 628–631.

Esehaghbeygi, A., Pirnazari, K., Sadeghi, M., 2014. Quality assessment of electrohydrodynamic and microwave dehydrated banana slices. LWT – Food Science and Technology 55: 565–571.

Feng, Y., Seyed-Yagoobi, J., 2004. Understanding of electrohydrodynamic conduction pumping phenomenon. Physics of Fluids 16: 2432–2441.

Fylladitakis, E.D., Theodoridis, M.P., Moronis, A.X., 2014. Review on the history, research, and applications of electrohydrodynamics. IEEE Transactions on Plasma Science 42 (2): 358–375.

Gallo, C.F., Germanos, J.E., Courtney, J.E., 1969. The effect of humidity and temperature variations on the behavior of wire-to-plane coronas. Research and Engineering Sciences Division, Rochester, New York 14603: 111–119.

Giri, S.K., Prasad, S., 2007. Drying kinetics and rehydration characteristics of microwave-vacuum and convective hot-air dried mushrooms. Journal of Food Engineering 78 (2): 512–521.

Grosu, F.P., Bologa, A.M., Paur, H.-R., Bologa, M.K., Motorin, O.V., 2014. Generalization of the Townsend current-voltage characteristics of a corona discharge. Surface Engineering and Applied Electrochemistry 50 (4): 306–310.

Hashinaga, F., Bajgai, T.R., Isobe, S., Barthakur, N.N., 1999. Electrohydrodynamic EHD drying of apple slices. Drying Technology 17 (3): 479–495.

Hashinaga, F., Kharel, G.P., Shintani, R., 1995. Effect of ordinary frequency high electric fields on evaporation and drying. Food Science and Technology International 1 (2): 77–81.

Henson, B.L., 1983. Toward a fundamental model for steady point-plane corona discharges. Journal of Applied Physics 5 (1): 150–157.

Isobe, S., Barthakur, N., Yoshino, T., Okushima, L., Sase, S., 1999. Electrohydrodynamic drying characteristics of agar gel. Food Science and Technology Research 5 (2): 132–136.

Kiousis, K.N., Moronis, A.X., Fruh, W.G., 2014. Electro-hydrodynamic (EHD) thrust analysis in wire-cylinder electrode arrangement. Plasma Science and Technology 16 (4): 363–369.

Kirschvink-Kobayashi, A., Kirschvink, L.J., 1986. Electrostatic enhancement of industrial drying processes. Industrial & Engineering Chemistry Process Design and Development 25 (4): 1027–1030.

Kudra, T., Martynenko, A., 2015. Energy aspects in electrohydrodynamic drying. Drying Technology 33: 1534–1540.

Kudra, T., Martynenko, A., 2019. Electrohydrodynamic drying: theory and experimental validation. Drying Technology. DOI: 10.1080/07373937.2019.1628773.

Lai, F.C., Huang, M., Wong, D.S., 2004. EHD-enhanced water evaporation. Drying Technology 22 (3): 597–608.

Lai, F.C., Wong, D.S., 2003. EHD-enhanced drying with needle electrode. Drying Technology 21: 1291–1306.

Li, K., Zhang, M., Mujumdar, A.S., Chitrakar, B., 2019. Recent developments in physical field-based drying techniques for fruits and vegetables. Drying Technology. DOI: https://doi.org/10.1080/07373937.2018.1546733.

Liang, Y-Z., Ding, C-J., 2006. High Voltage Electric Field Drying. In: Pan, Y-K., Wang, X-Z., Liu, X-D. (Eds.), Modern Drying Technologies, Second Enhanced Edition, Chemical Industry Press, Beijing. pp. 840–858 (in Chinese).

Martynenko, A., Astatkie, T., Riaud, N., Wells, P., Kudra, T., 2017b. Driving forces for mass transfer in electrohydrodynamic (EHD) drying. Innovative Food Science and Emerging Technologies 43: 18–25.

Martynenko, A., Bashkir, I., Kudra, T., 2019. Electrically enhanced drying of white champignons. Drying Technology. DOI: 10.1080/07373937.2019.1670672.

Martynenko, A., Kudra, T., 2016a. Electrically-induces transport phenomena in EHD drying – A review. Trends in Food Science and Technology 54: 63–73.

Martynenko, A., Kudra, T., 2016b. Electrohydrodynamic (EHD) drying of grape pomace. Japan Journal of Food Engineering 17 (4): 123–129.

Martynenko, A., Kudra, T., Yue, J., 2017a. Multipin EHD dryer: Effect of electrode geometry on charge and mass transfer. Drying Technology 35 (16): 1970–1980.

Maskell, B.R., 1970. The effect of humidity on corona discharge in air. Royal Aircraft Establishment. Technical report 70106. U.D.C. 533.276: 621.3.015.532.

Martynenko, A., Zheng, W., 2015. Electrohydrodynamic drying of apple slices: energy and quality aspects. Journal of Food Engineering 168: 215–222.

McLean, K.J., Ansari, I.A., 1987. Calculation of the rod-plane voltage/current characteristics using the saturated current density equation and Warburg's law. IEE proceedings 134A (10): 784–788.

Misra, N.N., Yadav, B., Roopesh, M.S., Jo, C., 2018. Cold plasma for effective fungal and mycotoxin control in foods: mechanisms, inactivation effects, and applications. Comprehensive reviews in Food Science and Food Safety 00: 1–15.

Monrolin, N., Plouraboe, F., Praud, O., 2017. Electrohydrodynamic thrust for in-atmosphere propulsion. AIAA Journal ISSN 0001–1452: 1–10.

Montgomery, D.C., 2017. Design and Analysis of Experiments. 9th edition. Wiley, New York.

Moreau, E., 2007. Airflow control by non-thermal plasma actuators. Journal of Physics D: Applied Physics 40: 605–636.

Moses, J.A., Norton, T., Alagusundaram, K., Tiwari, B.K., 2014. Novel drying techniques for the food industry. Food Engineering Reviews 6: 43–55.

Ngamwonglumlert, L., Devahastin, S., 2018. Food microstructure and its relationship with quality and stability. DOI: https://doi.org/10.1016/C2015-0-01352-1.

Panchenko, M.S., Mosiyevich, A.S., Voloshyn, O.M., Ivashchuk, Y.H., 1980. About drying under influence of constant non-uniform electric and magnetic fields. Surface Engineering and Applied Electrochemistry 3 (93): 76–80 (in Russian).

Peek, F.W., 1929. Dielectric Phenomena in High-Voltage Engineering. McGraw-Hill Book Company, Incorporation, New York.

Pirnazari, K., Esehaghbeygi, A., Sadeghi, M., 2016. Modeling the electrohydrodynamic (EHD) drying of banana slices. International Journal of Food Engineering 12 (1): 17–26.

Pogorzelski, M., Zander, Z., Zander, L., Wrotniak, M., 2013. Drying kinetics of plant material in the electrohydrodynamic (EHD) process. University of Warmia and Mazury, Poland.

Precht, J., 1883. Absolute messungen über das ausströmmen der electricität aus spitzen. Physikalischen Institut der Universität Bonn (in German).

Ramachandran, M.R., Lai, F.C., 2010. Effects of porosity on the performance of EHD-enhanced drying. Drying Technology 28: 1477–1483.

Robinson, M., 1961. Movement of air in the electric wind of the corona discharge. Journal of AIEE 80 (2): 143–150.

Singh, A., 2014. Electrohydrodynamic drying (EHD) and its associated effects on conformation of food proteins using molecular modeling concept. PhD Thesis, McGill University.

Singh, A., Orsat, V., Raghavan, V., 2013. A comprehensive review on electrohydrodynamic drying and high-voltage electric field in the context of food and bioprocessing. Drying Technology 30: 1812–1820.

Stuetzer, O.M., 1959. Ion drag pressure generation. Journal of Applied Physics 30 (7): 984–994.

Sumariyah, K.A., Fachriyah, E., 2018. Ion wind generation and its application to drying of wild Ginger slices (Curcuma Xanthorhiza). Journal of Physics: Conference Series 1025 012016: 1–6.

Sumorek, A., Pietrzyk, W., 2004. The influence of corona wind on the convective drying course. Physics and Chemistry of Solid State 5 (2): 377–381.

Tansakul, A., Lumyong, R., 2008. Thermal properties of straw mushroom. Journal of Food Engineering 87: 91–98.

Taylor, G. I., 1966. Studies in electrohydrodynamics. I. The circulation produced in a drop by an electric field. Proceedings of the Royal Society A. Mathematical, Physical and Engineering Sciences. DOI: https://doi.org/10.1098/rspa.1966.0086.

Thirumdas, R., Saragapani, C., Ajinkya, M.T., Deshmukh, R.R., Annapure, U.S., 2016. Influence of low pressure cold plasma on cooking and textural properties of brown rice. Innovative Food Science and Emerging Technologies 37: 53–60.

Tirawanichakul, S., Tasara, J., Tirawanichakul, Y., 2009. High electric field enhance drying and aging of rough rice. In: Commemorative International Conference on the Occasion of the 4$^{th}$ Cycle Celebration of KMUTT Sustainable Development to Save the Earth: Technologies and Strategies Vision 2050: (SDSE2008). Bangkok, Thailand. pp. 428–433.

Townsend, J.S., 1915. Electricity in Gases. Oxford. Clarendon Press.

Vega-Galvez, A., Ah-Hen, K., Chacana, M., Vergara, J., Martinez-Monzo, J., Garcia-Segovia, P., Lemus-Mondaca, R., Di-Scala, K., 2012. Effect of temperature and air

velocity on drying kinetics, antioxidant capacity, total phenolic content, colour, texture and microstructure of apple (var. Granny Smith) slices. Food Chemistry 132: 51–59.

Wang, D., 2016. Prediction of texture characteristics in apple drying using computer vision. MSc Thesis, Dalhousie University.

Warburg, E., 1927. About silent discharge in gases. Handbuch der Physik 14: 149–170 (in German).

Xue, G.R., Limoto, M., Uchino, T., 1996. Drying of shiitake mushrooms using ionic wind generated be corona discharge. Journal of the Japan Society of Agricultural Machinery 58 (4): 53–60 (in Japanese).

Xue, G.R., Uchino, T., Matsuo, M., 1994. Drying promotion of radish using corona discharge. Journal of the Japanese Society of Agricultural Machinery 56 (5): 35–42 (in Japanese).

Yabe, A., Mori, Y., Hijikata, K., 1977. EHD study of the corona wind between wire and plate electrodes. AIAA Journal 16 (4): 340–345.

Yang, M., Ding, C., 2016. Electrohydrodynamic (EHD) drying of the Chinese wolfberry fruits. SpringerPlus 5 (909): 1–20.

Zhang, B., He, J., Ji, Y., 2017. Dependence of the average mobility of ions in air with pressure and humidity. IEEE Transactions on Dielectric and Electrical Insulation 24 (2): 923–929.

Zheng, D.-J., Liu, H.-J., Cheng, Y.-Q., Li, L.-T., 2011. Electrode configuration and polarity effects on water evaporation enhancement by electric field. International Journal of Food Engineering 7 (2): 1–12.

# Appendices

## Table A.1 EHD drying of water and plant-based materials (A)

| Reference | Material | Discharge electrode | Collecting electrode | Environmental conditions | Gap, cm | Voltage, kV | E, kV/cm | Current | Drying kinetics | Major findings |
|---|---|---|---|---|---|---|---|---|---|---|
| Kirshvink-Kobayashi and Kirshvink (1986) ♦ | Wet filter paper, ($A$=0.0177 m$^2$) | Multiple needles | Metal plate | 90ºC heating from above<br>90ºC heating from below | 5.0 | 5<br>9<br>10<br>15 | 1<br>1.8<br>2<br>3 | AC<br>DC+<br>DC- | Linear | ▪ EHD increased drying rate 1.6-2.3 times compared to control (90ºC, no DC/AC)<br>▪ DC was more effective than AC |
| Chen and Barthakur (1991) | Potato slices ($l$=2.8-5 mm) | Sewing needle | Aluminum plate, $A$=0.0022 m$^2$ | 21ºC<br>30% RH | 1.0 | 5.25 | 5.25 | DC+ | Linear | ▪ EHD increased drying rate 2.2-3 times compared to control (no DC+) |
| Carlon and Latham (1992) | Wet towel paper | Copper disk, $A$=0.0028 m$^2$ | Copper disk, $A$=0.0028 m$^2$ | 25ºC<br>50% RH<br>small airflow | 2.0 | 0-14 | 0-7 | AC | Linear | ▪ Drying rate linearly increased with electric field strength<br>▪ Drying rate increased as RH decreased |
| Chen and Barthakur (1994) | Potato slices ($A$=0.0022 m$^2$, $l$ = 2, 4, 8 mm) | Sewing needle | Aluminum plate, $A$=0.0022 m$^2$ | 21.7±1.6ºC<br>29.9±3.6% RH | 1.0 | 5.25 | 5.25 | DC+ | Linear | ▪ EHD drying depends on sample thickness. The average ratios of EHD evaporation to free convection were 2.5, 2.5 and 2.1 for thickness 2, 4, and 8 mm, respectively |
| Xue et al. (1994) | Radish | Multiple needle | Stainless-steel mesh | 40, 50, 60ºC<br>20, 30, 40% RH<br>0.05, 0.2, 0.5 m/s | 2.0 | 10 | 5 | AC | Exponential | ▪ EHD drying rate was 1.2-1.3 times greater than sole forced convective drying under various air flow rates<br>▪ Effect of EHD decreased with increase of air flow<br>▪ Air temperature and RH did not affect EHD drying |

Table A.1 EHD drying of water and plant-based materials, Continued

| Reference | Material | Discharge electrode | Collecting electrode | Environmental conditions | Gap, cm | Voltage, kV | E, kV/cm | Current | Drying kinetics | Major findings |
|---|---|---|---|---|---|---|---|---|---|---|
| Barthakur and Arnold (1995) | Distilled water | Sewing needle | Aluminum plate, $A$=0.0026 m$^2$ | 20ºC 32.6% RH | 0.5<br>1.0<br>2.0 | 5.25 | 10.5<br>5.25<br>2.63 | DC+<br>DC- | Linear | ▪ Negative DC features higher drying rate than positive<br>▪ The optimal gap was 1.0 cm, giving maximum EHD enhancement of drying rate. Smaller (0.5 cm) and larger (2 cm) gaps resulted in lower drying rates |
| Hashinaga et al. (1995) | Water ($A$=0.0031 m$^2$) | Copper wire ($r$ =0.5 mm) or plate ($A$=0.06 m$^2$) | Copper plate, $A$=0.06 m$^2$ | 25ºC 30% RH | 1.5<br>2.0 | 8.6<br>12.8 | 4.3<br>8.53 | AC<br>DC+<br>DC- | Linear | ▪ Drying rate increased linearly with electric field strength<br>▪ EHD with gap larger than 5 cm did not affect drying rate<br>▪ Positive DC resulted in higher drying rate than the negative one<br>▪ Wire discharge electrode resulted in a higher drying rate than plate electrode |
| | Apple slices ($A$=0.0003 m$^2$, $l$=10 mm) | | | | | 0<br>5.7<br>7.9<br>10 | 0<br>2.85<br>3.95<br>5 | | Exponential | ▪ Drying was faster as electric field increased<br>▪ Natural convection took 16 h, while AC treated samples were dried until reaching the same moisture content only in 10 h |
| Xue et al. (1996) | Mushroom cups ($A$=0.0013-0.0028 m$^2$) | Multiple needle | Stainless-steel mesh | 45±0.5ºC 40±2% RH 0.1, 0.2, 0.3, 0.4 m/s | 2.0 | 6<br>8<br>10<br>12 | 3<br>4<br>5<br>6 | AC | Exponential | ▪ EHD drying rate increased with increasing of voltage and decreased with increasing of air flow rate<br>▪ EHD drying rate was 1.1-1.6 times higher than control |
| Isobe et al. (1999) | 1% agar gel ($A$=0.0024 m$^2$, $l$=5 mm) | Single needle | Titanium plate | 25, -14ºC 60% RH | 1.0<br>1.5 | 3-15 | 3-10 | DC+ | Linear | ▪ DR increased with increase of electric field and decreased logarithmically with increase of electrode gap at 25ºC<br>▪ The sublimation rate of EHD-exposed agar gel at -14ºC was higher than in natural convection |

Table A.1 EHD drying of water and plant-based materials, Continued

| Reference | Material | Discharge electrode | Collecting electrode | Environmental conditions | Gap, cm | Voltage, kV | E, kV/cm | Current | Drying kinetics | Major findings |
|---|---|---|---|---|---|---|---|---|---|---|
| Hashinaga et al. (1999) * | Apple slices ($A$=0.0058 m$^2$, $l$=2-3 mm) | 1-3 thick copper or thin stainless steel sewing needles | Aluminum plate | 18±1ºC 33-65% RH | 1.0-3.0 | 3-16.5 | 3-5.5 | AC | Exponential | ▪ EHD drying rate increased 3-4.5 times compared to control (no AC)<br>▪ 1.3 cm gap led to the maximum effect of EHD drying<br>▪ Stainless steel sewing needles resulted in 1.2 times higher drying rate than copper needles |
| Al Bdour (2000) | a) 0, 20, 40, 60 and 70% sugar with water;<br>b) 0.5:1, 1:1, 1.5:1, and 2:1 glycerin with water;<br>c) Agar gel | Single needle | Aluminum plate, $A$=0.0026 m$^2$ | 22±2ºC 45±15% RH 2.5 m/s | 1.0 | 5.25 | 5.25 | DC+ DC- | Linear | ▪ DRs of sugar solution at EHD and 2.5 m/s were 3-5 times higher than free convective drying and sole EHD, depending on viscosity<br>▪ DRs of glycerin-water at EHD and 2.5 m/s drying were 3-5 times higher than free convection drying<br>▪ DR of agar gel at EHD and 2.5 m/s and sole EHD drying were 4 and 3 times higher than free convection drying, respectively<br>▪ No significant difference between DR at DC+ (1.38 μA) and DC- (1.66 μA) |
| Bajgai and Hashinaga (2001a) * | Blanched radish slices ($l$=2 mm) | Multiple needle (7 needles, $r$ =0.8 mm, $r_{tip}$=0.015 mm) | Copper mesh | 25ºC 65% RH | 1.0 | 4.3 | 4.3 | AC | Linear | ▪ EHD drying removed almost the same amount of moisture as thermal drying at 60ºC after 7 h of drying, but at the rate 3.3 times higher compared to control (natural convection) |

Table A.1 EHD drying of water and plant-based materials, Continued

| Reference | Material | Discharge electrode | Collecting electrode | Environmental conditions | Gap, cm | Voltage, kV | E, kV/cm | Current | Drying kinetics | Major findings |
|---|---|---|---|---|---|---|---|---|---|---|
| Bajgai and Hashinaga (2001b) * | Pieces of spinach ($A$=0.0001-0.0002 m$^2$) | Multiple needle (7 needles) | Aluminum plate, $A$=0.0058 m$^2$ | 25ºC 65% RH | 1.0 | 4.3 | 4.3 | AC | Linear | ▪ EHD drying removed almost the same amount of moisture as thermal drying at 60ºC after 7 h of drying, but at the rate 4.2 times higher compared to control (natural convection) |
| Sumorek and Pietrzyk (2004) | Wheat grain | a) Metal plate b, c) Multiple needle | Metal plate | 30, 40, 50ºC 0.3-1.4 m/s | 3.0 | 6-12 | 2 3 4 | DC+ | Linear | ▪ Plate discharge electrode did not affect drying, only needle electrode increased drying rate twice as compared to control (forced air drying)<br>▪ Higher electric field increased DR, however positive effect disappeared at high air velocity (> 0.3 m/s) |
| Cao et al. (2004a) | Wheat grain ($A$=0.0189 m$^2$, $l$=10 mm) | Multiple needle (16 needles, $r$ =0.0005 mm) | Stainless-steel plate, $A$=0.0438 m$^2$ | 20, 35, 50ºC 55% RH | 3.0 4.0 5.0 6.0 | 10 20 30 | 1.67-10 | DC- | Linear | ▪ DR at 35ºC and electric field strength of 5, 7.5, and 10 kV/cm was 1.7, 2.0, and 2.1 times higher, compared to control (35ºC, no DC-)<br>▪ EHD DR at 6 kV/cm and 50, 35, and 20ºC was 1.5, 1.6, and 1.9 times higher than control (the same conditions). EHD effect decreased with air temperature |
| Cao et al. (2004b) * | Rice ($A$=0.0189 m$^2$, $l$=10 mm) | Multiple needle (16 needles, $r$ =0.0005 mm) | Stainless-steel plate, $A$=0.0438 m$^2$ | 25, 40, 50ºC 60% RH | 3.5 4.5 5.5 | 10 20 30 | 1.8-8.57 | DC- | Linear | ▪ DR at 40ºC, 4.5 cm gap and 10, 20 and 30 kV were 1.23, 1.43 and 1.59 times higher, respectively, compared to control (40ºC, no DC-)<br>▪ DR at 40ºC, 30 kV and 3.5, 4.5, and 5.5 cm gap increased by 1.81, 1.59, and 1.35 times, respectively, compared to control (40ºC, no DC-)<br>▪ EHD DRs at 30 kV, 4.5 cm gap and 25, 40 and 50ºC were 2.83, 1.59 and 1.63 times higher compared to control (25, 40, and 50ºC, no DC-) |

Table A.1 EHD drying of water and plant-based materials, Continued

| Reference | Material | Discharge electrode | Collecting electrode | Environmental conditions | Gap, cm | Voltage, kV | E, kV/cm | Current | Drying kinetics | Major findings |
|---|---|---|---|---|---|---|---|---|---|---|
| Lai et al. (2004) | a) Water<br>b) Water with glass beads of 3 and 6 mm in diameter | Single needle or wire ($r$ =0.25 mm) | Copper plate, $A$=0.0225 m$^2$ | 25ºC<br>1.0, 2.8 m/s | 1.28<br>2.54 | 9.6<br>19 | 7.5 | DC+<br>DC- | Linear | ▪ EHD DR increased linearly with increase of electric field strength<br>▪ DR at DC- was 1.16 times higher than DC+<br>▪ DR for needle was 1.31 times higher than for wire<br>▪ DR was higher for 6 mm layer of beads because of the larger pores and smaller capillarity<br>▪ For the first stage of drying (constant DR) effect of the surface conditions (roughness) was more pronounced than effect of inner porous structure |
| Liang and Ding (2006) ⁂ | a) Carrot slices (5 mm)<br>b) Potato slices ($l$=3 mm)<br>c) Cabbage ($l$=10 mm)<br>d) Green pepper ($l$=5 mm) | Multiple needle | Metal ground of $A$:<br>a) 2.0 m$^2$ (GXJ-2)<br>b) 16.0 m$^2$ (GXJ-16)<br>c) 10 m$^2$ (GTJ-1.7) | a) 36-42ºC for GXJ-2 and GXJ-16 models<br>b) >35ºC +vibration for GTJ-1.7 model | 10.0 | 35-40 | 3.5-4 | AC | n/a | ▪ EHD enhanced hot-air drying of carrots, potato, cabbage and green peppers by 30 to 43%<br>▪ Drying flux in pilot-scale prototype GXJ-2 and GXJ-16 was higher than 0.231 g/(s·m$^2$)<br>▪ Drying flux in pilot-scale prototype GTJ-1.7 was higher than 0.463 g/(s·m$^2$) |
| Bai et al. (2008) ⁎ | Kelp pieces ($A$=0.0056 m$^2$) | Multiple needle (25 needles, $r_{tip}$=0.01 mm) | Stainless steel plate, $A$=0.14 m$^2$ | 15±1ºC<br>65±3% RH | 9.0 | 5-55 | 0.6-6.1 | DC+ | Linear | ▪ EHD DR at 45 kV was 6.77 times higher compared to control (the same conditions), but 1.55 lower compared to thermal drying 60°C<br>▪ EHD DR at 55 kV was 9.8 times higher compared to control (the same conditions) |

Table A.1 EHD drying of water and plant-based materials, Continued

| Reference | Material | Discharge electrode | Collecting electrode | Environmental conditions | Gap, cm | Voltage, kV | E, kV/cm | Current | Drying kinetics | Major findings |
|---|---|---|---|---|---|---|---|---|---|---|
| Bai et al. (2010) ♦ | Tofu slices ($A$=0.0018 $m^2$) | Multiple wire with spacing a) 3-12 cm b, c) 9 cm | Stainless steel plate, $A$=0.14 $m^2$ | 18±1ºC 35±3% RH | a, c) 9.0 b) 5.0-11.0 | a) 45 b) 25-55 c) 0-50 | a) 5 b) 2.3-11 c) 0-5.6 | DC+ | Linear | ▪ DR of tofu slices increased linearly with voltage<br>▪ The highest DR was observed at 9 cm spacing between wires, 9 cm gap, and 45 kV, and it was almost 8 times higher than control (the same conditions) |
| Tirawani-chakul et al. (2009) ⁂ | Rice | Multiple needle (300 needles) | Aluminum plate | 40-70°C 2.0±0.1 m/s | 2.0 3.0 | 6 8 10 | 2-5 | AC | Linear | ▪ EHD at 4 kV/cm and 40°C significantly enhanced DR compared to control (the same conditions)<br>▪ EHD DR at 50°C was significantly higher at 2 cm gap than 3 cm |
| Basiry and Esehagh-beygi (2010) * | Rapeseeds ($A$=0.00011 $m^2$, $l$=10 mm) | Multiple needle (14 needles, $r$ =1.5 mm) | Aluminum plate, $A$=0.011 $m^2$ | 25°C 40% RH | 2.0 | 4 4.5 5 | 2-2.5 | DC+ | Linear | ▪ EHD DR at 4, 4.5, and 5 kV/cm was higher by 1.78, 2.11 and 2.47 times, respectively, compared to control (the same conditions)<br>▪ Final moisture content of dried samples decreased with increase of voltage to 17.1%, 15.43%, 13.03% on wet basis at 4, 4.5, and 5 kV/cm, respectively |
| Esehagh-beygi and Basiry (2011) ⁂ | Tomato slices ($l$=5 mm) | Multiple needle (14 needles, $r$ =1.5 mm) | Aluminum plate, $A$=0.011 $m^2$ | 24°C 30% RH | 2.0 | 6 8 10 | 3 4 5 | DC+ | Linear | ▪ EHD DR increased with voltage by 1.3, 1.43, and 2 times at 3, 4, and 5 kV/cm respectively, compared to control (the same conditions)<br>▪ Moisture content of dried samples decreased up to 11% at EHD 5 kV/cm. The same final moisture content was observed after thermal drying at 55°C, while after natural convection, the final moisture content was 49% |

Table A.1 EHD drying of water and plant-based materials, Continued

| Reference | Material | Discharge electrode | Collecting electrode | Environmental conditions | Gap, cm | Voltage, kV | E, kV/cm | Current | Drying kinetics | Major findings |
|---|---|---|---|---|---|---|---|---|---|---|
| Zheng et al. (2011) | Water ($A$=0.0084 m$^2$) | Single nickel-plated steel needle or multiple needle (space 1 cm) | Metal plate, $A$=0.1963 m$^2$ | 23-26ºC 30-40% RH | 4.0<br>6.0<br>8.0<br>10.0<br>12.0<br>16.0 | 5<br>10<br>15<br>20<br>25 | 0.31-5 | AC DC+ DC- | Linear | ▪ EHD DR increased with increase of electric field strength<br>▪ EHD DR was significantly higher at AC current compared to DC at both polarities |
| Alemrajabi et al. (2012) ⁂ | Carrot slices ($A$=0.0003-0.0007 m$^2$, $l$=2 mm) | Multiple needle (13 needles, $r$ =1 mm, $r_{tip}$=0.05 mm) | Stainless steel plate, $A$=0.0572 m$^2$ | 24±1°C 24.8% RH | 2.0<br>2.5<br>3.0 | 10<br>11.5<br>13 | 3.3<br>3.8<br>4<br>4.3<br>4.6<br>5<br>5.2<br>5.75<br>6.5 | DC+ DC- | Exponential | ▪ DRs for EHD at DC+ and DC-, and thermal drying at 55°C after the first hour of drying were 5.23, 5.08, and 4.62 times higher, respectively, and the amount of removed moisture after 5 h of drying was 3.62, 3.46, and 3.42 times higher, respectively, compared to control<br>▪ Electric field strength of 5.2 kV/cm resulted in the highest DR |
| Esehagh-beygi (2012) ⁂ | Rice ($l$=10 mm) | Multiple needle (14 needles, $r$ =1.5 mm) | Aluminum plate, $A$=0.0113 m$^2$ | 26°C 36% RH | 2.0 | 10 | 5 | DC+ | Linear | ▪ EHD at 10 kV reduced moisture content by about 4% in 50 minutes, while thermal drying at 45°C the time was 35 minutes |
| Dalvand et al. (2012, 2013) | Kiwi fruits slices ($A$=0.001-0.002 m$^2$) | Multiple needle (1, 9 or 17 stainless steel needles, $r_{tip}$=0.05 mm) | Metal plate or mesh, $A$=0.07 m$^2$: a) Galvanized iron b) Aluminum c) Copper | 24°C 20.8-21.4% RH | 0-8.0 | 6<br>10.5<br>15 | 4.5 | DC+ | Exponential | ▪ DR decreased with decrease of samples moisture content<br>▪ The highest DR was observed with aluminum plate, the smallest with galvanized iron<br>▪ Plate electrode resulted in a lower DR compared to mesh electrode and the difference increased with increase of voltage<br>▪ The highest DR was observed at EHD with one needle, decreasing with the increase of needle number |

Table A.1 EHD drying of water and plant-based materials, Continued

| Reference | Material | Discharge electrode | Collecting electrode | Environmental conditions | Gap, cm | Voltage, kV | E, kV/cm | Current | Drying kinetics | Major findings |
|---|---|---|---|---|---|---|---|---|---|---|
| Pogorzelski et al. (2013) ♦ | 0.0034 $m^2$ of: a) apples b) miscanthus c-f) carrots | Multiple needle: a) 102 needles b-f) 7 needles | Aluminum plate | 20.0±0.5°C 40-45% RH a, b) 1.45 m/s c, d) 1.33 m/s e) 1.09 m/s f) 1.18 m/s | 0.93 | a, b) 4.9 c, d) 4.5 e) 3.7 f) 4.0 | a, b) 5.27 c, d) 4.84 e) 3.98 f) 4.3 | a-c) DC+ d) DC- e, f) AC | Linear | ▪ The highest DR was observed at 4.84 kV/cm with DC+ (14 μA) and DC- (47 μA) with 7 needles<br>▪ Increase of needles' density from 7 to 102 resulted in the lowest DR with DC+<br>▪ Negative DC showed the best enhancement of DR. Positive DC was remarkable too, but caused breakdown<br>▪ EHD can increase DR of plant-based materials by 4 times compared to control (same conditions) |
| Esehagh-beygi et al. (2014) ⁂ Pirnazari et al. (2016) | Banana slices ($l$=3 mm) | Multiple needle (25 needles, $r$ =1.25 mm) | Stainless steel plate, $A$=0.0225 $m^2$ | 25°C 45±15% RH | 2.0 | 12 16 20 | 6 8 10 | DC+ | Exponential | ▪ DR increased with increase of electric field strength from 6 to 10 kV/cm<br>▪ EHD reduced convective resistance of banana slices to mass transfer, which became diffusion-limited |
| Singh (2014) ⁂ | Wheat grain | Single copper wire ($r$ =0.25 mm) | Aluminum plate, $A$=0.0025 $m^2$ | 20°C 45±15% RH 1, 1.5, 2 m/s | 1.5 2.0 2.5 | 7-25 | 2.8-16.7 | DC+ | Linear | ▪ EHD DR increased with increase of voltage and increase of air flow<br>▪ DR at EHD combined with air flow was significantly higher than control (the same conditions, no EHD) |
| Dinani et al. (2014) * ♦ | Blanched mushroom slices ($A$=0.00086 $m^2$, $l$=3.1-5 mm) | Multiple wire (6 thermocouple alloy wires, $r$ =0.127 mm) | Stainless steel plate, $A$=0.0758 $m^2$ | 60°C 10% RH | 5.0 6.0 7.0 | 17 19 21 | 2.4-4.2 | DC+ | Exponential | ▪ EHD DRs at 17, 19, and 21 kV and fixed gap 5 cm were 1.38, 1.41, and 1.43 times higher, compared to control after 2.5 h of drying.<br>▪ EHD DRs at 5, 6, and 7 cm and fixed voltage 21 kV were 1.52, 1.36, and 1.33 times higher, respectively, compared to control after 2.5 h drying. |

Table A.1 EHD drying of water and plant-based materials, Continued

| Reference | Material | Discharge electrode | Collecting electrode | Environmental conditions | Gap, cm | Voltage, kV | E, kV/cm | Current | Drying kinetics | Major findings |
|---|---|---|---|---|---|---|---|---|---|---|
| Dinani and Havet (2015) ♦ | Blanched mushroom slices ($l$=5 mm) | Single wire ($r$ =0.075 mm) | Metal mesh, $A$=0.0292 m$^2$ | 45°C 10% RH 0.4, 2.2 m/s | 6.0 | 20 25 30 | 3.33 4.17 5 | DC+ | Exponential | ▪ Effect of EHD was significant at 0.4 m/s, but was not significant at 2.2 m/s<br>▪ DRs at EHD (combined with 0.4 m/s) at 3.33, 4.17, and 5 kV/cm were 1.40, 1.56, and 1.78 times higher, respectively, compared to control (same conditions) after 5 h of drying<br>▪ DRs at EHD (combined with 2.2 m/s) at 3.33, 4.17, and 5 kV/cm were 1.08, 1.03, and 0.97 times higher, respectively, compared to control (same conditions) after 5 h of drying |
| Ding et al. (2015) ∗ | Carrots strips ($A$=0.00001 5 m$^2$, $l$=5 mm) | Multiple needle (135 needles, $A$=0.256 m$^2$, $r$ =0.5 mm) | Stainless steel plate, $A$=0.3696 m$^2$ | a) 21±2°C 30±5% RH b) 40±1°C 30±5% RH | 10.0 | a) 5, 10, 15, 20, 25, 30 b) 35 | a) 0.5, 1, 1.5, 2, 2.5, 3 b) 3.5 | AC DC (polarity was not given) | Exponential | ▪ EHD DR increased with voltage by 0.47, 0.75, 1.45, 1.49, 1.96 and 2.33 times at 0.5, 1, 1.5, 2, 2.5 and 3 kV/cm compared to control (the same conditions) after 0.5 h<br>▪ No electric current observed at 5 and 10 kV |
| Martynenko and Zheng (2015) ⁂ ⁂ | Apple slices ($A$=0.00138 m$^2$, $l$=8±0.5 mm) | Multiple needle (Stainless steel, $A$=0.009 m$^2$) | Aluminum plate, $A$=0.02 m$^2$ | 21±1°C 1, 3, 5 m/s | 2.5 | 0 5 10 15 | 0 2 4 6 | DC+ | Exponential | ▪ The highest EHD effect on DR was observed in the range of 4-6 kV/cm combined with 0-1 m/s air flow. EHD DR increased with increase of electric field strength. EHD effect on DR gradually decreased with increase of air flow from 1 to 5 m/s<br>▪ The highest DR was observed at 6 kV/cm and 1.0 m/s<br>▪ Mass transfer was faster at EHD 4-6 kV/cm combined with 0-1 m/s air flow compared to sole EHD |

Table A.1 EHD drying of water and plant-based materials, Continued

| Reference | Material | Discharge electrode | Collecting electrode | Environmental conditions | Gap, cm | Voltage, kV | E, kV/cm | Current | Drying kinetics | Major findings |
|---|---|---|---|---|---|---|---|---|---|---|
| Yang and Ding (2016) ⁂ | Chinese wolfberry fruit | Multiple needle (135 needles, $A$=0.256 m$^2$, $r$ =0.5 mm) | Stainless steel plate, $A$=0.3696 m$^2$ | 25±2°C 30±5% RH | 10.0 | a) 0, 20, 24, 28, 32 b) 28 | a) 0, 2, 2.4, 2.8, 3.2 b) 2.8 | a) AC b) DC+ DC- | Exponential | ▪ EHD DR increased with electric field strength and it was 1.88, 2.0, 2.37 and 2.66 times higher at 2, 2.4, 2.8, and 3.2 kV/cm, respectively, compared to control (the same conditions)<br>▪ EHD DR at AC 2.8 kV/cm was 1.40 times higher compared to that at DC 2.8 kV/cm after 5 h of drying. This could be explained by the level of current, which was 369 µA for AC and 10 µA for DC<br>▪ DR enhancement increased with the increase of voltage |
| Martynenko and Kudra (2016b) ⁂ | Grape Pomace ($l$=5-7 mm) | Multiple needle with spacing: a) 1 cm b) 2 cm | Aluminum plate, $A$=0.02 m$^2$ | 20°C 45±15% RH 1 m/s | 3.5 | 15 | 4.3 | DC+ | Linear | ▪ Discharge electrode with 2 cm spacing between needles provided higher DR than with 1 cm spacing<br>▪ EHD combined with air flow had a significantly higher DR than sole air flow (control)<br>▪ Effective moisture diffusivity at sole EHD drying was significantly higher than at force convective drying 1 m/s |
| Bardy et al. (2016) ♦ | Methylcellu-lose gel, mango slices ($A$=0.012 m$^2$) | Single wire ($r$ =0.25 mm) located: a) perpendicu-larly to air flow b, c) parallel | Copper plate, $A$=0.0225 m$^2$ | 35°C 20% RH 0.3 m/s | a) 7 b, c) 4 | a) 22 b) 10 c) 16 | a) 3.14 b) 2.5 c) 4 | DC (polarity was not given) | Exponential | ▪ EHD combined with airflow 0.3 m/s significantly increased DR compared to control (the same conditions) |

Table A.1 EHD drying of water and plant-based materials, Continued

| Reference | Material | Discharge electrode | Collecting electrode | Environmental conditions | Gap, cm | Voltage, kV | E, kV/cm | Current | Drying kinetics | Major findings |
|---|---|---|---|---|---|---|---|---|---|---|
| Elmizadeh et al. (2017) ⁂ | Quinces slices ($l$=2 mm) | Multiple needle (32 needles, $r_{tip}$=0.4 mm) | Metal plate | 70°C 1 m/s | 2.0 | 5<br>7<br>9 | 2.5<br>3.5<br>4.5 | DC+ | Linear | ▪ DR increased linearly with increase of electric field. DR at 3.5 kV/cm was higher by 1.24 times, and DR at 4.5 kV/cm higher by 1.66 times compared to 2.5 kV/cm<br>▪ EHD disturbed the boundary layer of quince slices and mass transfer was enhanced because of that |
| Martynenko et al. (2017b) | Wet tissue paper, wet sponge ($l$=5 mm) | Multiple needle (stainless steel, 143 with 1 cm spacing and 42 with 2 cm spacing, $r$ =0.675 mm) | Aluminum plate, $A$=0.02 m$^2$ | 20±1ºC 55-70% RH 0, 1 m/s | 3.5<br>4.0 | 14<br>19 | 3.5-5.43 | DC+ | Linear | ▪ DR increased with electric field strength, increasing with voltage and decreasing with gap<br>▪ EHD combined with 1 m/s airflow resulted in higher DR than sole EHD<br>▪ EHD DR at 42 needles (2 cm spacing) was higher than at 143 needles (1 cm spacing)<br>▪ EHD effect depends on the material surface smoothness. Calculated drying flux was 0.225 g/(s·m$^2$) for tissue vs. 0.180 g/(s·m$^2$) for sponge at 5.43 kV/cm |
| Sumariyah and Fachriyah (2018) * ♦ | Ginger slices ($A$=0.00007 9-0.0007 m$^2$, $l$=3 or 20 mm) | Single needle ($r_{tip}$=0.026 mm) | Multiple ring (3 rings, 0.008-0.024 m diameter) | 25°C | 0.4<br>0.6 | 4.3 | 7.17<br>10.75 | DC+ | Exponential | ▪ One needle and multiple ring collecting electrode created good local density of ionic wind |

Table A.1 EHD drying of water and plant-based materials, Continued

| Reference | Material | Discharge electrode | Collecting electrode | Environmental conditions | Gap, cm | Voltage, kV | E, kV/cm | Current | Drying kinetics | Major findings |
|---|---|---|---|---|---|---|---|---|---|---|
| Martynenko et al. (2019a) ⁂ | Mushroom slices ($A$=0.00126 m$^2$, $l$=5 or 10 mm) | Multiple needle (stainless steel, 143 with 1 cm spacing and 42 with 2 cm spacing, $r$ =0.675 mm) | Aluminum plate, $A$=0.02 m$^2$ | 20°C 20-70% RH 1 m/s | 3.0 3.5 | 12 14 15 16 18 22 | 4-6.3 | DC+ | Exponential | ▪ EHD DR decreased with increase of needles' density and by 1.47 times with increase of sample thickness from 5 to 10 mm<br>▪ EHD DR increased with decrease of RH from 70 to 30% by more than 3 times<br>▪ EHD DR increased with increase of electric field strength from 4 to 5.33 kV/cm at the same electrode gap<br>▪ Effective moisture diffusivity increased with increase of electric field strength at fixed gap. It was $3.29 \cdot 10^{-10}$ m$^2$/s at 4 kV/cm, $4.84 \cdot 10^{-10}$ m$^2$/s at 4.67 kV/cm, and $6.42 \cdot 10^{-10}$ m$^2$/s at 5.33 kV/cm<br>▪ EHD DR decreased proportional to initial moisture content of samples<br>▪ EHD DR was 4.76 times higher compared to control (natural convection) |

*Notes*. ∗ quality measurements are included; ♦ energy consumption is included; ⁂ quality and energy consumption are included. Material area was calculated per each separate sample/slice/piece.

**Copyright permission (B)**

RE: Permission to re-use graphical material

UJ

US Journal Permissions <USJournalPermissions@taylor

To Ivanna Bashkir

Wed 1/29

You forwarded this message on 1/29/2020 1:52 PM.

January 29, 2020

Dear Ivanna Bashkir on Behalf of Dalhousie University,

1. **Material Requested: Figure 1 from: Martynenko, A., Bashkir, I., Kudra, T., 2019. Electrically enhanced drying of white champignons. Drying Technology. DOI: 10.1080/07373937.2019.1670672.**
2. **Figure 5 from: Kudra, T., Martynenko, A., 2019. Electrohydrodynamic drying: Theory and experimental validation. Drying Technology. DOI: 10.1080/07373937.2019.1628773.**
3. **Figure 2 from: Martynenko, A., Kudra, T., Yue, J., 2017. Multipin EHD dryer: Effect of electrode geometry on charge and mass transfer. Drying Technology. DOI: 10.1080.07373937.2017.1285311.**

Thank you for your correspondence requesting permission to post your above mentioned material on **your institutions intranet or within the Institutional Repository of your institution and in your thesis.**

As you are the author of the above article, we will be pleased to grant entirely free permission on the condition that you make the following acknowledgement:

"This is an **Accepted Manuscript** of an article published by Taylor & Francis in *JOURNAL TITLE* on *date of publication*, available online at the Taylor & Francis Ltd web site: www.tandfonline.com and include a link to the article - http://

You will also need to obtain permission from any co-authors of this article.

Please note that this license does not allow you to post our content on any other third party websites.

This license does not allow the use of the Publishers version/PDF (this is the version of record that is published on the publisher's website) to be posted online.

Thank you for your interest in our Journals.

Sincerely,

**Mary Ann Muller** – Permissions Coordinator, US Journals Division

***My Work Schedule is Tuesday, Wednesday, and Friday.***

**Please note the current processing time is 6 weeks for all permission requests received in-house by the Journal permissions team.**

Find digital versions of our articles on: www.tandfonline.com to use RightsLink, our online permissions web page, for immediate processing of your permission request.

Instructions on the use of RightsLink is provided below:
(**https://taylorandfrancis.my.salesforce.com/sfc/p/** )

Do you need corporate or book permission? **Please contact our dedicated Corporate Permission TFCorpermissions@informa.com or Book Permission mpkbookspermissions@tandf.co.uk teams.**



Taylor & Francis Group
an **informa** business

530 Walnut Street – 8th floor
Philadelphia | PA | 19106 | United States of America
**Direct line**: 215-606-4334
**Main Office**: 215 625 8900, ext. 14334

maryann.muller@taylorandfrancis.com
www.taylorandfrancisgroup.com
www.tandfonline.com

**Copyright permission (C)**

AW: Request for Permission

DR

DeGruyter, Rechte <rights@degruyter.com>
To Ivanna Bashkir

11/14/2019

You forwarded this message on 11/14/2019 8:31 AM.

Dear Ivanna,

Thanks for reaching out. I am pleased to inform you that we grant you the permission to reuse the requested figures free of charge, provided that they have been created by yourself entirely and that full credit is given to the original publication and publisher.

Please note that our consent is given to the mentioned reuse only and this permission is non-exclusive and non-transferable. We kindly ask you to ensure, that any electronic content is password-protected, we cannot grant open access.

The permission is subject to full acknowledgement of the source material used and provides that full credit is given to the original publication and the publisher at appropriate place and according to the following credit line:

author(s)/editor(s) (ed.), title. subtitle, place: publisher, year, pp. xx - xx, fig./ill. xx - xx. or author(s), "title of article"; in: author(s)/editors(s) (ed.) of book/journal, title of book/journal, vol./issue number (if journal), place: publisher, year, pp. xx - xx, fig./ill. xx - xx.

Please do not hesitate to contact us in case you have any questions.

We wish you all the best
Sophie

Kind regards
De Gruyter Rights & Licenses Team

i.A. Sophie Schmale
Associate, Rights & Licenses
DE GRUYTER
Genthiner Straße 13
10785 Berlin, Germany
T +49 (0)30.260 05-337
F +49 (0)30.260 05-264
rights@degruyter.com
www.degruyter.com
Walter de Gruyter GmbH. Genthiner Str. 13. 10785 Berlin.

Domicile Berlin. Amtsgericht Charlottenburg HRB 143490 B. Rechtsform: GmbH.
Managing Director: Carsten Buhr
Chairman of the Advisory Board: Rüdiger Gebauer

-----Ursprüngliche Nachricht-----
Von: Ivanna Bashkir [mailto:IvannaBashkir@dal.ca]
Gesendet: Dienstag, 12. November 2019 14:31
An: DeGruyter, Rechte <rights@degruyter.com>
Betreff: Request for Permission

Dear Sir/Madam,

I am seeking your permission for the reprint of highly-modified by me two pictures, previously published by Berkeley Electronic Press in International Journal of Food Engineering.
I need your permission to reuse two figures from:

Zheng, D.-J., Liu, H.-J., Cheng, Y.-Q., Li, L.-T., 2011. Electrode configuration and polarity effects on water evaporation enhancement by electric field. International Journal of Food Engineering, Volume 7, Issue 2. ISSN (Online) 1556-3758. DOI: 10.2202/1556-3758.1794.
https://www.degruyter.com/view/j/ijfe.2011.7.2/ijfe.2011.7.2.1794/ijfe.2011.7.2.1794.xml

The required figures in the above paper are: Figure 10 and 11.
I have modified them highly and do not require any translation and additional work.

At the moment, I am MSc student at Dalhousie University, writing my review paper "Electrohydrodynamic drying of plant-based materials" where the above-mentioned pictures (Referred to Zheng et al., 2011) accounts roughly 1% of my new work. I am planning to submit this paper, which has 35-40 pages, to Critical Reviews in Food Science and Nutrition Journal published by Taylor and Francis. An expected date of my new publication is March-May 2020.
Please, give me your permission to reuse the above mentioned graphical material with high modifications.

Thank you,
With Best Regards,

Ivanna Bashkir,

MSc Candidate
Department of Engineering
Faculty of Agriculture
Dalhousie University
Truro, NS, B2N 5E3
P: (902) 893-6696
F: (902) 893-1406